1997009

Final Report 1999-36

Research

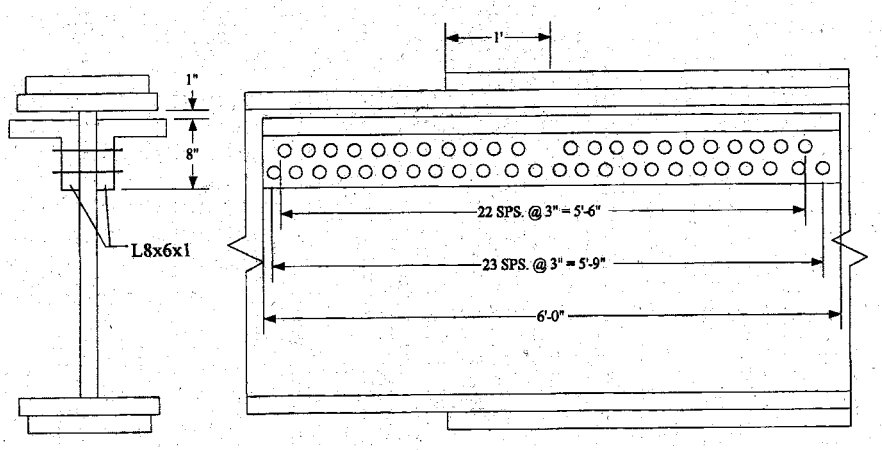

Acoustic Emission Monitoring of Fatigue Cracks in Steel Bridge Girders

Technical Report Documentation Page

1. Report No.	2.	3. Recipients Accession No.
MN/RC - 1999-36		

4. Title and Subtitle	5. Report Date
ACOUSTIC EMISSION MONITORING OF FATIGUE CRACKS IN STEEL BRIDGE GIRDERS	September 1999
	6.

7. Author(s)	8. Performing Organization Report No.
Jay McKeefry Carol Shield	

9. Performing Organization Name and Address	10. Project/Task/Work Unit No.
University of Minnesota Department of Civil Engineering 122 CivE Bldg., 500 Pillsbury Dr., S.E. Minneapolis, Minnesota 55455-0220	11. Contract (C) or Grant (G) No. 74708 TOC # 44

12. Sponsoring Organization Name and Address	13. Type of Report and Period Covered
Minnesota Department of Transportation 395 John Ireland Boulevard, Mail Stop 330 St. Paul, Minnesota 55155	Final Report 1997 - 1999
	14. Sponsoring Agency Code

15. Supplementary Notes

16. Abstract (Limit: 200 words)

This report presents results from a laboratory study and field implementation of acoustic emission monitoring of fatigue cracks in cover-plated steel bridge girders. The acoustic monitoring successfully detected growing fatigue cracks in the lab when using both source location and a state of stress criteria. Application of this methodology on three field bridges also proved successful by detecting a propagating crack in two of the bridges and an extinguished crack in a third bridge.

Researchers tested a double angle retrofit, designed by the Minnesota Department of Transportation, both in the lab and in the field of girder with fatigue cracks in the top flange. This retrofit does not require removal of concrete deck, and only involves bolting the retrofit to the bridge girder web. The double angle retrofit applied to laboratory test girder resulted in a reduction of flange stresses by 42 percent. Field implementation of the retrofit had mixed success. On one bridge, stress ranges in the cracked flange was reduced by 43 percent. However, on a second test bridge, the reduction was only 8 percent, likely due to the inadequate space for proper installation of the retrofit.

17. Document Analysis/Descriptors		18. Availability Statement
Acoustic Emission	Repair	No restrictions. Document available from:
Fatigue	Steel Bridge Girders	National Technical Information Services,
		Springfield, Virginia 22161

19. Security Class (this report)	20. Security Class (this page)	21. No. of Pages	22. Price
Unclassified	Unclassified	138	

ACOUSTIC EMISSION MONITORING OF FATIGUE CRACKS IN STEEL BRIDGE GIRDERS

Final Report

Prepared by:

Jay A. McKeefry
Carol K. Shield

Department of Civil Engineering
University of Minnesota

September 1999

Published by

Minnesota Department of Transportation
Office of Research Services
First Floor
395 John Ireland Boulevard, MS 330
St. Paul, Minnesota 55155

ACKNOWLEDGEMENTS

Funding for this research was provided by the Minnesota Department of Transportation (Mn/DOT) and the University of Minnesota. I would like to thank both for the financial support given.

Many people also assisted by giving a helping hand or providing knowledge, these include: Dr. Theodore V. Galambos, Dr. Robert J. Dexter, William Saari, Joe Hanus, John Timm, and Carl Osberg all at the University of Minnesota as well as Dan Ruffelle, Eric Evans, Terry Moravek and the bridge maintenance crews at Mn/DOT.

TABLE OF CONTENTS

Chapter 1 - Introduction 1
Chapter 2 - Literature Review 5
2.1 Acoustic Emission Monitoring 5
2.2 Fatigue Cracks and Fatigue Life 12
Chapter 3 - Laboratory Setup 15
3.1 Load Frame 15
3.2 Crack Initiation Procedure 16
3.3 Acoustic Emission Monitoring Equipment 16
3.4 Acoustic Emission Monitoring Before Retrofit 19
3.5 Strain Gage Setup Before Retrofit 20
3.6 Double Angle Retrofit Design 21
3.7 Acoustic Emission Monitoring After Retrofit 22
3.8 Strain Gage Setup After Retrofit 23
Chapter 4 - Laboratory Experiment Results 25
4.1 AE Results Before Retrofit 25
4.2 Beam Stresses Before Retrofit Application 26
4.3 Fatigue Crack Growth After Retrofit Application 26
4.4 AE Results After Retrofit Application 27
4.5 Beam Stresses After Retrofit Application 28
Chapter 5 - Test Bridges Setup 33
5.1 Test Bridges 33
5.2 Acoustic Emission Setup 35
5.3 Strain Gage Setup Before Retrofit 37
5.4 Strain Data Filtering 38
5.5 Mn/DOT Retrofit Design 40
5.6 Strain Gage Setup After Retrofit 41
Chapter 6 - Bridge Experiment Results 43
6.1 Stresses Produced by Sand Trucks Before Retrofit 43
6.2 Bridge Stress Ranges Produced by Random Traffic 47
6.3 AE Results 50
6.4 Bridge Stresses Produced by Sand Truck After Retrofit 52
Chapter 7 - Conclusions 57
7.1 Effectiveness of AE Monitoring to Determine Fatigue Crack Propagation 57
7.2 Effectiveness of Retrofit to Reduce Flange Stress and Stop Crack Propagation 58
7.3 Fatigue Life of Cracked Girders 60
7.4 Final Recommendations 60
References 63
Tables 65
Figures 67
Appendix A Section Properties
Appendix B Bridge Details
Appendix C Ultrasonic Inspection Reports
Appendix D Programs

LIST OF TABLES

Table 5.1: Truck Weights for Bridge Testing 65
Table 6.1: Bridge Stress Distributions for Traffic Data Collected 65
Table 6.2: Values of C_1 for Each Bridge 65
Table 6.3: Values of N_i for Varying Stress Ranges 66
Table 6.4: AE Events to Sand Truck Pass Ratio 66
Table 6.5: Percent Reduction of Stress Ranges Due to Sand Truck Loading 66

LIST OF FIGURES

Figure 3.1: Load Frame Setup 67
Figure 3.2: Crack Initiation Detail 67
Figure 3.3: Bottom Flange Section Loss at 1,773,000 cycles 68
Figure 3.4: Bottom Flange Section Loss at 1,983,000 cycles 68
Figure 3.5: Acoustic Emission Monitor Setup and Transducer Location 69
Figure 3.6: Determination of Stress Wave Velocity in Lab Beam 69
Figure 3.7: Typical AE Signal 70
Figure 3.8: Loading Conditions that Create Crack Propagation 70
Figure 3.9: Location of Strain Gages Before Retrofit 71
Figure 3.10: Laboratory Double Angle Retrofit Detail 71
Figure 3.11: Laboratory Beam Moment of Inertia Values 72
Figure 3.12: AE Transducer Configuration After Retrofit (Single Array) 72
Figure 3.13: AE Transducer Configuration After Retrofit (2-Dimensional Array) 73
Figure 3.14: AE Transducer Configuration After Retrofit (Double Linear Array) 73
Figure 3.15: Location of Strain Gages on Retrofit 74
Figure 4.1: AE Crack Events vs. Cycle Before Retrofit 74
Figure 4.2: Cracked Section Stresses Just Prior to Retrofit 75
Figure 4.3: AE Crack Events vs. Cycle After Retrofit Application 75
Figure 4.4: Cracked Section Stresses Just After Retrofit Application 76
Figure 4.5: Cracked Section Stresses After Full Flange Cracking 76
Figure 4.6: Final Web Crack of Laboratory Specimen 77
Figure 5.1: Cover Plate Detail 77
Figure 5.2: Pier Layout West 7th Street Bridge 78
Figure 5.3: Pier Layout I-94 78
Figure 5.4: Pier Layout TH-36 79
Figure 5.5: Typical AE Transducer Location on Bridges 79
Figure 5.6: Strain Gage Locations on Bridges Before Retrofit 80
Figure 5.7: Typical Unfiltered Stress Data 80
Figure 5.8: Order Effects on Low Pass Butterworth Digital Filter 81
Figure 5.9: Fast Fourier Transform of Unfiltered Data 81
Figure 5.10: Typical Filtered Stress Data 82
Figure 5.11: Mn/DOT Retrofit Detail (West 7th Street Bridge and TH-36 Bridge) 82
Figure 5.12: Mn/DOT Retrofit Detail (I-94 Bridge) 83
Figure 5.13: Strain Gage Locations for Bridges After Retrofit 83
Figure 6.1: West 7th Street Bridge Northbound Stress History 84
Figure 6.2: West 7th Street Bridge Northbound Stress History Offset Gage 84
Figure 6.3: West 7th Street Bridge Northbound Stress Distribution 85
Figure 6.4: West 7th Street Bridge Southbound Stress History 85
Figure 6.5: West 7th Street Bridge Southbound Stress History Offset Gage 86
Figure 6.6: West 7th Street Bridge Southbound Stress Distribution 86
Figure 6.7: I-94 Bridge Stress History Before Retrofit 87
Figure 6.8: I-94 Bridge Stress History Before Retrofit Offset Gage 87
Figure 6.9: I-94 Bridge Stress Distribution Before Retrofit 88

Figure 6.10: TH-36 Bridge Stress History Before Retrofit 88
Figure 6.11: TH-36 Bridge Stress Distribution Before Retrofit 89
Figure 6.12: Three AE Crack Events for One Truck Pass 89
Figure 6.13: Crack Rubbing Event on I-94 Shown Against Bottom Flange Stress 90
Figure 6.14: Strain in the Bottom Flange of TH-36 with Trucks Adaquately Spaced 90
Figure 6.15: Strain in the Bottom Flange on TH-36 with Trucks too Closely Spaced 91
Figure 6.16: West 7th Street Bridge Northbound Stress History After Retrofit 91
Figure 6.17: West 7th Street Bridge Northbound Stress History Angle Gage After Retrofit ... 92
Figure 6.18: West 7th Street Bridge Northbound Stress Distribution After Retrofit 92
Figure 6.19: West 7th Street Bridge Southbound Stress History After Retrofit 93
Figure 6.20: West 7th Street Bridge Southbound Stress History Angle Gage After Retrofit ... 93
Figure 6.21: West 7th Street Bridge Southbound Stress Distribution After Retrofit 94
Figure 6.22: I-94 Bridge Stress History After Retrofit 94
Figure 6.23: I-94 Bridge Stress Distribution After Retrofit 95

EXECUTIVE SUMMARY

Methods for detecting propagating fatigue cracks and retrofitting bridge girders with fatigue cracks were investigated. Several cover plated rolled steel girders bridges in the Minneapolis Metropolitan area are known to have fatigue problems in the top flange near the cover plate detail. Previous methods of repair involved removal of the bridge deck requiring a disruption in the traffic over the bridge. In order to minimize the number of bridges that require this type of repair, acoustic emission monitoring was implemented to determine if the existing cracks were propagating. In addition, the effectiveness of a double angle retrofit that involved bolting through the web only was investigated.

Acoustic emission (AE) monitoring of a steel girder in the University of Minnesota structures lab indicated that AE monitoring could detect growing fatigue cracks if both a source location and a state of stress criteria were used. Application of this methodology on three field bridges also proved successful by detecting a propagating crack in two of the bridges and an extinguished crack in a third bridge.

The double angle retrofit was applied to the laboratory test girder and resulted in a reduction of flange stresses by 42%. Field implementation of the retrofit had mixed success. On one bridge, stress ranges in the cracked flange were reduced by 43%. However, on a second bridge tested, the reduction was only 8%, likely due to the inadequate space to properly install the retrofit.

Chapter 1 - Introduction

Fatigue cracks in the flanges of rolled steel beams originating at the ends of welded cover plates have been discovered on several bridges in the Twin Cities metro area. These cracks could propagate further into the flange and possibly down into the web resulting in member failure. Some fatigue cracks have already propagated into the web and have needed extensive repair. When the crack was in the top flange, these repairs required removal of the concrete deck and bolting of plates on the top and bottom of the flange across the crack. Periodic ultrasonic testing has indicated the propagation of some small cracks, while indicating that other cracks or flaws appear not to be growing and thus, pose a lesser threat of failure. Crack propagation detection and fatigue crack repair, are the two main objectives of this research. A method for determining the rate at which cracks continue to grow may reduce unneeded repair of girders with slow growing cracks. In addition, a procedure that could repair top flange cracks without having to remove a portion of the bridge deck is desirable, because of the expense associated with deck removal.

Various methods of nondestructive evaluation (NDE) have been employed in discovering fatigue cracks in steel bridges. Of these methods, both visual and ultrasonic testing have been used by the Minnesota Department of Transportation (Mn/DOT) to inspect bridges. Visual inspection does not allow examination of welded cover plate terminations that reside on top of the top flange of a girder because of the concrete bridge deck above. In these locations, ultrasonic testing has been used to determine if the weld toes of the cover plates are cracked. While ultrasonic testing is a good tool for discovering fatigue cracks that are not visible to the eye, its ability to determine crack activity is limited. Ultrasonic testing must be performed many times over long periods to determine if the cracks are indeed growing. Another NDE method that could determine crack propagation is acoustic emission (AE) monitoring. AE monitoring to detect fatigue crack propagation has been performed on bridges previously with mixed results [1]. Advances in the equipment and increased speed of personal computers has allowed AE monitoring to be a practical option for fatigue crack propagation detection [2].

Acoustic emissions are transient stress waves created when stressed material has a sudden release of strain energy [1]. These waves travel in all directions in the material and

eventually travel along the material surface. The stress waves then excite an AE transducer that is placed on the material surface to detect such emissions. AE transducers are constructed of piezoelectric material that can transform strain into voltage. These voltage signals generated by the transducer are amplified and sent to the AE monitoring equipment. The AE monitor has the ability to take signals from many transducers and determine the location where the emission was created [3].

The University of Minnesota has investigated the use of acoustic emission technology in determining fatigue crack growth of fatigue cracks near cover plates. A laboratory study was performed to evaluate the ability of AE to detect crack propagation of a fatigue crack. A fatigue crack was initiated in the bottom flange of a W27x94 rolled steel beam. Once the crack had been initiated in the section, AE transducers were placed in positions where crack growth could be monitored. Various transducer arrangements were investigated to determine optimal placement of the transducers for use in the second portion of the study in the field, on a cracked girder in a bridge. Acoustic emissions from the crack were monitored during cyclic loading of the laboratory girder and AE data was correlated to visual crack growth over many cycles.

Once the crack in the laboratory reached a severity that was worse than those found in the field, the girder was fitted with a double angle retrofit developed by Mn/DOT to stop the progression of the fatigue crack. This retrofit comprised two angles bolted with a slip critical connection through the web of the member. Strain gages were used both before and after retrofit attachment to determine how the retrofit changed the stress distribution through the section. Acoustic emission monitoring was also performed after the retrofit had been affixed to see if crack propagation could be monitored.

Chapter 2 presents a review of previous research done in the field of both AE monitoring of bridges and strain gage testing of bridges. The information learned in these studies was used as a knowledge base for the current research.

Chapter 3 discusses the setup of the girder in the laboratory and the procedure implemented to generate the fatigue crack. Details are given as to the AE transducer arrangement and the testing methods performed on the member both before and after the implementation of the double angle retrofit. Strain gage layout is also discussed for both the

girder and the retrofit angles. A discussion about the retrofit design theory is also presented in Chapter 3.

Chapter 4 discusses the results from work performed on the laboratory specimen. AE monitoring data and strain gage data are presented and rationalized. Information is given for both before and after the retrofit attachment, allowing for an evaluation of the performance of the double angle retrofit. The laboratory study provided the needed background of both AE monitoring procedures and retrofit performance to successfully embark on the next phase of the research, the bridges.

Three bridges in the Twin Cities metro area were instrumented with both AE monitoring equipment and strain gages. BR 62066, West 7th Street over railroad tracks, BR 27855, I-94 over TH-55, and BR 9276, TH-36 over Cleveland Ave were the three bridges tested. The bridges were chosen because of the existence of fatigue cracks at cover plate terminations at all three locations.

Testing was performed both before and after the implementation of the retrofit to evaluate how adding the angles affected girder stress ranges. Loaded Mn/DOT supplied sand trucks were used to apply a known load to the bridges for two reasons. The trucks would allow for a comparison of before and after effects due to the double angle retrofit. In addition, the trucks provided a consistent load for producing any AE that would emanate from the fatigue crack, if that crack were propagating.

Chapter 5 presents the procedures used on the bridges for acquiring both AE and strain data. General information is given about each bridge and locations of AE transducers and strain gages are discussed. Problems with testing in the field are presented and the solutions to overcome them are subsequently discussed.

Chapter 6 includes a discussion of the results of all the testing performed in the field. The predictions made after studying the AE monitoring data are presented. Stress ranges before and after retrofit are also presented to determine the effectiveness of the retrofit.

Chapter 7 gives the answers to the questions posed by the need for this research. There were three main objectives studied in this project. The first concerns the use of AE monitoring to determine if fatigue cracks in bridges are propagating. The second objective was to find out if the retrofit proposed by Mn/DOT was effective in lowering cracked flange stress ranges and if

the retrofit could stop the flange from cracking. Remaining fatigue life of the member was also an objective that is discussed.

Chapter 2 - Literature Review

This study combines previous knowledge from two research areas. One part of the previous research pertains to the use of acoustic emission monitoring of fatigue cracks in bridges. The other type of previous research that is of interest is strain gauging and the determination of remaining fatigue life in cover plated steel bridge girders. These two topics will be discussed in this chapter starting with the information that has been gathered about AE monitoring of fatigue cracks. Following that will be a discussion of determining stress ranges in bridge girders and how that information can be used to obtain the remaining fatigue life of the member.

2.1 Acoustic Emission Monitoring

Steel bridges may be damaged by continued loading over the life of the structure. Cyclic loads imposed by truck traffic can create fatigue cracks in bridge members. Certain attributes of a member may make it more susceptible to fatigue cracking such as the magnitude of the truck loads imposed, the number of times these loads are imposed, and the structural details the member contains [1]. Welded structural details are most often the location where fatigue cracks will initiate in a member [4].

Earlier in this century, steel bridges were constructed from built up, riveted members [4]. These members had built up redundancy, thus if part of the member were to fail by fatigue cracking, it would fail only one piece which would be noticed and repaired without collapse of the entire structure. Welded details began to be introduced into steel bridges with initial hesitation because of the knowledge that cracking problems may arise [4]. Because design data for welded members was inadequate at the time, low fatigue strength details were commonly used [4]. One of these poor details is the partial length cover plate.

Partial length cover plates are vulnerable to fatigue cracks for two main reasons, flawed welds and stress concentrations. The ends of cover plates often contain welds that possess irregularities and imperfections that are oriented transverse and perpendicular to stress flows which leads to initiation of fatigue cracks. The changes in member section properties at the ends

of cover plates also create high stress concentrations. These large stress concentrations have the most influence on fatigue crack growth [4].

Few steel bridges have failed catastrophically, those that have include: Kings Bridge in Melbourne, Australia (1962), the Silver Bridge in West Virginia (1967), and a span of the Mianus River Bridge in Connecticut (1983) [5]. These failures and other bridge closings have brought about the need for regular inspections of bridges. The Federal Highway Administration (FHWA) has become involved in promoting the need for regular bridge inspection and has fueled research of certain nondestructive evaluation (NDE) procedures [6].

Visual inspection has been used in the past to detect fatigue cracks in steel members, but some small fatigue cracks may not be detected in a simple visual inspection. Paint may cover cracks, obscuring them. Cracks that form on the top side of the top flange can not be visually detected until they have propagated through the flange. Methods that aid in discovering small fatigue cracks need to be found.

Some of the methods that are now used to inspect bridges for cracks include magnetic particle testing, dye-penetrant testing, florescent surface testing, eddy-current testing, and ultrasonic testing [7]. Research performed by the Kentucky Transportation Research Program (KTRP) was done to evaluate these methods of locating cracks in steel bridge members.

Magnetic particle testing is performed by blowing iron particles onto the testing surface with a squeeze bottle in the presence of a magnetic field. Surface cracks are present when the particles lie in an aligned manner. If the particles are distributed in a random manner then no cracks are present. A drawback of this method is that if too much powder is dispensed on the testing surface, cracks could be masked and not detected. However, this method can be used on painted surfaces but it cannot be used to detect cracks below the surface.

Dye-penetrant testing uses a solvent-removable dye that is sprayed onto the testing surface. After the surface is cleaned of the dye, cracks can be detected by the presence of traces of dye left behind in the crack. This method is advantageous on surfaces free of obstructions, if used near filet welds; indications that do not correspond to cracks may be present. This method cannot be used to detect sub-surface cracks.

Florescent magnetic particle testing uses a black light and particles similar to those used in visual magnetic particle testing. This method was found to be much slower than visual

magnetic particle testing and needed low light conditions to be successful. Below surface cracks cannot be detected with florescent magnetic particle testing.

The eddy-current testing device creates a magnetic field around a coil. The coil is brought near the test specimen and a field is then created in the steel of the specimen. A crack in the specimen disrupts the electronic and magnetic fields which is detected by the eddy current probe. This method is also a surface technique, it cannot be used from the back side of the member. The method found cracks not previously detected by visual methods but false indications of cracks were likely due to material variations and welding imperfections.

Ultrasonic testing was the only testing method that was capable of discovering cracks on the back surface of a steel specimen. Ultrasonic testing uses piezoelectric transducers that are coupled to the test specimen using a fluid. A sound wave is sent into the specimen by the transducer, when the wave interacts with features of the specimen it reflects back to the transducer. These features can be the back side of the specimen or a flaw. A signal is created when the wave gets back to the transducer and the time difference between when the wave was sent out and received can be used to determine the thickness of the member or location of the flaw. If the timing of the return signal indicates it is from something other than the back side of the specimen, then a flaw is indicated. A drawback to ultrasonic testing is the extensive training required to use the equipment properly. Although all the NDE methods mentioned involve the scanning of the surface for existing cracks, none of the methods can be used in a single inspection to determine if the crack is propagating. KTRP suggest a two-phase system of bridge inspection. The first phase would be to detect cracks and other discontinuities in the members, this would be the scanning phase. The second phase would be flaw evaluation. This phase would determine if the crack that was detected poses a threat of failure. The previously mentioned NDE methods all may be used for the scanning phase. The authors suggest that the use of acoustic emission monitoring would be beneficial in the evaluation phase.

Acoustic emission monitoring is an NDE method that detects only active flaws in a steel member. Transient stress waves are produced when there is a rapid release of strain energy due to a crack that is propagating. AE monitoring equipment uses piezoelectric transducers to detect these stress waves. A drawback to using AE monitoring is the background noise present on bridges [8]. Earlier versions of AE monitors lacked the ability to distinguish between AE caused

by fatigue crack propagation and AE caused by bridge fretting [1]. These early versions of AE monitoring instruments were used by KTRP to detect cracks in steel members. Research was suspended for a time until the equipment improved and made bridge monitoring possible. The emphasis then was on finding an AE system that could effectively distinguish AE produced by crack propagation from AE caused by mechanical noise.

KTRP started using a new AE monitoring system created by GARD in 1982, the acoustic emission weld monitor (AEWM) [1]. The AEWM was initially designed to test welding operations but KTRP thought it might be suited for bridge monitoring. The system used a three criteria process to determine if AE was crack produced or background noise. The first of the three criteria was that cracks would produce multiple AE events over a short period of time. This was known as the event-rate criteria. The second criteria was that AE events had a discrete energy level, this was an energy criteria. The final criteria was that AE crack activity came from a distinct region, or a location criteria. The AEWM used software that analyzed the AE data to recognize cracks and determine their location [1].

The AEWM was employed on many different bridges by both KTRP [9] and GARD to determine fatigue crack propagation of known cracks. The first bridge tested was I-24 over the Tennessee River near Paducah, Kentucky in 1982. There were visible cracks at the end connections that were caused by out-of-plane bending in the floor beams. Five crack locations were tested and two sensor arrays were used to surround the crack location; these locations were near bolted splices that were producing AE by mechanical rubbing. Normal service loads were the only loads present to generate AE by fatigue cracking. One of the five sites produced AE that the AEWM determined to be generated from fatigue cracking. Subsequent tests of the same crack location showed that AE due to fatigue cracking was decreasing with time. This crack was determined to be self-extinguishing, as some out-of-plane cracks are, and not repaired in any manner.

Another bridge tested by KTRP [9] was the I-75 Bridge over the Ohio River in Covington, Kentucky. Here welded cover plates on the bottom flanges of girders in the approach span were monitored for crack activity. Strain gages had been used to measure the stress ranges present in the lower flanges and the recorded values exceeded those recommended by AASHTO. AE indications present were determined not to be produced by fatigue cracking because the

indications were not passing the location criteria. Other sensors were used as guard sensors to eliminate the false AE indications. No repairs were recommended by KTRP for this bridge.

KTRP determined that the AEWM was successful in determining the propagation of existing fatigue cracks in steel bridge members. AE monitoring was considered a viable NDE method for the fatigue crack evaluation phase of bridge inspections. KTRP also determined the four phases of AE monitoring. The first phase is to properly locate the AE sensors to receive fatigue crack induced AE. The second phase is to calibrate the array location by injecting ultrasound at specified points along the array. The third and fourth phase actually occur simultaneously and include suitable loading of the bridge members being tested and acquisition of AE data.

Later research was performed by Vannoy and Azmi [8] at the University of Maryland in 1986, to further the use of AE monitoring in determining crack propagation in steel. Their research addressed the problem of AE produced by mechanical rubbing interfering with determination of fatigue crack growth by AE monitoring. Signal characteristics were used to discriminate between AE produced by fatigue crack growth and AE produced by mechanical noise.

The beams tested were W14x30 that were 15.5 ft. in length. Cyclic loading was performed by an actuator attached to the center of the beam. The loading was a sinusoid function at 0.75 Hz, amplitudes varied to produce a bottom flange stress that was no more than 22 ksi in tension.

The AE monitor was a Physical Acoustics SPARTAN model. Two types of transducers were used, model R15I and model WD, these were calibrated by the ultrasonic white noise method and by hand using pencil lead. Thresholds for the system were set between 22 and 30 dB. Two transducers were placed on the top of the bottom flange of the member and another transducer was placed in the center of the beam on the web.

Results of the testing showed that amplitudes of the AE signals produced by cracks fell on a bell-shaped curve over the fatigue life of the beam. AE produced by cracks showed no distinct feature that could make it distinguishable from AE produced by mechanical noise. It was also shown that welds generated AE very early in the fatigue life of the member. These AE signals were thought to be produced by micro-crack initiation in welds.

Research was performed at the University of Wisconsin-Milwaukee by Ghorbanpoor and Rentmeester [10] to find methods to distinguish crack produced AE from noise related signals. Researchers believed that attributes associated with the AE signal, such as state of stress and event location, could be used to distinguish crack growth AE from noise produced AE. Both a laboratory experiment and a field test were performed.

In the laboratory, steel plates of both 3/8 in. and 3/4 in. thickness were cut into 2 in. by 16 in. specimens. The specimens had notches cut into the side at the midpoint to act as a stress raiser and accelerate the start of a fatigue crack and to direct where the crack would initiate. Sinusoidal loading was imposed at a rate from 1 to 4 Hz; this produced tension stresses ranging from 0.9 ksi to 20 ksi. Specimens were loaded until a fatigue crack had started and ultimately propagated to failure.

The AE monitoring was done using 4 transducers on each specimen in a linear array. The two inner transducers were responsible for source location of crack produced AE and the outer transducers were used to guard against background noise. The applied load value was input into the AE monitor, yielding knowledge of the state of stress in the specimen at the time of each acoustic emission. All AE that was produced by the crack was recorded for the entire time the test proceeded.

AE events were screened by both a state of stress and location criteria. Only those AE events occurring at a high stress state were considered possible AE events produced by crack propagation. In addition, the location of the event was used to screen out those events that did not occur at the crack location. The result of this screening process was a figure showing AE crack events against the number of cycles for the specimen. The figure shows a high number of AE events very early in the fatigue life, this was attributed to the formation of a plastic state near the notches in the specimen before a crack had been initiated. The number of AE crack events dropped for about 100,000 cycles until a sharp increase in AE events was noted at about 150,000 cycles. This corresponded very well to the crack growth rate as measured by a microscope. It was proven that a program of AE monitoring using both a stress state and location criteria to screen AE events, can effectively determine fatigue crack propagation in small steel specimens tested in the laboratory.

The field portion of the research was conducted on a steel bridge with known active fatigue cracks. The problematic detail that was chosen for testing was a field splice weld on the top flange and web. The crack lengths for these details ranged from 1.25 in. to 1.875 in. Four transducers were place in a rectangular arrangement and a strain gage was attached to the bottom flange. The strain gage values were input into the AE monitor to give state of stress for each AE event. Because fatigue crack growth would only occur when the flange was in tension, only those events that occurred when the crack was in tension were considered crack growth events.

Field testing occurred under two loading conditions. Random traffic loads were utilized for the first AE test and the second test involved the use of controlled loads. The second test loading was provided by two loaded tandem-axle dump trucks with a front axle weight of 14,700 lbs. and rear axle weight of 30,400 lbs. Trucks made passes over the bridge that created tensile stresses in the top flange of the member. Approximately 50 truck passes were made and AE data was recorded for each.

The results of AE monitoring did show possible crack propagation for both the random traffic loads and the truck loads. Researchers noted the importance of the strain gage information to successfully distinguish crack related AE from noise that occurred from mechanical rubbing and crack closure. The location was tested ultrasonically 5 years later and confirmed the findings of the AE monitoring, the crack size had increased 1.5 in. since the previous inspection.

Another research project that attempted to use AE monitoring for determining fatigue crack propagation was performed at the University of New Mexico by Maji and Kratochvil [2]. Their research did not include the use of a source location algorithm and used only an oscilloscope to receive the AE data. Field tests were performed on the I-40 bridge over the Rio-Grande River in Albuquerque, NM.

AE signals were produced only by heavy trucks and tractor-trailers. No AE data was noticed for other types of traffic. Ultimately the researchers used only an AE event rate to determine fatigue crack growth. Subsequent inspections of the bridge showed no signs of propagation and thus all AE produced was attributed to rubbing of the bolted connections.

2.2 Fatigue Cracks and Fatigue Life

Fatigue cracks at the ends of welded cover plates have been discovered on many bridges throughout the United States. In the Fall of 1970, many of these kinds of cracks were found on the Yellow Mill Pond Bridge in Bridgeport Connecticut [11]. The first crack discovered on this bridge extended from the toe of the cover plate into the flange and continued into the web 16 in. This and two other cracks were repaired with bolted splice plates on both the flange and web. Later in 1976, 40 of the same kinds of cover plate details were visually inspected on the bridge and 22 were found to have cracked [11].

Methods to retrofit the cracks were subsequently studied by Fisher, Pense, Slockbower, and Hausammann [11] at Lehigh University. Three methods of repair were reported by the researchers including: grinding of the weld toe, air hammer peening of the weld toe, and remelting of the weld toe using a gas tungsten arc process. Grinding the weld toe primarily was beneficial by removing slag inclusions and lowering the stress concentrations. This method was found to only be beneficial at lower stress ranges. Details subjected to large stress ranges showed no apparent improvement. Peening the weld toe was beneficial because there would be residual compression stresses imposed on the weld. This method also was only beneficial at low stress ranges but was found more reliable than the grinding method. Some fatigue life improvement was witnessed at high stress ranges (10 ksi) but not as much as for lower stresses (1 ksi). The most beneficial process for lengthening the fatigue life of the cover plate detail was gas tungsten arc remelting. Gas tungsten arc remelting works by eliminating the nonmetalic fragments present in the weld and smoothing the toe thus reducing the stress concentrations. Once the details were remelted, the method of fatigue failure was now controlled by the weld root rather than the weld toe.

Both the weld tow peening and gas tungsten arc process were used to retrofit the Yellow Mill Pond Bridge cracks. Peening was the method chosen when visible cracks could not be detected by ultrasonic inspection because the cracks were less deep. Cracks greater than 0.125 in. were gas tungsten arc remelted.

A study performed by Hahin, South, Mohammadi, and Plepeddi [12] included acquisition of strain data from fatigue cracked bridge girders and fatigue life calculations for the members. Fifteen bridges were chosen throughout the state of Illinois. Foil type strain gages collected data

for 3 to 8 hours. Bridge traffic for the various structures ranged from 125 to 15,800 trucks per day.

Nine of the 15 bridges tested had cracks at the ends of welded cover plates on the lower flange. Strain gages were placed on the bottom of the lower flange and readings were recorded with a single channel data acquisition system. Histograms of the stress ranges were produced using increments of 0.5 ksi. Stress ranges below 0.5 ksi were discarded. The histograms made were linearly extrapolated to show values for a 24 hour period. A histogram for the life of a structure was obtained by multiplying the 24 hour histogram times the number of days that the bridge had been in service. Researchers noted that the longer data was collected the more representative the histograms would be of the actual stress ranges in the members.

To determine fatigue damage sustained for each crack site, the authors used the Palmgren-Miner linear damage rule. The rule takes the form:

$$\sum_{i=1}^{n} \frac{n_i}{N_i} = \frac{n_1}{N_1} + \frac{n_2}{N_2} + \frac{n_3}{N_3} + \ldots\ldots = 1, \qquad (1)$$

where n_i is the number of stress cycles for a 0.5 ksi stress range increment and N_i is the number of allowable cycles to failure at that stress range. The n_i were reported in a histogram for the life of a bridge. The cycles available at each stress range, N_i, were found by using:

$$N = c(S)^m, \qquad (2)$$

where N is the total cycles available to failure, S is the stress range given in ksi, c is a fatigue coefficient, and m is a fatigue exponent. The authors used values obtained by Munse et al. [13] for c and m. For a girder with welded cover plates Munse suggested $c = 4.218 \times 10^9$ and $m = -3.256$. Values were also given for the various AWS fatigue categories for both c and m.

The research also looked at future increases in both traffic amounts and truck weights. The histograms for each bridge were modified to account for higher numbers of vehicles and heavier axle weights. The future damage was then calculated and fatigue lives were estimated.

The previous research studied was used as a foundation for the methods used in the current research project. The method of using location and state of stress criteria to screen out mechanical rubbing AE events was of particular help. The Palmgren-Miner linear damage rule was also used to determine remaining fatigue life.

Chapter 3 - Laboratory Setup

A steel girder was tested in the laboratory to simulate a fatigue crack found on the test bridges. A fatigue crack first had to be initiated in the bottom flange of the section. This chapter describes the setup for loading the girder, and the crack initiation detail. A discussion on how acoustic emission technology works is presented. The layout of all AE monitoring equipment is discussed as well as the location of all strain gages. Additionally, laboratory retrofit design principles are presented as well as the procedure that was followed to attach the angles to the member.

3.1 Load Frame

The laboratory setup was designed to model field conditions of the cracked girders. Although the field girders had the fatigue cracks on the top flange, the cause behind the cracking was a tensile stress created during negative bending. This same tensile stress was produced in the laboratory with a positive bending moment, with the crack in the bottom flange. The same types of stresses were modeled in the laboratory, but the specimen was upside down from what it was in the field. In addition, no concrete deck was present above the crack location in the laboratory specimen.

A 15 ft. simply supported W27x94 A36 member was loaded in positive bending as shown Fig.3.1. The load frame comprised two columns connected by a load tube and a spreader beam. A 77 kip MTS hydraulic actuator was connected to the load tube, the spreader beam and specimen, supplying a force to the center of the test girder. The forcing function was a sine wave ranging from 2 kips to 60 kips downward at a rate of 2 Hz, creating a maximum of 198 kip-ft of positive moment at beam centerline under the actuator. This moment produced a nominal 9.8 ksi of tensile stress in the bottom flange of the member. This stress range was much larger than the stress ranges expected in the field girders.

The bearings for the girder were 1 ft. sections of 2 in. diameter steel rod placed in channel sections so the bearings would not roll away. This produced a true simple support. Neoprene pads were used initially instead of the steel rod, but the pads were producing unwanted acoustic emissions. When neoprene pads were replaced with the rods, the number of acoustic

emissions was greatly reduced. The channel sections holding the bearings were placed on top of a steel plate that was leveled and positioned with hydrocal, quick setting grout that has a high compressive strength. The entire bearing assembly was placed on top of concrete reactions blocks, approximately 3 ft. tall and 2 ft. wide.

3.2 Crack Initiation Procedure

To facilitate crack initiation in the bottom flange of the member, two 0.75 in. x 3 in. x 8 in. plates were welded to the beam butted up to each other at the centerline of the beam as shown in Fig. 3.2. After 800,000 cycles a crack propagated through the weld material at the junction of the two plates. At 923,000 cycles, a crack was verified as entering the flange extending from the weld cracks. Loading continued until 1,773,000 cycles at which time the plates that assisted in initiating the crack were cut off because of the unwanted acoustic emission noise that the weld created. Subsequently, the flange crack was tested ultrasonically by Eric Evans of Mn/DOT, and the crack depth was determined to be about 10% of the flange thickness, or about 0.06 in. The approximate flange section loss at 1,773,000 cycles illustrated in Fig. 3.3.

Cycling continued after the removal of the plates until the crack progressed upwards in the flange and was visible at the top of the flange. This occurred around cycle 1,983,000 and concluded the first stage of the laboratory study. Section loss at this stage is illustrated in Fig. 3.4. The crack now simulated a worst case field crack. The crack length was 3.6 in. on the bottom of the flange, 0.9 in. on the top of the flange, north side and 0.3 in. on the top of the flange, south side. No more girder cycling occurred until the retrofit was attached.

3.3 Acoustic Emission Monitoring Equipment

All of the acoustic emission monitoring was performed with a MISTRAS 2001 AE monitor, manufactured by Physical Acoustics Corporation. The system consisted of AE transducers that were attached to the steel by magnetic holdowns and coupled to the steel with petroleum jelly. Transducers were connected to preamps that filtered and amplified the signal. The preamps, also manufactured by Physical Acoustics Corporation, provided 40 dB gain and 50 Hz high pass filtering. Preamps were connected to the MISTRAS 2001 by BNC cables. The MISTRAS 2001 is an AE monitor that performs feature extraction and source location for the

AE signals. Also connected to the MISTRAS 2001 was the output from the conditioned strain gage on the top flange of the specimen. This signal was sampled every 0.05 seconds as well as every time an AE event occurred, and was used to determine the state of stress of the girder when an acoustic emission event occurred. A depiction of the AE setup can be seen in Fig. 3.5.

Some terms used when talking about acoustic emission data are AE hits and AE events. The excitation of a single AE transducer above a set threshold due to a stress wave traveling in the material is termed an AE hit. If the wave amplitude is smaller than the threshold setting the wave will not be recorded as a hit by the system. An AE event occurs when two or more channels receive hits emanating from the same source. The MISTRAS 2001 uses algorithms to determine the location of AE events from multiple hits. This process will be described in greater detail later.

The threshold for each AE channel was determined by placing the transducers on the member with the actuator hydraulics on but not applying load. While watching the hits being received, the threshold was lowered incrementally until a level where the hits being received was continuous. The threshold was then set a few dB above this value. Once the threshold was set correctly there were no hits received until loading commenced. The threshold for the laboratory testing was 40 dB.

For the acoustic emission system to successfully predict crack growth, two pieces of information are necessary, source location of the AE event, and state of stress in the cracked flange at the time of the AE event. As previously stated the state of stress for an AE event was determined by the use of the top flange strain gage data input into the AE monitor. Source location was determined by using two AE transducers located in a linear array and the AE software for the MISTRAS 2001. Before the software could be used for source location, the speed of the AE wave in steel needed to be determined. To accomplish this a series of lead breaks using 4H lead at predetermined locations between the two transducers was done. The location of the break referenced to both transducers and time difference of the stress wave passing each transducer as determined by the AE monitor was recorded. By using the following equation, the stress wave velocity was determined and used for source location;

$$V_s = \frac{L - 2X}{dt} \tag{3}$$

where L is the distance between the two AE transducers, X is the location of the lead break referenced to one transducer, and dt is the time difference between arrival of the stress wave at the two transducers. A linear regression of L-$2X$ vs. dt yielded the velocity of the stress wave, 132,000 in./sec with a correlation coefficient of $r^2 = 0.9963$. A graph showing the regression of L-$2x$ and dt is given in Fig. 3.6. The AE system used a different form of this same relation, where wave velocity, time difference, and distance between transducers were all known, to calculate the location of each AE event. This is the basis of AE source location.

When working with materials that have one dimension smaller than the others, reflections of stress waves will create what seem to be multiple AE events that actually all stem from one emission. Stress waves will travel in all directions, reflect off material surfaces, and reach the same transducer at different times. Therefore, not every pair of AE hits will be able to be used to determine the location of an AE event and more than one event location may be reported for a single acoustic emission.

Wave velocity was not the only system parameter that needed to be decided upon before AE monitoring could progress. Other guidelines for how the system interpreted the AE signals were gathered. Three of these values are known as system timing parameters and are tailored for specific materials and structures. The system timing parameters help the AE system to correctly identify the proper attributes of an AE hit and reset the system to be prepared for the next hit. A typical AE signal is shown with the different system timing parameters labeled in Fig. 3.7.

The Peak Definition Time (PDT) is the time allowed for the peak amplitude of the wave to occur after the wave initially crosses the system threshold. This system timing parameter allows the AE system to correctly establish the largest peak of an AE hit. This is important because smaller peaks might preclude the larger true peak of a waveform. If the correct peak is not established then proper time differences may not be acquired thus causing an incorrect location associated with an event. The MISTRAS 2001 manual suggested a value for PDT as the sensor spacing divided by the velocity of the fastest wave [3]. A value of 400 μs was selected and was within acceptable range for steel structures.

A second important system timing parameter is Hit Definition Time (HDT). The HDT is the time allowed for a hit's reflections to keep exciting the transducer and the transducer to ringdown. This time value ensures that a single hit is recorded as one hit only and is not

misinterpreted to be multiple hits. HDT must not be too long as this will not allow for high data throughput. The AE system hardware controlled the value used for the HDT, because the system requirements mandated that the HDT be at least twice as much as the value used for PDT. Therefore, in this case the HDT was selected to be 800 μs.

The final system timing parameter is the Hit Lockout Time (HLT). The HLT is a time that the system will wait after the HDT is over before it gets ready for the next hit to come. If this delay was not present, hit reflections after the true hit peak would be recorded as separate hits. For structures with low damping, this value may be quite high to discard hits that are reflecting off numerous surfaces. A reasonable value for this is the length of the structure divided by the stress wave velocity. Conservatively a value of 2000 μs was used. The accuracy of the system was checked by using lead breaks at specific locations and associating these with locations given by the AE monitor.

3.4 Acoustic Emission Monitoring Before Retrofit

Two transducers were placed equidistant from the fatigue crack on the top side of the bottom flange. The transducers were located on the top side of the bottom flange because in the field access to the side of the flange containing the crack (outer side of the top flange in the field) was not possible due to the presence of the bridge deck. Each transducer was placed 20 in. on either side of the center of the crack. A coordinate system was set up with 0 being at the crack location. All events that showed a location between -1 in. and 1 in. were events that met the location criteria for determining crack growth. A buffer of 1 in. on either side of the crack was chosen because the AE monitor can only locate sources within about 0.5 in. tolerance. Also the transducer location is not a point, as the active area of the transducer is approximately 0.5 in., therefore the range of -1 in. to 1 in either side was used as the crack location criteria. Another set of two transducers was placed in a linear array directly below the actuator and above the fatigue crack location on the web of the girder. This second linear array was used to determine if acoustic emissions were coming from the actuator-girder connection. Upon inspection of the AE data it was shown that the connection did not produce such events, therefore the linear array placed on the bottom flange was all that was necessary to observe crack growth events.

Acoustic emission tests were conducted throughout the crack growing portion of beam cycling, cycles 0 to 1,983,000. To be consistent with each other, AE was collected for 10 minute intervals during the 2 Hz cycling to encompass 1200 cycles. Events that occurred when the bottom flange was at a tensile stress within 75% of the maximum stress achieved, either loading or unloading, were considered crack propagation events. Events happening at stresses lower than 25% of the peak stress were discarded as crack rubbing. Figure 3.8 shows loading conditions that were considered for possible crack propagation. Both the location criteria and girder stress state criteria needed to be met for an event to be associated with crack growth.

Data for each test was stored on the hard drive of the personal computer that ran the AE software. AE data falls under two categories, time driven data and event driven data. Time driven data was that data that was sampled at certain instances in time, in this case every 0.05 sec. The only value obtained for time driven data was the strain of the top flange for a given time. Event driven data was recorded every time an AE event occurred and included not only the top flange strain but also the location of the AE event. These two types of data were put together to determine if the crack was propagating. A feature of the AE software is the ability to replay the data stored for a certain test and export it to a text file. These text files containing both the time driven and event driven data were downloaded into a commercially available spreadsheet program. A macro was written to sort event data by location and all events that had source locations within 1 in. of the crack were examined. Stress in the top flange was then examined for each event that passed the location criteria; those that occurred at high enough stress were counted as possible crack events. The number of events for the 1200 cycle test were then compared with other tests to create a plot that showed AE activity over various cycles of loading, this plot will be discussed later in the laboratory results, Section 4.1.

3.5 Strain Gage Setup Before Retrofit

In addition to AE monitoring the laboratory specimen was also instrumented with resistive type strain gages. The type of strain gages used were three-wire, Tokyo Sokki Kenkyujo type FLA-3-11-3LT gages with a gage factor of 2.13. Attachment of the strain gage included the following steps. The steel was first ground clean using a mini-grinder and conditioned using M-Prep conditioner and neutralizer. Cyanoacrylate strain gage adhesive was

used to adhere the strain gages to the steel. The gage lead wires were connected to an OPTIM signal conditioner and data acquisition system for collection of strain data. Actuator load and stroke values were also taken with strain readings. The data collection rate was 10 Hz for static tests where loading was a 0.08 Hz ramp function, and 100 Hz when loading was a cyclic 2 Hz sine wave.

Locations of the gages were limited to locations accessible on the field bridge girders. Because of the concrete deck present on the field girders, gages could not be located on the outer side of the cracked flange; gages were mounted on the inner side of the flanges. An illustration of gage layout before attachment of the retrofit can be seen in Fig. 3.9. One gage was placed in the cracked section at the bottom of the top flange. Two gages were located on the web of the cracked section, one 8.75 in. from the bottom of the member and another 19.25 in. from the bottom. All other gages were located at various positions on the top of the bottom flange; two gages located at the cracked section and another two gages placed 6 in. away from the cracked section.

3.6 Double Angle Retrofit Design

The design philosophy for the double angle retrofit was provided by Mn/DOT. The detail for the retrofit can be seen in Fig. 3.10. The concept behind the retrofit design was to transfer tensile stresses away from the damaged flange and into the double angles by means of a slip critical bolted connection. A bolted connection was desired because of the greater fatigue life that is achieved over welded connections, as welded connections were the primary cause of the existing fatigue problems. The laboratory retrofit was designed to have the area of the angle flanges develop their full yield strength providing a force capacity near that of the original rolled girder flange. Angle sizes were restricted to those that did not have legs projecting out past the original girder flange width. Two L6x4x5/8 Grade 50 angles were placed on either side of the web, centered on the cracked section. The strength provided by the angle flanges ($A_s f_y$)was 250 kips compared to 270 kips for the uncracked girder flange. A strong axis moment of inertia, I_{xx}, of 3251 in^4 was obtained for the combined angles and girder acting without a bottom flange, as shown in Fig. 3.11 b. Significantly increasing the moment of inertia over that of cracked flange

member, I_{xx}, of 1467 in^4 as shown in Fig. 3.11 c. The retrofitted section I_{xx} of 3251 in^4 is near that of the uncracked section moment of inertia I_{xx} of 3270 in^4, also shown in Fig. 3.11 a.

The number of bolts used to connect the retrofit was selected so that the angle legs, acting as the new flange, could develop their full yield strength. The connection was designed as a slip-critical connection so that slip would not occur until the angle flanges achieved yield. The resulting required bolt force was 250 kips. Using A325 7/8 in. bolts in double shear, 20.4 kips can be produced by each bolt, requiring 14 bolts on each side or 28 bolts for the entire connection. Bolts were spaced at 3 in., in two rows making the retrofit length 42 in.

The procedure for attaching the retrofit was as follows: One angle was drilled with all 28 holes. Angles were clamped back to back and two outer holes were drilled in the opposing angle to ensure proper alignment. An outer hole was then laid out on the beam web and drilled, the two angles were then attached by a single bolt. The other outer hole was then drilled through the web using the first angle as a template, again to ensure alignment, and a second bolt was installed and tightened. The angles, now snug against the web, were used as the template for the remaining 26 holes. The remaining bolts were put into place and tightened in order from the outside working in. All bolts were initially torqued to 150 lb.-ft., then to 300 lb.-ft., and finally to 448 lb.-ft., the required torque for this grade and size of bolt to achieve a slip critical connection.

3.7 Acoustic Emission Monitoring After Retrofit

It was thought that after the retrofit had been attached, the use of AE for monitoring crack growth would not be feasible because of the amount of AE that would be generated by rubbing of the bolted connection. This noise would make monitoring crack growth by means of the linear array impossible because most of the noise emissions would be coming from the same linear location as the crack and could not be distinguished from AE originating from the crack. Other means were necessary to find out if in fact the bolted connection was causing extraneous AE activity.

The first AE setup used was to establish the increase in AE after the retrofit had been attached. This setup was the same as the setup used for monitoring before the beam had been retrofitted, with the only change being the two transducers had to be placed 44 in. apart. This

additional distance was necessary because the angles were longer than the original transducer spacing, so the transducers were placed 1 in. past either side of the angle. This AE configuration can be seen in Fig. 3.12.

Two other AE setups were examined in an effort to show that noise was being generated by the bolted connection. A two-dimensional array, where both x and y coordinates were calculated for each AE event, was attempted with four transducers placed in a rectangular arrangement. This two dimensional array was simply the joining of two parallel linear arrays, one placed on either side of the beam web. Rectangular dimensions for this setup were 44 in. along the beam and 8 in. for the cross dimension. A graphical representation of the two dimensional array is shown in Fig. 3.13.

The final setup for AE monitoring after attachment was another set of two linear arrays as shown in Fig. 3.14. The first array was the original linear array placed on the top of the bottom flange of the beam with a spacing of 44 in. The second linear array had one transducer placed 3 in. below the top of the beam directly above the crack location. The second transducer was put on the bottom of the beam centered directly under the web and under the crack. It should be noted that the use of this setup in the field was not possible because of the concrete deck present on top of the cracked flange (where the AE transducer would need to be placed.

3.8 Strain Gage Setup After Retrofit

Strain gages were also placed on the retrofit to determine the stress distribution in the double angles. Four gages were placed on the angle webs, and another four were located on the angle flanges. Locations of the gages on the retrofit can be seen in Fig. 3.15. These gages were put on after installation of the retrofit for fear of damaging a gage in the drilling and tightening process.

A gage was placed on the angle web at the cracked section 2.5 in. above the angle bottom to see if stress was being transferred into the angle by the bolts. Gages were placed on the inside of the angle flanges 2 in. above the bottom of the girder, at the cracked section to determine how much stress was being carried by the flanges. One gage was placed on the outside of the angle flange 2 in above the bottom of the girder, at the crack section to see if stresses were being transferred out to the angle flange tip and to determine the amount of shear lag. Finally, gages

were placed on the angle flange 6 in. away from the cracked section to see how force was being picked up by the bolts along the length of the angle.

Testing was performed to find out if crack growth could be monitored by use of the MISTRAS 2001 and to see if the double angle retrofit would reduce bottom flange stresses. The next chapter presents the results of the testing and gives indications of AE monitoring and retrofit performance in the lab.

Chapter 4 - Laboratory Experiment Results

Five sets of results are presented in this section. The first are acoustic emission results of the beam before the retrofit was attached, later AE results from after the retrofit attachment are presented. Strain gage readings for both before and after retrofit attachment are given to make a determination of retrofit performance. In addition, a visual account of crack growth after the retrofit was attached is presented, again to determine how the retrofit performed.

4.1 AE Results Before Retrofit

Acoustic emission events were collected during cycling as described in Section 3.4. AE events that were considered as coming from crack propagation are shown plotted against the number of cycles from start of fatigue cycling in Fig. 4.1. Each data point represents the sum of events occurring during a 1200 cycle period. In theory, for crack propagation from a single mechanism the plot should start very small and grow exponentially as the crack gets larger over many loading cycles. However, the plot starts out at a relatively high number of events and then actually decreases before it starts to grow larger again. This can be explained by knowing that the detail used to grow the crack first had to crack through its own weld before a crack started in the flange of the girder. AE from the initial weld propagation can be seen increasing from cycles 600,000 to 650,000. Immediately after the weld cracked through the growth rate was reduced because now the crack had to start into the flange and this reduction in growth rate is shown as a reduction in AE from cycles 650,000 to 1,050,000. Once the crack started in the beam flange the growth rate increased dramatically, as indicated by the increase in AE activity. The number of events continued to increase as the crack continued to progress up toward the web and show through the top of the flange. This trend is a good indication of crack propagation and shows the applicability of AE monitoring for this purpose.

The results of tests after 1,750,000 cycles are misleading because the detail that was employed to initiate the crack was torched off at 1,773,000 cycles. The removal of the fins by use of an oxy-acetylene torch created stress concentrations on the underside of the flange, which initiated many AE events with the peak at 1,800,000 cycles. This test is not necessarily representative of crack growth because of the number of AE events not associated with the crack.

However, AE from the vicinity of the crack immediately decreased after these stress concentrations were relieved. The rate of events again rose prior to the installation of the double angle retrofit. Cycling would have continued further to extend this increasing trend however at this time the crack had progressed so that it was visible from the top of the bottom flange. Because the crack was progressing more rapidly, it was thought that the retrofit should be attached to determine if the retrofit could stop the progression of the fatigue crack.

4.2 Beam Stresses Before Retrofit Application

Static load tests to acquire the stress distribution at the midspan of the girder were performed immediately prior to attachment of the double angle retrofit. These stresses were the baseline that the performance of the retrofit was compared against. A graph depicting the stress in the beam at the cracked section can be seen as the solid line in Fig. 4.2. A 60 kip load induced these stresses producing a positive moment of 198 kip-ft. An uncracked W27x94 steel girder would develop 9.8 ksi in both the top and bottom fibers of the section for this imposed moment as calculated by Euler beam theory. This theoretical uncracked girder stress distribution is shown as the dashed line in Fig. 4.2. As can be seen in Fig. 4.2 the cracked section stress in the bottom fiber reached 9.8 ksi in tension while the top fiber stress only reached 7.6 ksi in compression. Although the bottom flange is close to the uncracked predicted stress of 9.8 ksi, there is an obvious shift in neutral axis upward from the uncracked girder neutral axis indicating partial loss of section of the bottom flange. The neutral axis for an uncracked section is approximately 13.5 in. from the bottom fiber, but in the cracked girder, the neutral axis was 15.2 in. above the bottom fiber. This shift of 1.7 in. up clearly shows the loss of section in the bottom flange. Had the entire flange been severed the neutral axis would have risen to 17.6 in. above the bottom fiber as seen in Fig. 3.11 c. The position of the neutral axis will be of importance when determining how the retrofit performed.

4.3 Fatigue Crack Growth After Retrofit Application

Beam cycling continued immediately after the retrofit had been installed. Again the cyclic load imposed on the beam was a sinusoidal wave ranging from 2 kips to 60 kips downward at a rate of 2 Hz. The crack length could not be measured on the top of the flange

because of the proximity of the angles to the top of the bottom flange. There was only a ¾ in. gap between the two surfaces so the crack progression could only be witnessed from the bottom of the flange.

No crack growth was noticed on the bottom of the bottom flange for the first 425,000 cycles after installation of the retrofit. Crack length on the bottom of the bottom flange was 3.6 in. at this point, the same as before the retrofit had been installed. At 525,000 cycles after the installation of the retrofit, this length had grown to 4.3 in. By 870,000 cycles after the installation of the retrofit the length was only 4.7 in. and did not reach 5 in. until 986,000 cycles. The crack reached the 6 in. mark at 1,270,000 cycles and continued at a high rate of growth until the entire flange had been severed at cycle 1,730,000.

At this point, the retrofit was taking all tensile force that previously was present in the bottom flange. Loading continued after this point to see whether the retrofit would fail soon after complete flange section loss. Loading stopped after 3,750,000 cycles after retrofit installation (2,020,000 cycles after the flange had been completely severed). It was felt that further loading was unnecessary, as the system showed no signs of distress or failure.

4.4 AE Results After Retrofit Application

AE monitoring continued after the retrofit had been installed on the beam. Although there was no appreciable crack growth immediately after the installation of the retrofit, AE events continued at a high rate. Figure 4.3 shows the AE events vs. the number of cycles, after the addition of the retrofit. As can be seen the number of events is much higher than before the retrofit was applied as shown in Fig. 4.1. In an effort to find out where these events were coming from, two alternate setups were studied to pinpoint the location.

One setup was the two-dimensional array configuration shown in Fig. 3.13 and described in Section 3.7 Results for this setup were very poor at determining source location. The number of events located for a ten minute AE test were less than 10 in all testing attempts compared to one to two thousand events per test for the previous linear array used. Numerous attempts were made to get this setup to work but it was felt that the proximity of the transducers to the edges of the flange created too many wave reflections and thus the poor performance of the setup for

locating emissions. Another setup needed to be found to determine the cause of the increase in AE activity following the retrofit installation.

An alternate setup shown in Fig. 3.14 and discussed in Section 3.7 had better success than the two-dimensional array, for source location. The linear array that was positioned above and below the crack on the web was utilized for this purpose. Tests were immediately taken after installing the retrofit to see where the AE was emanating from through the cross section. These tests were conducted long before the crack was present in the web. It was shown that 70% of the AE events were coming from the area of the web where the retrofit was attached. Less than 3% of the AE events came from the bottom flange (the crack). Because of this large number of events emanating from the retrofit, acoustic emission monitoring can not be used to determine crack propagation when such a retrofit is used to correct the problem. Surface rubbing and bolt to steel contact produced too much excess noise in the region where fatigue crack emissions also emanate from. There is no way to decipher between the two emissions in the field because it would be impossible to attach the second linear array that was used to determine the location of events through the section due to presence of the concrete deck above the crack.

4.5 Beam Stresses After Retrofit Application

Static load tests, consisting of a ramp loading at 10 kips/sec., were performed to evaluate how the addition of the retrofit affected the stiffness and neutral axis of the system. Shown in Fig. 4.2 is the state of stress through the section at 60 kips, just before the retrofit was attached (after cycle 1,983,180). The stress at the bottom flange (0.0 in.) was 9.8 ksi for the cracked section with no retrofit. After the retrofit had been applied, another static load test was performed. The stress distribution from this test is shown in Fig. 4.4. Stresses measured on the girder are denoted by diamonds, stresses measured on the retrofit angle web and outside flange are shown by circles and a box respectively. For the same 60 kip load, the stress as measured by the gage on the top of the bottom flange was only 5.7 ksi. Hence, the retrofit reduced the bottom flange stress by 42%. The neutral axis also shifted down from 15.2 in. for the cracked section to 12.1 in. for the retrofitted section. Stress at the inside of the retrofit angle flange near the web was 4.6 ksi and the stress on the outside edge of the retrofit angle flange was 4.2 ksi. Stress values 6 in away from the cracked section on the angle flange were 4.3 ksi. This was smaller

due to the smaller moment at the 6 in. offset section. Because these stress values are relatively close, very little shear lag was occurring through the cross section of the retrofit at the crack location.

The stress reduction achieved by the retrofit was compared to the theoretical reduction. Details of this calculation are provided in Appendix A. To determine the predicted stress reduction, the equation for flexural stress was used:

$$\sigma_b = \frac{M}{S_b}, \tag{4}$$

where σ_b is the stress in the bottom fiber of the section for an imposed moment M and S_b is the section modulus to the bottom of the beam. Because the bending moment was the same for tests before and after application of the retrofit, the reduction of bottom fiber stresses from before the retrofit application to after it are given by:

$$1 - \frac{\sigma_{after}}{\sigma_{before}} = 1 - \frac{S_{b_{before}}}{S_{b_{after}}}, \tag{5}$$

where the subscript *before* denotes the uncracked section properties (Fig. 3.11a) and the subscript *after* denotes the retrofitted cracked section properties (Fig. 3.11b).

The reduction of bottom fiber stresses was determined from the measured stresses to be 42%. The calculated bottom fiber section modulus increase was 38% (Appendix A). The S_b prior to the retrofit application was assumed to be 243 in^3 (refer to the LRFD) and the post retrofit S_b was calculated as 390 in^3. The achieved reduction was greater than that expected by beam theory. However, the calculation for the girder prior to retrofit was based on an uncracked flange when in actuality, the girder flange was partially cracked but the flange was still taking a substantial amount of load. The uncracked properties were chosen instead of cracked section properties for ease of calculation when determining retrofitted properties. Had the lower S_b for the cracked section been used for the before retrofit condition the section modulus increase would have been higher than 38%. Thus, the stress reductions witnessed by the retrofit application were near what was expected.

The retrofit also caused the crack growth rate to slow considerably. As stated previously, prior to the attachment of the retrofit, the crack had gone from 10% depth and 2.5 in. in length at cycle 1,773,000, to 100% flange depth and 3.2 in. in length at cycle 1,983,000. In a span of

210,000 cycles the crack had grown more than in the previous 1,773,000 cycles it had gone through. After the retrofit was applied and cycling continued, the crack did not grow appreciably until an additional 425,000 cycles had been applied. Full flange cracking did not occur until 1,730,000 cycles after retrofit application.

Shown in Fig. 4.5 are stresses at the cracked section once the flange was completely cracked through (cycle 1,730,000). The measured stresses on the girder are denoted by diamonds, stresses measured on the retrofit angle web and outside flange are shown by circles and a box respectively. Stress in the retrofit increased due to the continued cycling, as the angle picked up the tensile force that was previously taken by the girder flange alone. The strain gage on the bottom flange of the girder indicated a stress of 0 ksi, as expected the girder flange at the crack was no longer taking any tensile force. The stress in the angle flange varied from 8.2 ksi near the angle web to 7.2 ksi at the angle flange tip shown by the diamond and box at 2 in. above the bottom of the section. Some shear lag can be seen through the angle flange for this case. The stress value 6 in. offset from the cracked section on the angle flange was 6.2 ksi, this is much smaller than the stress at the cracked section. This could be due to less moment at the section and more moment being taken by the girder flange at the 6 in. offset section than the girder flange takes at the cracked section. The stress in the top flange increased after the bottom flange cracked through as well. This was expected as the strong axis moment of inertia, I, of the section decreased when the flange was severed. The use of the double angle retrofit considerably decreased the rate at which crack growth was occurring in the laboratory specimen.

Loading continued after the bottom flange had completely cracked through for an additional 2,020,000 cycles, in an attempt to get the girder to fail by fatigue. The cracked girder and retrofit combination continued to perform well and additional cycling was thought to not be necessary at this point. The total number of cycles that the girder with the retrofit sustained was 3,750,000 with the amount needed to fail it in fatigue being unknown. The angles were removed after 3,750,000 cycles in order to visually inspect the girder. The crack had gone into the web and arrested itself in one of the lower bolt holes. A photo of the final crack can be seen in Fig. 4.6. The crack had propagated straight up until it reached the centerline of the first row of bolt holes and then turned 90° and arrested itself in the first bolt hole.

Stress levels used in the laboratory experiment were significantly higher than stress levels typically observed in the field study. The possibility exists that the retrofit used in the field may stop crack growth by lowering the stresses to levels that do not cause fatigue propagation.

Chapter 5 - Test Bridges Setup

In this chapter background information on all three bridges is given as well as testing dates for both the pre and post retrofit test periods. The first round of testing was performed on all three bridges and included both AE monitoring and strain measurements before retrofit attachment. The second round of testing was performed only on the West 7th Street Bridge and I-94 Bridge and included only strain measurements after the retrofit had been attached. The AE transducer locations and AE testing procedures on the bridges are discussed. Strain gage layout and the field data acquisition equipment is presented. Finally, theory behind the retrofit used by Mn/DOT to repair the fatigue cracks is reviewed and the procedure that Mn/DOT used to attach the retrofit is given.

5.1 Test Bridges

Three bridges in the Twin Cities metropolitan area were tested with acoustic emission equipment and strain gages: BR 62066, West 7th Street over railroad tracks, BR 27855, I-94 over TH-55, and BR 9276, TH-36 over Cleveland Ave. The bridges all had rolled steel girders with welded cover plates on both the top and bottom flanges extending out over the piers about 10 ft. Each had a fatigue crack or other defect in the top flange near the end of the cover plate that was discovered by periodic ultrasonic testing. The cover plate detail is shown in Fig. 5.1. Two of the bridges were chosen because the existing cracks located by ultrasonic tests were thought to be active, the West 7th Street Bridge and TH-36 Bridge. The I-94 Bridge defect was thought to have extinguished itself do to a widening of the bridge in 1992.

A two day testing period was used for each bridge with instrumentation and system checkout taking place on the first day and data acquisition and load testing on the following day. A lift truck supplied by Mn/DOT was used to perform instrumentation of the girders.

The West 7th Street bridge is a four span structure located south of downtown St. Paul and has a heavy commercial volume of 670 trucks daily. Mn/DOT performed the traffic count for this bridge in 1996. Heavy commercial vehicles are designated as those vehicles with more than two axles. This bridge was designed in 1970. The member tested was the center girder of a seven girder structure. This member at the crack location was a W36x160 with a 10.5 in. wide

and 1.375 in. thick cover plate tapered down to 3 in. wide at the end. The girder and cover plate detail for this bridge can be seen in Appendix B. The crack was in the third of four spans from the south and was located 10 ft. south of Pier No. 3; the entire span length was 83 ft. The entire pier layout for the West 7th Street Bridge can be seen in Fig. 5.2. The crack surface was ultrasonically measured to be approximately 0.1875 in. from the top of the flange. Ultrasonic test reports are in Appendix C. The original testing of this bridge took place on June 8, 9, and 10 of 1998. Secondary testing, after the retrofit had been installed, was performed on October 15 and 16 of 1998.

Bridge 27855, I-94 over TH-55, is a seven span structure located southeast of downtown Minneapolis; it carries 7,840 heavy commercial trucks per day. This traffic information was also obtained by Mn/DOT in 1996. The bridge was designed and built in 1966. The cracked girder that was tested was a fascia girder of the bridge as originally constructed. Two girders were added outside the tested girder later when the bridge was widened to add another lane in 1992. The girder tested was a W36x135 and the span length was 69.65 ft. A detail of the girder and cover plate can be seen in Appendix B. The crack location was approximately 10 ft. west of Pier 2. The crack depth was not listed on the ultrasonic report given. The ultrasonic report can be found in Appendix C. The entire pier layout for the I-94 Bridge can be seen in Fig. 5.3. Original testing of the I-94 Bridge took place on June 22 and 23, 1998 with secondary testing occurring on October 22 and 23, 1998.

The final bridge investigated was TH-36 over Cleveland Ave. located northeast of downtown Minneapolis. It is a two span structure that carries 1480 heavy commercial trucks per day and was designed in 1962. Again, the commercial traffic information was obtained by Mn/DOT in 1996. The girder investigated was a W36x150 and was the south fascia girder with a span length of 80 ft. 10 in. The crack location was 10 ft. east of the center pier at the 2 in. tapered end of the 10 in. wide and 1 in. thick cover plate. The details for both the girder and cover plate are given in Appendix B. A figure showing the pier layout is shown in Fig. 5.4. The crack surface was shown by ultrasonic testing to extend downward 0.1875 in. from the top of the flange. The ultrasonic report is found in Appendix C. Testing on the TH-36 bridge took place on June 24 and 25, 1998.

5.2 Acoustic Emission Setup

The AE monitoring equipment was implemented on the field bridges in the same fashion as it was in the laboratory study prior to the addition of the retrofit. The only difference between the two setups was the placement of the transducers on the top flange in the field, as opposed to the bottom flange in the lab. The field setup for AE can be seen in Fig. 5.5. The linear array on the flange was used to locate events emanating from the fatigue crack. The secondary web array was used as a precaution to isolate emissions that might have come from the lower flange cover plate welds, similar to isolating actuator noise in the laboratory. The state of stress input to the AE monitor used in the field was the conditioned output from the strain gage located on the bottom flange in the same section as the crack. Sample rate for the bottom flange strain gage was 20 Hz, the same rate used in the laboratory.

The transducers were connected exactly as they were in the lab by using petroleum jelly as the couplant and magnetic holdowns to attach to the steel. Preamps were set to 40 dB gain and were housed in a waterproof box that was clamped to the lower flange about 4 ft. from the transducers. The AE channel thresholds for each bridge were determined by decreasing the threshold level incrementally while watching the number of hits the MISTRAS unit received. The threshold was then set a few dB above that level where continuous hits were received. When the threshold levels were properly set, no hits were seen when the structure was not loaded. The threshold level for all the bridges was 35 dB.

Between 50 and 250 ft. of BNC cable was used to connect the preamps to the MISTRAS 2001. The West 7th and I-94 bridges had shorter runs of cable whereas the TH-36 bridge had 250 ft. of BNC cable. The MISTRAS 2001 and the PC that runs the AE software were housed in a minivan as close to the crack location as possible. The power supply for the AE equipment was a small 30 amp gasoline generator that was connected to a surge protector. The surge protector offered little help in providing a clean power signal to the equipment as will be seen when discussing bridge results. The power to the West 7th Bridge was conditioned with an uninterruptible power supply (UPS). The UPS was not available on the other bridges.

AE testing in the field was unlike laboratory testing because the field loading was performed by Mn/DOT supplied sand trucks rather than an actuator. These sand trucks were tandem axle dump trucks loaded with sand so the total weight of the vehicle was approximately

50,000 lbs. Exact truck weights for each bridge are given in Table 5.1. AE monitoring was performed as the sand trucks made passes in the lane closest to the girder being monitored. The equipment was paused in between sand truck passes so the data files that were created were not too large. Exact times that trucks passed over the bridge were also recorded to correlate with AE data.

For the first round of testing a total of 49 sand truck passes were made on the West 7th Street Bridge. The speed limit for that location is 45 MPH. For the I-94 bridge 38 sand truck passes were made. The speed limit on the I-94 Bridge was 55 MPH. Finally, on the TH-36 Bridge, 42 sand truck passes were performed. The speed limit for TH-36 at this crossing is 55 MPH. At all the locations, only dynamic load testing was performed. No static loads were recorded because of the difficulty in stopping traffic at these locations.

The AE data was converted to text files that could be imported and examined using a spreadsheet program. Two sets of data were created for each AE file. One set consisted of the bottom flange strain gage readings sampled at 0.05 seconds. The second set of data consisted of event location, bottom flange strain gage reading, and time for each AE event. The two portions of data were combined into the same spreadsheet file, with time and bottom flange strain reading being the two parameters shared by both sets of data. Data was sorted by event location and events emanating from within 1 in. of either side of the crack location were marked to set them apart from other events. The data was then sorted by time and those events that were caused by sand truck passes were marked. From this data, any event that was marked as emanating from the correct location and being truck induced were considered as possible fatigue crack events. The final check was to look at changes in the bottom flange strain both before and after a marked event to see if the stresses were such that might cause crack propagation or those that would be crack rubbing. The field state of stress criteria was that the top flange must be in tension. Those events that passed all three criteria, event location, truck pass induced, and high tensile stress state, were counted. The number of events occurring was compared to the number of sand trucks that made passes to get a ratio that could be used to compare AE activity among the bridges.

5.3 Strain Gage Setup Before Retrofit

Strain gages were also employed in the field in the same manner that they were in the laboratory. Gages used were Tokyo Sokki Kenkyujo three-wire resistance gages type WFLA-3-11-3LT with a gage factor of 2.11. The gage resistance for these gages was 120 Ω. The only difference between the gages used in the field and the laboratory gages was that field gages had a plastic protective backing on the gage whereas those in the lab did not. This backing protected the gage from the elements. Locations of the gages were the same as in the laboratory with reference to the crack. One gage was placed on the lower flange of the member directly under the crack, two were located in the cracked section on the web and four on the top flange. Two gages were placed on either side of the web at the cracked section and two more gages were placed 6 in. away on either side of the web. A schematic of gage location and a table showing dimensions to the gages for each bridge can be seen in Fig. 5.6.

The procedure for attaching the gages to the steel was the same as that used in the laboratory. Paint was removed by a mini-grinder and the steel was conditioned with M-Prep gage conditioner and neutralizer. Cyanoacrylate strain gage adhesive was used to adhere the strain gages to the girders. Gage wires were connected to the Measurements Group model 2100 quarter bridge strain gage conditioner and amplifier using 22 gage copper instrumentation wire. The conditioner-amplifier system was powered by the gasoline powered generator. Output voltages from the conditioner were read by a National Instruments DAQCard-AI-16E-4 PCMCIA analog to digital card plugged into a laptop computer using a sampling rate of 50 Hz. The software for data acquisition, converting, and filtering, was written using National Instruments Lab Windows CVI, which is a C based programming environment with special subroutines written specifically for data acquisition and reduction. The data acquisition program read the voltages for all strain gage channels and wrote the data to a binary file. The converting program read the binary file created by the data acquisition program and wrote it to a text file. A copy of the program for both data acquisition and data conversion can be found in Appendix D. Strain gage tests were taken in 15 minute increments for ease of use in the spreadsheet program that helped to graph and reduce strain data.

Random traffic strain data was collected continuously for approximately 3.5 hours at each bridge location (in 15 minute long files). Along with random data, strains of the girder

under sand truck loading were also recorded to provide a view of the stress state in the member for a known load that could be reproduced after the retrofit had been applied. These truck records were subsequently removed from the random data when histograms of the stresses for each bridge were compiled so they would not affect what should have been random traffic. The histogram was computed for each data file in Microsoft Excel using a Visual Basic program. A copy of the stress counting program is found in Appendix D.

5.4 Strain Data Filtering

Much of the strain data collected by use of the laptop computer and DAQ card was noisy. A high frequency noise with an amplitude of approximately 10 $\mu\varepsilon$ (0.05 volts) was present in all files. Spikes in the data as high as 60 $\mu\varepsilon$ (0.3 volts) were also seen regularly in both the I-94 Bridge data as well as that data taken on TH-36. No spikes were present in the West 7th Street Bridge data, possibly because a UPS was used to condition the power. This noise posed two major problems; the actual stress ranges were affected because the noise would alter the stress peaks. Secondly, the large voltage spikes would be interpreted as large stress ranges by the program written to find stress ranges.

The noise was thought to stem from not having a good ground for the system or from unclean power supplied by the gasoline generator. It should also be of note that the noise was much worse when the MISTRAS and strain equipment were both turned on. Having the MISTRAS on made noise in the strain signal about 20 $\mu\varepsilon$ (0.1 volts), or about the same strain caused by a sand truck. This data was useless because the strain difference caused by traffic could not be differentiated from all the noise. For this reason random strain data had to be taken after all AE testing was complete as not to interfere with the data being collected.

Digital filtering had to be performed on the strain data so that it could be used to determine stress ranges caused by random traffic. Fig. 5.7 shows a typical unfiltered stress history for a sand truck pass. Because the noise in the system was at a high frequency, a simple low pass filter was employed. Put simply, a low pass filter allows low frequency signals through with little amplitude change but high frequency signals are attenuated, or have a large amplitude decrease. The specific type of filter used was a low pass Butterworth, which is given by the equation:

$$\frac{V_{OUT}}{V_{IN}} = \frac{1}{[1+(f/f_c)^{2n}]^{1/2}} \tag{6}$$

where f is the frequency of the signal, f_c is the cutoff frequency, n is the filter order, V_{out} is the output voltage, and V_{in} is the input voltage [14]. The coding for the filter itself was performed in the same programming environment used for data acquisition and conversion, National Instruments, Lab Windows/CVI. A copy of the program can be found in Appendix D. The Lab Windows environment had many built in filters that could be used for this purpose. The filtering was performed in the same program that converts the binary data to an ASCII file. The low pass Butterworth filter was chosen because of its ease of use and effectiveness for the characteristics associated with this noise, namely high frequency signals.

Before the filter could be used, two parameters had to be chosen, cutoff frequency and filter order. Cutoff frequency is that value at which signals with a lower frequency are allowed to pass through while higher frequency signals are attenuated. No digital filter is perfectly binary, there is no absolute passing of lower frequency signals or complete stopping of higher frequency signals. There is an area near the cutoff frequency that all amplitudes are changed, amplitudes of signals with frequencies just lower than the cutoff frequency are affected little. Signals that have a frequency just higher than the cutoff have their amplitude affected much more. Filters with a low order have a large range of affected frequencies, while those with high order tend to be more precise in how they pass or stop. The simple diagram of Fig. 5.8 shows how changes in filter order can affect the way in which frequencies near the cutoff frequency are either passed or stopped. Filters with orders that are set too high are sometimes unstable so care must be given to the choice of filter order as well as cutoff frequency.

A Fast Fourier Transform was performed on the unfiltered strain data. The results of this transform can be seen in Fig. 5.9. The stresses in the bridge caused by truck traffic tended to have a frequency below 1.5 Hz, depending on the truck speed. There were three main frequencies associated with the noise, one was near 3.6 Hz, another between 18 and 20 Hz and yet another near 23.2 Hz. A cutoff frequency had to be chosen high enough so as not to affect the stress peaks caused by this traffic, but also low enough that unwanted noise was filtered out. A series of cutoff frequencies were examined to see how low the cutoff frequency could be set without adversely affecting the signal amplitude. A high filter order was used so the filter would operate as close to the cutoff frequency as possible. For this study, a cutoff frequency of 3.5 Hz

and a filter order of 8 was used. Shown in Fig. 5.7 is a typical truck history without filtering and subsequently in Fig. 5.10 is the same truck history with digital filtering. This filtered data was then used to properly determine stress ranges in bridges for random traffic.

5.5 Mn/DOT Retrofit Design

The design philosophy used to design the laboratory retrofit was the same as that used by Mn/DOT to design the bridge retrofit for repairing fatigue cracks initiated at the ends of cover plates. The two retrofit schemes look very similar with the exception of bolt patterns, type of angles used, and retrofit length. The detail of the Mn/DOT retrofit for the West 7th Street Bridge and the TH-36 bridge can be seen in Fig. 5.11. The retrofit detail used on the I-94 Bridge can be seen in Fig. 5.12, notice the center of the retrofit was not placed at the crack location. This was due to a splice plate in the girder located 2 ft. from the crack location, therefore the retrofit location had to be shifted. The angle size used at all three bridge locations was a L8x6x1, with 7/8 in. bolts. The laboratory retrofit used L6x4x5/8 angles (the detail for the laboratory retrofit can be seen in Fig. 3.10).

The field attachment procedure was similar to that used in the laboratory. Mn/DOT predrilled all holes on both angles before installing. In the laboratory only one angle had all holes predrilled, this ensured a proper fit but also took longer to attach because of the longer drilling time to go through both the web and second angle. Field holes were 15/16 in., the standard hole size for a 7/8 in. bolt. A template of the two outer holes was manufactured out of plywood so that the first two holes could be drilled in the web without lifting the angle up to the top flange. In the lab, the angle could rest on blocks in the correct position, whereas in the field, because the angle was placed on the top flange, it had to be held in place by hand. Once the two outer holes were drilled the first angle was lifted and held in place by two bolts. Drilling continued through the web using the first angle for the template. Once all holes were drilled, the second angle was lifted and attached. All bolts were then tightened by hand. The entire process out in the field to attach one retrofit took about one day.

Because of the length of the retrofit angles, their weights were about 265 lbs. each. Manual lifting of the angles into place was quite difficult. For this reason if the retrofit is to be adopted into regular use to repair fatigue cracks in girders, a lifting stand should be manufactured

to allow easier placement of the angles. This may also reduce the time it would take to put the retrofit in place, thus cutting down on the length of time traffic control is needed. This recommendation will not only save Mn/DOT money by cutting down on time of installation but it will also ensure a proper attachment which will result in better retrofit performance.

5.6 Strain Gage Setup After Retrofit

Once the retrofit had been placed on the bridge girder, sand trucks were again used to dynamically load the bridge. The trucks used were approximately 50,000 lbs. and the strain data collected was used to re-evaluate the stress ranges due to a known load for comparison to the stress ranges prior to the retrofit. Locations of strain gages on the retrofit were the same as those used to test the laboratory retrofit, as shown in Fig. 5.13. The procedure used to attach the strain gages on and record their data was exactly that used before the retrofit had been attached; the only difference being no AE data was taken at this time. For logistical and safety reasons only the West 7th Street and I-94 bridges were tested after the retrofit application.

During the second set of tests, a total of 46 sand truck passes were made over the West 7th Street Bridge. The posted speed limit for West 7th at the bridge location is 45 MPH. At the I-94 Bridge, 14 sand truck passes were made. There were many less passes made at the I-94 location because it was much more difficult for the trucks to turn around. In addition, stress histories were similar for each truck pass so it was deemed that 14 passes were sufficient. The speed limit at the I-94 Bridge is 55 MPH. Again, no static loading was done because of the difficulty in stopping traffic in these locations, only dynamic data was recorded.

Chapter 6 - Bridge Experiment Results

This chapter presents the results from the testing of the bridges including: acoustic emission results, girder stresses before retrofit attachment, and girder stresses after retrofit attachment. Fatigue crack propagation is investigated by comparing rates of AE from the 3 bridges. Information on stresses before the retrofit will serve two purposes. The effectiveness of the retrofit is assessed by determining the reduction in stress range from a known loading due to the application of the retrofit. In order to determine remaining fatigue life, stress ranges due to random traffic were measured.

6.1 Stresses Produced by Sand Trucks Before Retrofit

The West 7th Street bridge had two different stress history shapes for sand trucks, depending on the direction the truck was traveling. West 7th was the only bridge to have two way traffic affecting the cracked girder because the other two bridges were one way structures. Because the tested girder was in the center of the bridge, trucks traveling in both north and south directions had to be investigated. Shown in Fig. 6.1 is a typical stress history caused by a sand truck traveling northbound. Gages shown, all on the same side of the beam, include: a bottom flange gage, both top and bottom web gages, and one top flange gage. The average stress range attained at the top flange gage due to sand truck loading was 0.76 ksi with a standard deviation of 0.066 ksi. The average stress range for the bottom flange gage due to sand truck loading was 1.60 ksi with a standard deviation of 0.107 ksi. Gages that were offset 6 in. to the south, away from the cover plate on the top flange, showed little difference in stress than those directly at the cracked section, as shown in Fig. 6.2. The gage offset 6 in. has a stress range of about 0.79 ksi for this truck pass, almost exactly that of the 0.8 ksi seen at the cracked section top flange gage. Gages located 6 in. to the south also precede the stresses in time by less than 0.1 sec., this is about the time it takes for a truck traveling 40 MPH to travel 6 in.

A cross-sectional stress distribution for the peaks of the northbound stress history of Fig. 6.1 is shown in Fig. 6.3. The figure displays the stress distribution for three distinct times, corresponding to the three peaks in the bottom fiber stress, denoted by 1, 2, and 3 in Fig. 6.1. Stress distributions were calculated by taking values of each gage at the same time when the

bottom gage was at a peak value. The actual gage values are shown by either a block or triangle. A linear interpolation of the strains through the cross section is also displayed. The first peak is obtained when the sand truck is near the middle of the span containing the crack. The second peak is obtained when the truck is over the cracked section. The final peak occurs when the truck passes over the pier and again creates negative moment similar to first peak.

The neutral axis stayed the same for the last two cases approximately 31.6 in. above the bottom of the member. The section acted slightly different for the first peak when the truck was farther away from the crack location, the neutral axis shifted down 2 in. to 29.6 in. A possible reason why this section behaved in this way was due to changes in composite action. The more the concrete deck acted composite with the section, the higher the neutral axis was. There were no shear studs placed in the area near the cover plate for this bridge as can be seen on the girder detail in Appendix B, thus any composite action came from friction between the concrete and the steel. This composite action was greatest when the truck was closest to the crack, which was true for the second case where the truck was directly over the crack. For the first case, the truck was in the center of the span, approximately 40 ft. away, not creating as much normal force to induce friction and creating less composite action. When the truck reached the crack, its weight helped create more composite action than the first peak and it stayed more composite as the truck progressed over the pier during the third peak.

When the sand truck traveled southbound on West 7th Street a slightly different stress history was achieved. The southbound stress history is shown in Fig. 6.4, with stresses depicted from the bottom flange gage, both web gages and the top flange gage. For the southbound direction the average stress range produced in the top flange due to sand truck loading was 0.63 ksi with a standard deviation of 0.031 ksi. The bottom flange average stress range was 1.42 ksi and the standard deviation was 0.067 ksi. These values are less than those achieved in the northbound direction. The strain measured by the 6 in. offset top flange gage differed considerably from the top flange gage at the cracked section. Shown in Fig. 6.5 are these two gages; the 6 in. offset gage only had a stress range of 0.46 ksi for this sand truck compared to the 0.69 ksi achieved at the cracked section. The time the signal from the gage at the cracked section now precedes the signal from the gage offset by 6 in. because the truck traveled over the cracked section first.

The cross-sectional stress distribution for the peaks of the southbound stress history of Fig. 6.4 is shown in Fig. 6.6. Again three time instances are depicted; the first of these was when the truck was approaching the pier on the opposite span, north of the crack denoted by a 1 in Fig. 6.4. The second instance was when the truck had just passed over the pier and was over the cracked section creating positive moment in the section, denoted by a 2 in Fig. 6.4. The third case was when the truck was on the same span as the crack traveling away from it with negative moment being produced, denoted by a 3 in Fig. 6.4.

The neutral axis shifted more for these three cases than it did for the stresses caused by a northbound traveling truck. For the southbound direction the neutral axis rose considerably for the second case where the deck appeared to have taken all compressive stresses, the neutral axis was very close to the interface between the deck and girder. This was expected because the greatest composite action should have occurred when the truck was closest to the cracked section. In both negative moment cases the neutral axes changed very little for the stresses caused by a southbound truck from the stresses caused by a northbound traveling truck. Both neutral axes moved up 0.6 in., this was understandable because there was greater composite action in the section when a truck was traveling southbound, as was just shown for the second peak case. Again, the peak that occurred when the truck was on the north side of the pier from the crack had a higher neutral axis because the truck was closer to the crack than for the third peak.

A typical stress history for a sand truck pass over the I-94 bridge is shown in Fig. 6.7. Gage stresses shown are for the bottom flange gage, both top and bottom web gages and top flange gage. Member stress behavior was similar to that of the northbound West 7th Street Bridge stress history; this is understandable because the layout of the bridges was similar and the truck passes proceeded as they did in the northbound direction on the West 7th Street Bridge. The average stress range for the top flange due to sand truck loading was 0.59 ksi with a standard deviation of 0.014 ksi. The bottom flange average stress range was 1.49 ksi and the standard deviation was 0.058 ksi. The stresses from the 6 in. offset gage on the top flange can be seen plotted with the stresses from the top flange gage located at the cracked section in Fig. 6.8. Just as for the West 7th Street location, the 6 in. offset gage stresses preceded the stresses present at the cracked section by about 0.1 sec, again attributed to the travel time of the sand truck. The

stress range is not as large at the offset gage, 0.4 ksi for the sand truck depicted. This could be due to a reduced moment at this section. This was similar to the difference seen on the West 7th Bridge for the northbound truck.

Cross-sectional stress distribution for the I-94 Bridge for the stress history depicted in Fig. 6.7, is presented in Fig. 6.9. Three instances are plotted; these coincide with the minimum and maximum stresses achieved at the bottom flange gage for the stress history shown in Fig. 6.7 and are denoted by a 1, 2, and 3. The first minimum was produced when the sand truck was traveling near the center of the span where the fatigue crack is located, denoted by a 1 in Fig. 6.7. The maximum stress was produced when the truck was over the cracked section producing positive moment, denoted by a 2 in Fig. 6.7. The final minimum was achieved as the truck passed over the pier and was on the third span of the bridge, denoted by a 3 in Fig. 6.7.

The location of the neutral axis stayed very consistent for all three cases; located approximately 29.5 in. above the bottom of the member. About the same amount of composite action was present in the I-94 Bridge as was in the West 7th Bridge for a northbound traveling truck. For the I-94 Bridge the neutral axis was not affected by truck position on the span, which would conclude that the composite action was constant for the bridge, independent of truck placement. This makes sense because there were channels located along the entire girder length, and especially at the crack location to create composite action. The channel designation was C4x7.25 and 8 in. long. These channels can be seen on the beam detail in Appendix B.

TH-36 was also a bridge that allowed traffic to move in one direction, in this case, from east to west across its spans. The stress history for two sand trucks on the TH-36 Bridge is shown in Fig. 6.10. The sand trucks were traveling so close together that the stress histories overlapped. Stresses depicted come from the top flange gage, both web gages and the bottom flange gage. Stress ranges achieved by the flanges are quite different from those of the previous two bridges. Because of the proximity of the sand trucks to each other, both trucks affected the cracked section stresses and it must be of note where both trucks were at each time instance. The bridge is a two span structure and the trucks are on the span that does not include the fatigue crack first producing negative moment, this time is denoted by a 1 in Fig. 6.10. When one truck passes over the pier to create positive moment at the cracked section, the other truck was still on the first span producing a negative moment that counteracted the effect of the first truck, this is

denoted by a 2 in Fig. 6.10. The two produce negative moment once the first truck moves toward the center of the span containing the crack and this was seen as the bottom flange reaches another minimum, this occurs at point 3 in Fig. 6.10. The second truck passed over the crack location and again produced a small positive moment, denoted by a 4, that was visible before the section again moves into negative moment, denoted by a 5. The last negative moment produced was about half that of the previous two valleys shown, only one truck was present on the span to produce this. The average top flange stress range due to sand truck loading was only 0.15 ksi with a standard deviation of 0.019 ksi. The average stress range at the bottom flange was 2.07 ksi and the standard deviation was 0.31 ksi.

The cross-sectional stress representation for the stress history depicted in Fig. 6.10, is shown in Fig. 6.11. Again, three cases are shown for the minimum and maximum stresses achieved at the bottom flange gage, and are denoted by a 1, 2, and 3 in Fig. 6.10. The neutral axis was much higher for this bridge than it was for both the West 7th location and the I-94 bridge. For TH-36 the neutral axis was very near the top of the steel member for both negative moment cases and for the positive moment case the neutral axis moved up into the concrete deck about 0.7 in. This can be explained by the detailing of the girder for TH-36 at the crack location. Shear channels, designation C4x7.25, were placed along the top flange of the beam, even in the area containing the cover plate. One channel was placed 4 in. away from the end of the cover plate, the exact location of the crack, this can be seen in the girder detail shown in Appendix B. The TH-36 Bridge was designed for composite action in this section and as seen by the results of the testing, it was achieving a great deal of it. Similar to the other bridges tested, the greatest amount of composite action was seen for the positive moment case.

6.2 Bridge Stress Ranges Produced by Random Traffic

Stresses caused by random truck traffic were also recorded. Stress ranges near the cracks were determined by investigating the data recorded by the gages on the top flange. The stress histories of the sand trucks were removed from the data that contained the stresses caused by random traffic so the randomness of the data would be preserved. After removing the data caused by the sand trucks, the random data was sorted into 0.5 ksi stress range levels and put into

a histogram. All stress ranges that were below 0.5 ksi were discarded and not considered important in determining remaining fatigue life.

Approximately 3.5 hours worth of typical traffic data was taken at the West 7th Street location. Collection started around 9:30 AM and continued until 1:45 PM. The random traffic created 42 stress ranges that fell in the 0.5 ksi to 1.0 ksi range, as well as 1 stress range in the 1.0 ksi to 1.5 ksi range. No stress ranges higher than 1.5 ksi were recorded at the West 7th Street Bridge.

Stress ranges on the I-94 bridge were recorded for 4 hours, from 9:10 AM until 1:25 PM, however; the MISTRAS 2001 AE monitor was being utilized for 2 of the 4 hours and created electrical problems that made the strain data too noisy to be useful. An attempt was made to filter the data that was corrupted by the AE monitor. Because the amplitudes of the noise were so great (0.5 ksi) and the noise signal frequency was near that of the random traffic stresses, the filter needed would have decreased traffic stress amplitudes as well. Of the 2 hours that were not corrupted, 28 stress ranges between 0.5 ksi and 1.0 ksi were recorded. No stress ranges greater than 1.0 ksi were recorded at this site.

A total of 4 hours of random stress data was recorded for the TH-36 bridge, but again, the MISTRAS 2001 corrupted about 1.5 hours of it. Data recording started at 9:50 AM and continued until 2:15 PM. The amplitude of the noise was again near 0.5 ksi and could not be filtered due to the degrading of the stress values imposed by random traffic. For the remaining 2.5 hours of data that was useful, only 2 stress ranges were recorded in the 0.5 ksi to 1.0 ksi range with no stress ranges being greater than 1.0 ksi.

A table showing the amount of data collected and a histogram of stress ranges for the crack location on each bridge tested is located in Table 6.1. Stress ranges recorded at all three bridges were not of the magnitude or frequency to cause concern for fatigue failure on any of the girders tested. Only one bridge recorded a stress range higher than 1.0 ksi, and that occurred only one time on the West 7th Street Bridge. Typically stress ranges above 2.5 ksi are required to cause crack propagation in the welded cover plate detail. No bridge tested recorded a stress range higher than 1.5 ksi. There is cause for concern, because the cracks did exist, therefore some past loading had to occur to cause the girder flanges to crack. There is a strong possibility

that this loading was still occurring randomly, but was not experienced during the few hours that traffic data was taken at each site.

A possible solution to this concern would be to set up a weigh in motion scale at each bridge to get a larger sample of truck weight data. These weights could then be converted into stress ranges by using the stress range from a known weight, i.e. the sand trucks. Data could be taken over a much longer period of time to get a larger random sample and over an entire 24 hour period to detect overweight trucks traveling in the middle of the night. These are the vehicles that cause the most fatigue damage. The scales should be placed in the same lane that the sand trucks traveled, West 7th Street Bridge traffic weights would need to be taken in both the northbound and southbound directions.

As an example, if traffic weights were collected for the I-94 Bridge, each weight collected could be turned into a stress range by knowing the relationship between the sand truck and the stress range it caused in the top flange. The equation is given as

$$\Delta\sigma_{Traffic} = C_1 \times W_{Traffic} \tag{7}$$

where $\Delta\sigma_{Traffic}$ is the stress range in ksi caused by a vehicle, the vehicle weight in lbs. is given by $W_{Traffic}$, and C_1 is a constant relating the stress range caused by a sand truck divided by the weight of the sand truck causing that stress range. The constant C_1 will be different for each bridge. For the West 7th Street Bridge Northbound direction, C_1 = 1.58 x 10^{-5} and for the Southbound direction C_1 = 1.31 x 10^{-5}. The I-94 Bridge has a C_1 = 1.19 x 10^{-5}, and TH-36 has a C_1 = 3.00 x 10^{-6}. These values of C_1 are summarized in Table 6.2. For the West 7th Street bridge it would take a truck weighting approximately 165 kips to cause a 2.5 ksi stress range. Likewise, for the I-94 bridge, a truck weight of approximately 205 kips would be needed to generate a 2.5 ksi stress range.

Once a histogram is established for a given period (day or week), the values can be multiplied by the number of periods (days or weeks) the bridge has been in service. This will give the total number of stress cycles for a particular stress range that the bridge has experienced (n_i). To find the incremental fraction of fatigue life consumed for a stress range, the number of cycles sustained by the bridge at that stress range should be divided by the total cycles available at that stress range. The total cycles available at that stress range can be found by the equation [12]:

$$N = c(S)^m \tag{8}$$

where N is the total cycles available to failure, S is the average value of the stress range given in ksi, c is a fatigue coefficient, and m is a fatigue exponent. Values provided for c and m for a wide flange section with welded cover plate are $c = 4.218 \times 10^9$ and $m = -3.256$ [13]. A value for N can be calculated for all stress ranges and then divided into the number of cycles actually experienced at that stress range. This gives the incremental fraction of fatigue life consumed at that stress range. Values of N for various stress ranges are given in Table 6.3. To find the total fatigue life consumed, sum up all incremental fatigue lives for all stress ranges present in the histogram; $\sum \frac{n_i}{N_i}$. By following this procedure, Mn/DOT will be able to get a better determination of crack fatigue life for the bridges tested. As of the writing of this report, weigh-in-motion data for the bridges tested was not available.

6.3 AE Results

Acoustic emission results for the bridges were much different than those obtained in the laboratory for two main reasons. One, the AE result for each bridge was only one point in the life of a fatigue crack on that bridge girder. In the laboratory, AE was collected periodically over many cycles throughout the life of the fatigue crack. Secondly, the loading in the laboratory was producing nominal stresses near 10 ksi consistently throughout cycling. AE was collected for periods of time that contained 1200 cycles in the lab. In the field, stress ranges barely reached 1 ksi for each sand truck and only about 20 to 40 passes were made for each bridge. The AE produced by fatigue cracks in the field will only be comparable to AE produced by fatigue cracks on the other bridges tested and not directly to results obtained in the laboratory.

For the West 7th Street Bridge, the sand truck made 43 passes over the girder prior to retrofit attachment. The number of events that were considered possible crack events was 37. This bridge had the highest ratio of AE events to sand truck passes of any of the bridges tested at 0.86 crack events per truck pass. This is high considering the low stresses compared to that of the laboratory girder. In the lab, the highest number of crack events over a 1200 cycle test was 63. This yields an event to cycle ratio of 0.052 events per stress cycle.

Often on the West 7th Street Bridge, multiple events were recorded for a single truck pass. An example of this is shown in Fig. 6.12, where three possible crack events are plotted along with the bottom flange live load stress history for the sand truck pass. The AE events occurred just prior to the peak in tension for the top flange. This is a good indication of fatigue crack produced AE, multiple events occurring near the peak in tension for the crack. The high AE event to sand truck ratio and the multiple events per truck indicated that the fatigue crack tested on the West 7th Street Bridge was actively being reopened.

The I-94 Bridge was the second bridge to be tested. A total of 18 sand truck passes were monitored with only 1 event meeting the criteria of a crack propagation emission. The lowest ratio of AE events to sand truck pass was obtained for this bridge, 0.055 crack events per truck pass. A few events had the correct location to be considered possible crack events, but occurred at the end of a sand truck history, when top flange stresses would be coming back to baseline values. This type of event is more indicative of crack rubbing. Figure 6.13 shows one such event. With such a low AE event to sand truck pass ratio, this fatigue crack was probably no longer propagating. The crack may have been created when the member was a fascia girder, but since has stopped growing because of the addition of the two girders adjacent to it.

TH-36 was the third and final bridge to be monitored for AE activity. The sand truck passes made here were sometimes different than the previous two bridges because the trucks were often not separated enough to cause two distinct stress histories. As can be seen in Fig. 6.14, the two trucks were separated enough that two distinct stress histories were created. However, in Fig. 6.15 the trucks were too close together and only one distinct history can be seen. This complicates the determination of the number of truck passes, and hence makes it difficult to come up with a reasonable event to truck pass ratio. Each history was looked at carefully and those that resemble Fig. 6.14, with ample truck spacing, were considered two truck passes and those that resemble Fig. 6.15 were only counted as one truck pass. Although 24 total truck passes were made, only 16 distinct truck histories were recorded. A total of 6 possible crack events were counted for the 16 truck histories. This results in a ratio of 0.375 crack events per truck history.

This fatigue crack showed some indication of propagation but perhaps was not as active as the West 7th Street Bridge. Certainly the TH-36 Bridge fatigue crack tested was more active

than that tested on I-94. A summary showing number of AE events, number of truck passes and AE event to truck pass ratio is presented in Table 6.4.

6.4 Bridge Stresses Produced by Sand Truck After Retrofit

Once the retrofit had been attached to each bridge another round of sand truck load testing was performed to evaluate stress changes in the section. Only two bridges were tested after the application of the retrofit, West 7th Street and I-94. The sand truck weight for the West 7th Street Bridge increased by 4%, going from 48,120 lbs. for the first test, to 50,040 lbs. for the second round of testing after the retrofit. Sand truck weight for the I-94 Bridge testing increased by only about 1%, going from 49,580 lbs. and 49,300 lbs. for the two trucks used on the first round of tests, to 49,900 lbs. for the second round of tests.

The stress history for a typical sand truck for the West 7th Street bridge with the truck traveling in the northbound direction after the retrofit can be seen in Fig. 6.16. Stresses depicted in this figure are from the bottom flange gage, both web gages and the top flange gage. Stress ranges experienced in the section were less than those before the retrofit had been applied. The average stress range for all sand truck passes at the bottom of the top flange was 0.43 ksi with a standard deviation of 0.013 ksi. The bottom flange average stress range for all sand trucks was 1.44 ksi with a standard deviation of 0.05 ksi. Stresses were reduced by an average of 43% in the top flange by the addition of the retrofit and bottom flange stresses were reduced by 10%. A listing of before and after retrofit stress ranges and percent reductions is shown in Table 6.5.

A simple comparison of before and after retrofit stress range and before and after retrofit section modulus was performed to check the validity of the reductions similar to that described in Section 4.5. A copy of the calculation is provided in Appendix A. The stress range reduction for the top flange was measured to be 43%, while the calculated top fiber section modulus increase was 44%. The section modulus before retrofit attachment was 542 in^3 and 973 in^3 after retrofit. The calculation was performed assuming the beam with retrofit only, composite action from the concrete deck action was not taken into consideration. The reduction in stress due to retrofit was very close to computed values of section modulus increase and thus the amount of recorded stress reduction seems valid.

Figure 6.17 shows stress results for some of the gages located on the retrofit angle plotted along with the gage on the top flange of the girder for reference. Gages on the flange of the retrofit angles stay in live load compression the entire time although the gage located on the flange of the girder starts out in live load tension before it goes into live load compression.

A cross-sectional view of the stresses through the cracked section for the stress history depicted in Fig. 6.16, is shown in Fig. 6.18. Just as before the retrofit, the three cases depicted are the minimum and maximum stresses achieved at the bottom flange strain gage denoted by a 1, 2, and 3 in Fig. 6.16. For the northbound direction, the first minimum is achieved when the sand truck was on the cracked span moving toward the crack, producing negative moment. The maximum stress occurs when the truck was over the cracked section inducing positive moment at the section. The third and final case was when the truck had passed over the pier and again created negative moment at the section.

For the first peak shown the neutral axis was located 29.5 in. above the bottom of the section, approximately where it had been before the retrofit was applied for the same loading condition. The second case, where the section was in positive moment, the neutral axis shifted up to 33.4 in above the bottom of the section, 1.8 in. above what it had been before the retrofit was put on. Finally for the last case, the neutral axis was located 32.2 in. above the member bottom. This is only 0.6 in. above what it was prior to the angles being attached. These shifts in neutral axis seem reasonable when compared with the calculation comparing before and after retrofit section properties shown in Appendix A. The calculation showed a rise in neutral axis of 4.75 in. from 18 in. for before the retrofit to 22.75 in. after the retrofit. Again, this calculation does not take into account the concrete deck, if it had the neutral axis would not move as much. Therefore, the 1.8 in. movement of the neutral axis for the positive moment case seems reasonable.

A southbound sand truck on West 7th Street created different stresses in the section than did a northbound truck. Figure 6.19 shows a stress history for a typical southbound sand truck. Stresses plotted are for the bottom flange gage, both girder web gages and the girder top flange gage. The stress ranges were reduced from those seen previously without the retrofit for this truck direction also. The average top flange stress range for all sand trucks was 0.39 ksi with a standard deviation of 0.015 ksi. The bottom flange of the section had an average stress range of

1.23 ksi and a standard deviation of 0.08 ksi. Stress reductions due to the retrofit were on average 38% for the top flange and about 14% for the bottom flange. As seen previously the reductions in stress range shown here appear to be valid when compared to the calculation showing changes in section properties due to the retrofit shown in Appendix A.

For the southbound truck direction, stresses in the angles themselves were smaller and varied slightly between live load compression and live load tension throughout the history. Shown in Fig. 6.20 are the stresses seen in the retrofit for the same truck that was depicted in Fig. 6.19. The angle flange tip stresses were very close in value to those seen in the angle flange gage closer to the web. This would indicate that little shear lag was present.

The cross-sectional stress representation for the stress history depicted in Fig. 6.19, are shown in Fig. 6.21. Again, the loading conditions for the southbound truck occurred in the opposite order than those for a northbound truck. The truck approached from the span on the other side of the pier away from the crack, denoted by a 1 in Fig. 6.19. Once it passed over the pier it was directly over the cracked section, denoted by a 2 in Fig. 6.19. The truck then proceeded away from the crack toward the center of the cracked span inducing negative moment at the cracked section, denoted by a 3 in Fig. 6.19.

The first peak neutral axis position is almost exactly that of the same loading condition before the retrofit was attached at 32.3 in. above the girder bottom. Moreover, for the second truck position the neutral axis moved dramatically with the addition of the retrofit however. Before the retrofit was applied, the neutral axis for this case was located 1.7 in. into the deck. With the addition of the retrofit, the neutral axis moves up 2.2 in. above the top of the girder into the concrete bridge deck. The final case neutral axis is at 29.9 in. above the bottom of the section, almost unchanged from that before the retrofit application. The two negative moment cases mimicked the change in behavior exhibited by the negative moment cases for the northbound truck stresses.

The other bridge load tested after retrofit was the I-94 Bridge. A stress history for a sand truck after the retrofit application is shown in Fig. 6.22. Stresses were reduced somewhat with the addition of the retrofit. The average stress range for all sand truck passes at the top flange strain gage was 0.54 ksi with a standard deviation of 0.026 ksi. The average bottom flange stress range was 1.36 ksi and a standard deviation of 0.068 ksi. Reductions in stress due to the retrofit

were on average 8.5% for the top flange and 8.7% for the bottom flange. These stress range reductions are not as much as those reported for the West 7th Street Bridge. Explanations as to why the reductions were not as much are two fold. First, the retrofit could not be attached properly due to a splice in the girder that was too close to the crack location. The splice plate was about 2 ft. from the crack and therefore the retrofit angles were shifted over so the crack was not in the center of the retrofit. Secondly, the bolts were not tightened using a torque wrench, this may have left the bolts with less torque than was required for a slip critical connection. If this is true, the retrofit may slide when loaded and thus not be able to divert much stress into the angle flanges.

A cross-sectional stress representation of the cracked section for the stress history depicted in Fig. 6.22, is shown in Fig. 6.23. The three loading cases shown correspond to the peaks achieved in the bottom flange stress and are denoted by a 1, 2, and 3 in Fig. 6.22. When the location of the neutral axis for these three cases after the retrofit was compared to those before the retrofit, no change was witnessed. This was expected after noticing that there really was not substantial reduction in stress ranges for the section, due to the addition of the retrofit. This finding also points to the theory that the retrofit was not taking stress away from the section to aid in stress reduction in the top flange.

Chapter 7 - Conclusions

There were three main questions to be answered by this research. The first, can acoustic emission monitoring be used to determine if fatigue cracks are propagating in cover plated bridge girders? Second, will the retrofit that was proposed by Mn/DOT stop the crack propagation of these cracked girders and how much were stress ranges in the top flange reduced by the application of the retrofit? Third, what is the expected fatigue life for the girders tested on the three bridges that were studied?

7.1 Effectiveness of AE Monitoring to Determine Fatigue Crack Propagation

Good correlation existed between the results obtained by AE monitoring of the laboratory girder and the crack propagation witnessed on its lower flange. By using both the location of the AE event and the stress state near the crack at the time of the AE event, it was possible to isolate AE events caused by crack growth from AE events due to other sources. These other sources including crack rubbing and bearing noise, exist in both the laboratory and field settings. As explained in Section 4.1, the number of AE events that were caused by fatigue crack propagation increased as the crack continued to grow into the flange of the lab specimen and up towards the web.

This same principle can be used in the field on a fatigue cracked bridge girder. The AE monitoring setups used in both the laboratory and in the field were almost identical. Both included the use of a linear array placed on the inside of the cracked flange to determine AE event location. Both the laboratory and field setups made use of a strain gage output to determine the state of stress in the member at the time of the event. The only major difference between the laboratory and field study was the presence of a concrete bridge deck above the fatigue crack in the field. Another difference in AE monitoring between the lab and the field is that the AE data obtained in the field for one bridge is only for one point in time during the life of a crack, whereas the laboratory girder had many times throughout its life monitored.

Two of the bridges tested seemed to have propagating fatigue cracks. An examination of the ratio of AE events to sand truck passes indicated that the West 7th Street Bridge had an event to truck ratio of 0.86. This was the most active crack tested according to AE monitoring. The

second most active crack as determined by AE monitoring was that found on the TH-36 Bridge. A ratio of 0.375 crack events per sand truck resulted from the testing performed there. The West 7th Street Bridge and the bridge on TH-36 most likely contained propagating fatigue cracks. AE testing of the fatigue crack on the I-94 Bridge indicated this crack was not propagating. Only one event could have been considered a possible propagating acoustic emission. This bridge resulted in the lowest crack event to sand truck ratio of 0.055.

In the wake of these conclusions, it has been shown that AE monitoring can be used to determine fatigue crack propagation on bridges with positive results. With recent advances in AE technology and proper techniques used, a rational judgement now can be made to determine if cover plated girder fatigue cracks are propagating or not. The use of AE monitoring can give results as to growth during a single test whereas, ultrasonic testing must be performed many times to determine crack growth. However, the AE equipment can not continue to monitor crack activity after the retrofit has been attached, as once was hoped, due to excessive noise coming from the connection region of the retrofit. Once the retrofit is in place, neither AE nor ultrasonic testing can be employed to inspect the crack. Another suitable method of NDE should be developed to monitor the cracks with the retrofit in place. The reliability of the retrofit if the bolts loosen is unknown, and may lead to continued crack propagation through the girder web. To implement AE testing of the field bridges, cheaper permanent AE transducers and vibrating wire strain gages could be placed on the member with permanent cables installed. Periodic AE monitoring could be performed (perhaps once a year). The amount of AE obtained from crack activity could be compared with previous results to determine if crack propagation rate has increased.

7.2 Effectiveness of Retrofit to Reduce Flange Stress and Stop Crack Propagation

The retrofit was conceived by Mn/DOT to serve two main purposes, to reduce flange stresses in the girder and to stop the propagation of the fatigue crack into the flange. The retrofit used in the laboratory was similar in concept to that used on the bridges. The laboratory retrofit was successful in reducing stresses in the flange. Stresses were immediately decreased by 42% in the bottom flange after the addition of the retrofit.

Stress reductions seen on the West 7th Street Bridge were similar to that obtained in the laboratory. When comparing average stress ranges in the top flange due to sand truck loading, an average stress range reduction of 43% occurred after the retrofit had been attached. This performance is very close the 42% reduction recorded in the laboratory. Stress reductions achieved on the I-94 Bridge were not as promising, but some reduction was observed. An 8.5% reduction in average stress range was obtained. This poor performance of the retrofit was likely due to the limited length of the retrofit on one side of the crack.

The retrofit was successful in achieving one of the two purposes it was designed for, reduce stress ranges in the top flange of the girder. The retrofit also reduced stresses in the bottom flange as well, but this was not the objective of the design. However, had the stress ranges in the bottom flange increased that would have been a disadvantage of the retrofit, due to concern of the bottom cover plate possibly developing fatigue cracks from an increased stress range.

Whether or not the retrofit will stop the fatigue cracks from propagating is not as simple an answer. The laboratory retrofit did stop cracking for 425,000 cycles but then the crack continued to grow all the way through the flange and into part of the web up to the first row of bolt holes. However, this propagation was the result of stress ranges that were near 10 ksi nominal in the laboratory. Stress ranges in the field were on the order of 0.5 ksi after the retrofit had been attached. The possibility exists that the stresses were reduced to below the level needed to propagate the cracks. Even if crack propagation continues, it will be at a slower rate than prior to the introduction of the retrofit, simply because of the stress range reduction.

An encouraging fact is that the laboratory retrofit performed as well, with a severed beam flange, as a new beam under fatigue loading. The retrofit did not fail under continued fatigue loading and the same performance should be expected of the retrofit in the field. However, the laboratory retrofit was not tested for ultimate load once the flange was severed. The actuator used to supply the many cycles of fatigue type loading was not powerful enough to test the ultimate load that could be withstood by the beam with retrofit.

One recommendation for future use of the retrofit is in reference to the installation procedure. When tightening the bolts of the retrofit, special care should be used to ensure that the proper torque is reached. Bolts not torqued enough may not allow full transfer of force from

the girder flange to the retrofit angles. Bolts torqued too much may fracture and not be useful at all for transferring force. Methods to ensure proper bolt tightening include turn of the nut method, torque wrench tightening, and twist off bolts. The retrofit also should not be used where the existence of splice plates does not allow proper alignment of the angles over the crack, the retrofit must be centered on the crack section.

7.3 Fatigue Life of Cracked Girders

Mn/DOT should perform weigh-in-motion data acquisition for the three bridges tested to gain a better understanding of remaining fatigue life. Stress ranges obtained during testing were not large enough to ever cause concern of fatigue failure, however, the amount of data collected was small and better representative samples should be taken by using weigh-in-motion equipment. Large overweight trucks are what produce a majority of fatigue damage in girders. To properly account for these loads, longer testing periods should be performed, consisting of at least 24 hours, to obtain nighttime drivers that might try to haul larger loads than are legal. A procedure for determination of fatigue life based on truck weight data was outlined in Section 6.2. Values of C_1 were based on before retrofit stress ranges, this is conservative since the retrofit reduced stress ranges in the top flange.

7.4 Final Recommendations

The goals of this project were met and the results of the research are encouraging for the future of AE monitoring. Mn/DOT may want to implement an AE monitoring program to evaluate fatigue crack activity over time. The AE results obtained in the laboratory were over the life of the fatigue crack and correlated well with fatigue crack growth. Data obtained in the field was only for one instance in time. More testing should be performed in a couple of years to compare crack activity. Permanent transducers could be placed on the girders and the wires brought to a central location near the pier so setup would be quick, requiring less traffic control. Preamps would need to be hooked up each time data would be collected but that could be performed quickly with the use of a lift truck. The AE results could be used to obtain an AE event to sand truck pass ratio and compared to previous ratios obtained for that crack. If the ratio increased from the previous AE tests, it would mean that the crack has grown and is propagating

at a greater rate. If the ratio is less than previous testing or close to zero it would mean that the crack has arrested. By repeated AE monitoring the activity of the crack could be determined with greater accuracy than by a single isolated test.

The retrofit was a success at repairing the fatigue cracks found at the end of the welded cover plates. If used properly the double angle retrofit could be counted on to effectively reduce top flange stress ranges. The most important parameters regarding installation are that the retrofit be properly aligned with the crack in the center of the angles and that the bolts be tightened to the proper torque with one of the approved methods. A crack arresting hole should be drilled in the web for all instances when the retrofit is used in case the crack propagates further into the flange and eventually the web.

Some recommendations for Mn/DOT concerning future use of AE monitoring and the double angle retrofit are as follows:

- Only use the double angle retrofit so it can perform in the way it was designed, this would include paying special attention to both proper alignment of the angles and proper bolt tightening techniques.
- Drill a crack arresting hole just below the crack in the web in all cases when using the double angle retrofit.
- Construct a lifting stand that could be used to assist in the installation of the retrofit on future bridges.
- Periodically inspect the retrofit to check for continued crack propagation through the web, and loose bolts holding the angles on to the web.
- Acquire weigh-in-motion data for the test sites to give a better approximation of remaining fatigue life.
- Routine use of AE monitoring for fatigue crack growth in cover plated girders is not recommended.

References

1. Hopwood, Theodore II., "Acoustic Emission Inspection of Steel Bridges", *Public Works,* Vol. 119, No. 6, May, 1988, 66-69.
2. Maji, A. K., Kratochvil, T., "Acoustic Emission Monitoring of Steel Bridges", *Structures Congress XII Proceedings of the Structural Congress 94,* ASCE, New York, NY, 1994, 1322-1327.
3. MISTRAS 2001 Users Manual, Physical Acoustics Corporation, Princeton, NJ, 1995.
4. Fisher, J. W., Hanson, J. M., Lally, A., Scheffey, C., Salgo, M. N., "Fractures - Problem for Welded Steel Bridges", *Civil Engineering,* Vol. 48, No. 4, April, 1978, 70-73.
5. Verma, Krishna K., McNamara, Michael P., "A Conceptual Approach to Prevent Crack-Related Failure of Steel Bridges", *Engineering Journal - American Institute of Steel Construction,* Vol. 25, No. 1, First Quarter, 1988, 17-19.
6. Chase, Stephen B., "NDE for Steel Bridges", *Civil Engineering,* Vol. 65, No. 5, May, 1985, 49-51.
7. Hopwood, Theodore II, Oka, Vishwas K., Deen, Robert C., "Reliability Assessment of High-Risk Steel Bridges by Nondestructive Test Methods", Kentucky Transportation Research Program, College of Engineering, University of Kentucky Transportation Research Building, Lexington, Kentucky, October, 1987.
8. Vannoy, Donald W., Azmi, Mohammad, "Acoustic Emission Detection and Monitoring of Highway Bridge Components", Maryland Department of Transportation State Highway Administration Research Report, Department of Civil Engineering, University of Maryland, College Park, MD, April, 1991.
9. Hopwood, Theodore II, Prine, David W., "Acoustic Emission Monitoring of In-Service Bridges", Kentucky Transportation Research Program, College of Engineering, University of Kentucky Transportation Research Building, Lexington, Kentucky, August, 1987.
10. Ghorbanpoor, A., Rentmeester, Alan T., "NDE of Steel Bridges by Acoustic Emission", Structural Engineering in Natural Hazards Mitigation Proc Symp Struct Eng Nat Hazard Mitigation, ASCE, New York, NY, 1993, 1008-1013.

11. Fisher, John W., Pense, Alan W., Slockbower, Robert E., Hausammann, Hans, "Retrofitting Fatigue Damaged Bridges", *Transportation Research Board*, Washington, D.C., 1978, 102-109.

12. Hahin, C., South, J. M., Mohammadi, J., Polepeddi, R. K., "Accurate and Rapid Determination of Fatigue Damage in Steel Bridges", *Journal of Structural Engineering,* Vol. 119, No. 1, January, 1993, 150-167.

13. Munse, W., Wilbur, T., Tefralian, M., Nicoll, K., Wilson, K., "Fatigue characterization of fabricated ship details for design", *SSC-318,* Ship Structure Committee, Washington, D.C.

14. Horowitz, Paul, Hill, Winfield, *The Art of Electronics,* Second Edition, Cambridge University Press, Cambridge, U.K., 1989

Tables

Table 5.1: Truck Weights for Bridge Testing

Bridge	Sand Truck Weight (lbs.)
Before Retrofit Testing	
West 7th Street (BR 62066)	48,120
I-94 over TH-55 (BR 27855)	49,580
	49,300
TH-36 over Cleveland (BR 9276)	50,000
	50,080
After Retrofit Testing	
West 7th Street (BR 62066)	50,040
I-94 over TH-55 (BR 27855)	49,900

Table 6.1: Bridge Stress Distributions for Traffic Data Collected

Bridge	Hours of Data Collected	Stress Distribution	
		0.5 to 1.0 ksi	1.0 to 1.5 ksi
West 7th Street (BR 62066)	3.5	42	1
I-94 over TH-55 (BR 27855)	2	28	0
TH-36 over Cleveland (BR 9276)	2.5	2	0

Table 6.2: Values of C_1 for Each Bridge

Bridge	Stress Range	Truck Weight	C_1
West 7th Street (BR 62066) NB	0.76	48,120	1.58×10^{-5}
West 7th Street (BR 62066) SB	0.63	48,120	1.31×10^{-5}
I-94 over TH-55 (BR 27855)	0.59	49,400	1.19×10^{-5}
TH-36 over Cleveland (BR 9276)	0.15	50,000	3.00×10^{-6}

Table 6.3: Values of N_i for Varying Stress Ranges

Stress Range	N (cycles)
0.5 - 1	1.08×10^{10}
1 - 1.5	2.04×10^{9}
1.5 - 2	6.82×10^{8}
2 - 2.5	3.01×10^{8}
2.5 - 3	1.56×10^{8}
3 - 3.5	9.09×10^{7}
3.5 - 4	5.70×10^{7}
4 - 4.5	3.79×10^{7}
4.5 - 5	2.64×10^{7}
5 - 5.5	1.19×10^{7}

Table 6.4: AE Events to Sand Truck Pass Ratio

Bridge	AE Events	Truck Passes	AE Event to Truck Pass Ratio
West 7th Street (BR 62066)	37	43	0.86
I-94 over TH-55 (BR 27855)	1	18	0.055
TH-36 over Cleveland (BR 9276)	6	16	0.375

Table 6.5: Percent Reduction of Stress Ranges Due to Sand Truck Loading

Bridge	Stress Range Before Retrofit (ksi)	Stress Range After Retrofit (ksi)	Measured % Reduction
Laboratory	9.8	5.7	42
West 7th Street (BR 62066) NB	0.76	0.43	43
West 7th Street (BR 62066) SB	0.63	0.39	38
I-94 over TH-55 (BR 27855)	0.59	0.54	8.5

Figures

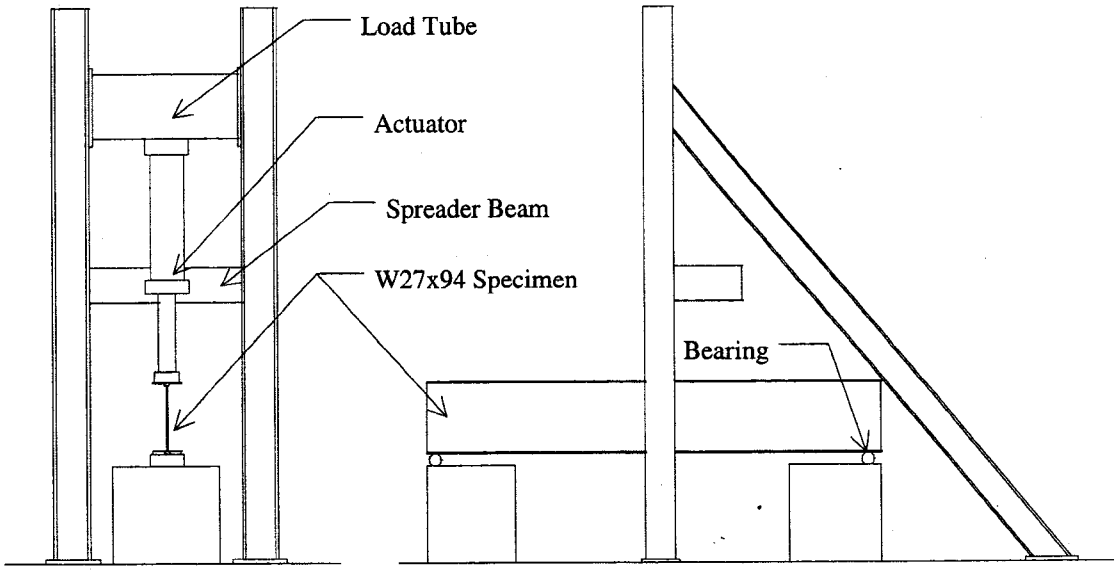

Figure 3.1: Load Frame Setup

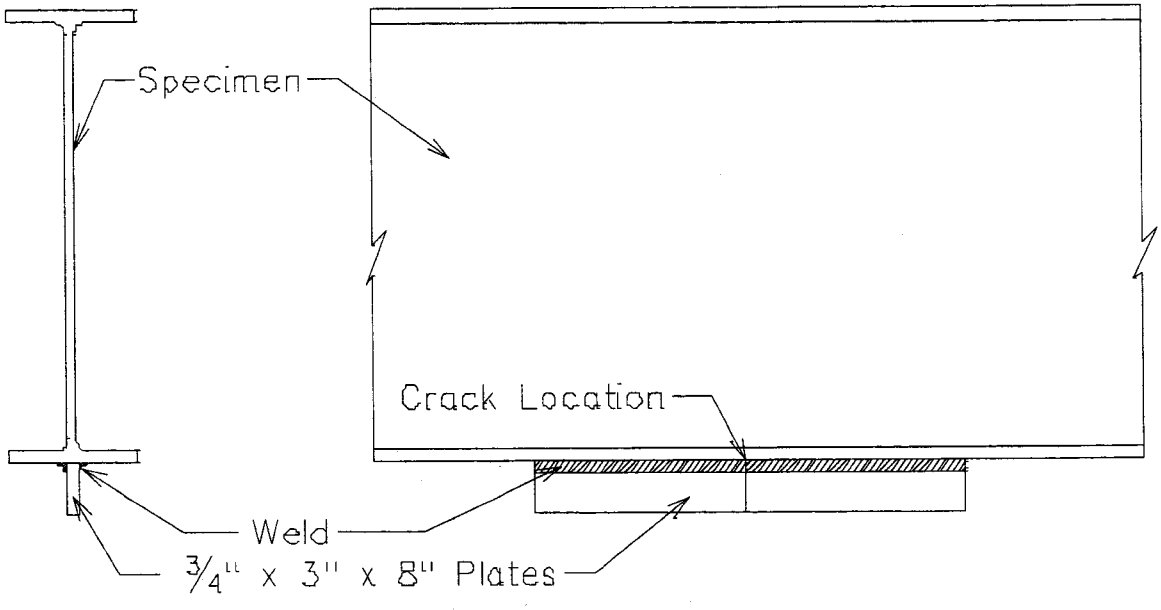

Figure 3.2: Crack Initiation Detail

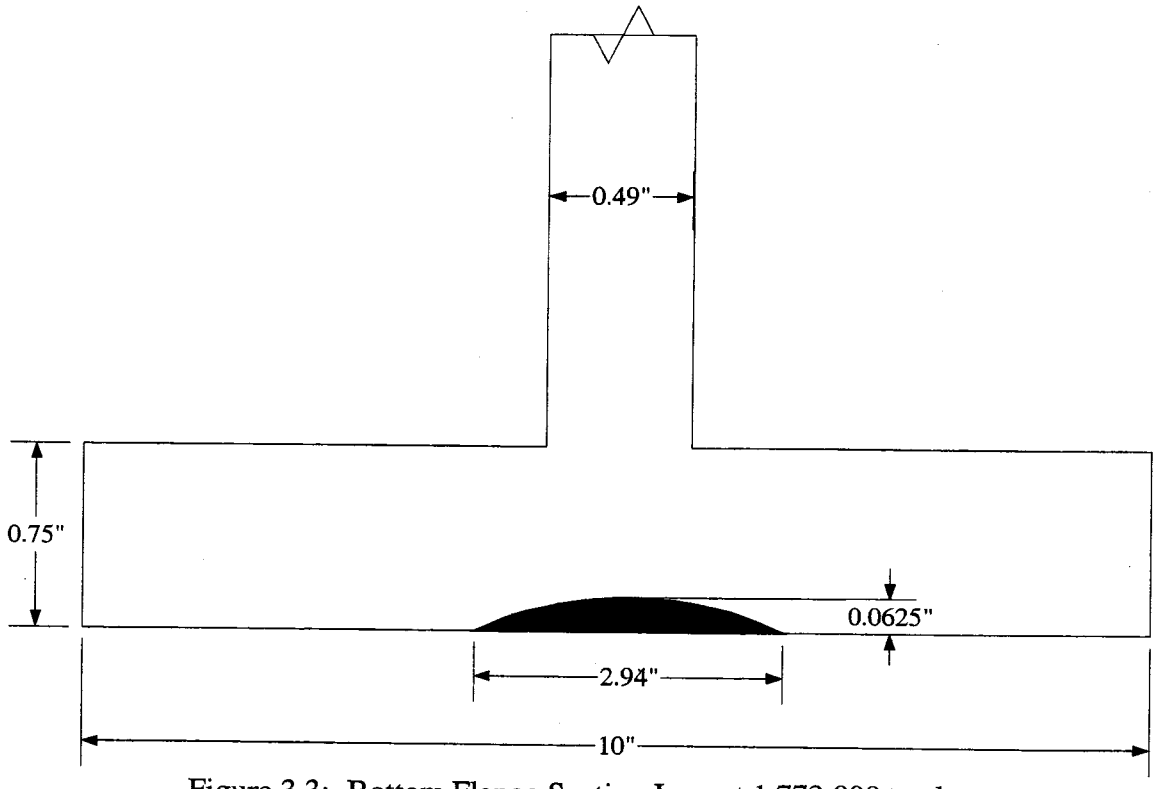

Figure 3.3: Bottom Flange Section Loss at 1,773,000 cycles

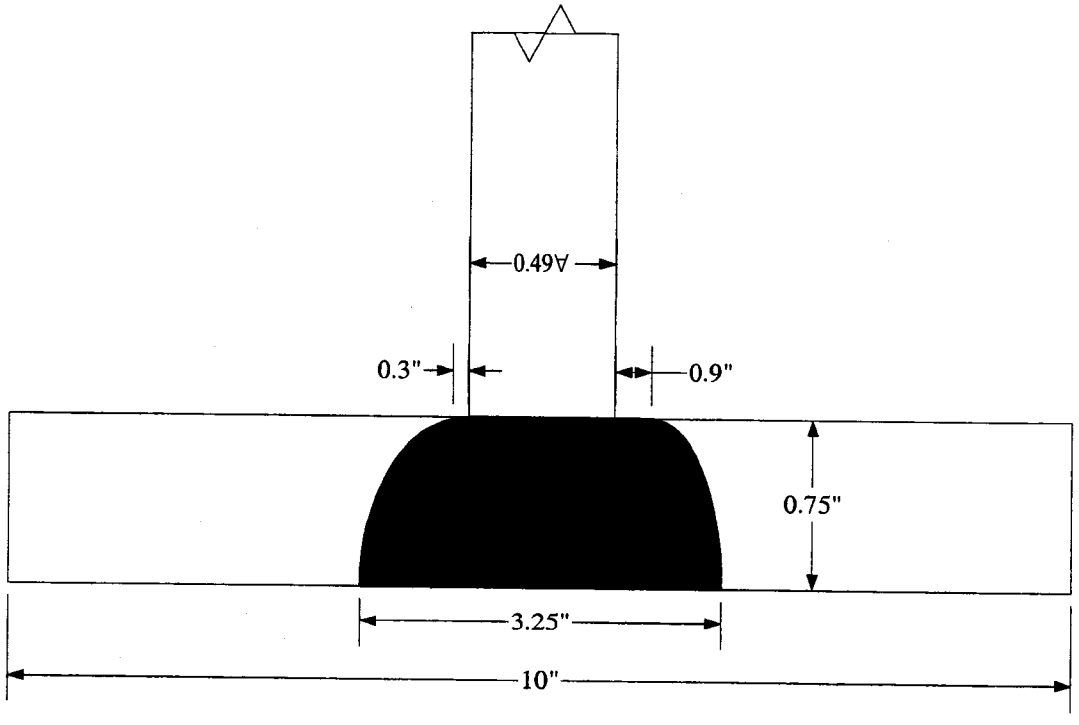

Figure 3.4: Bottom Flange Section Loss at 1,983,000 cycles

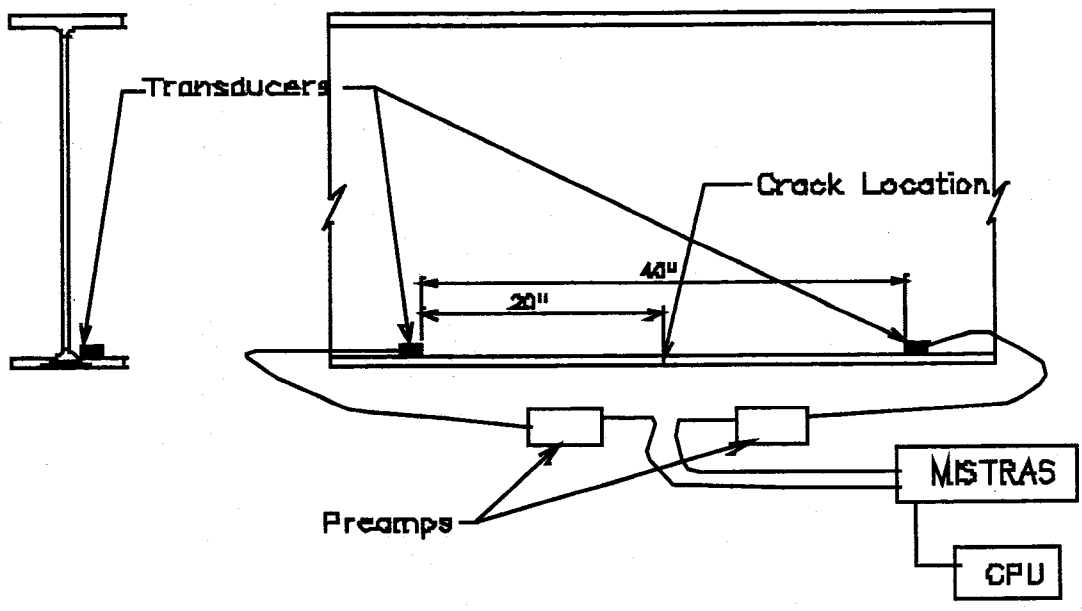

Figure 3.5: Acoustic Emission Monitor Setup and Transducer Location

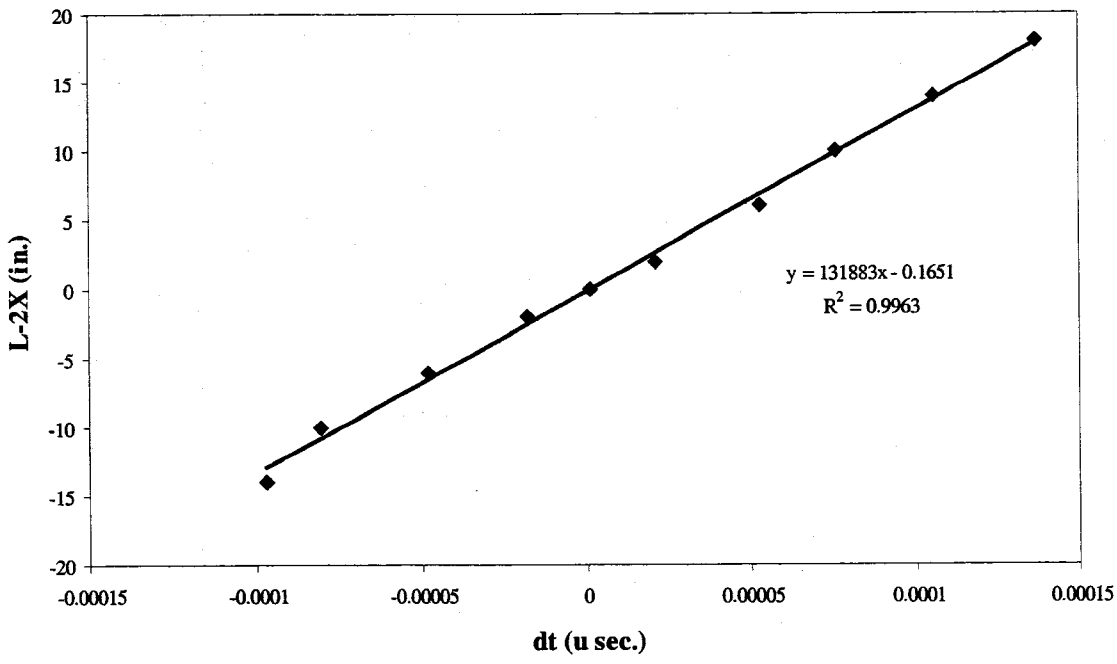

Figure 3.6: Determination of Stress Wave Velocity in Lab Beam

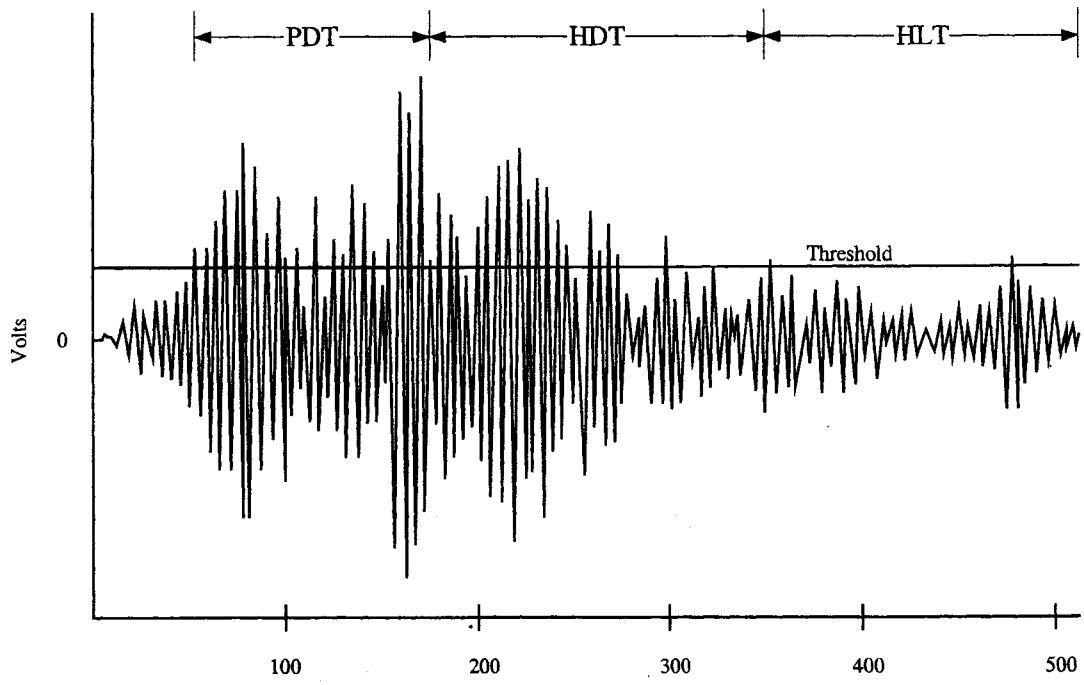

Figure 3.7: Typical AE Signal

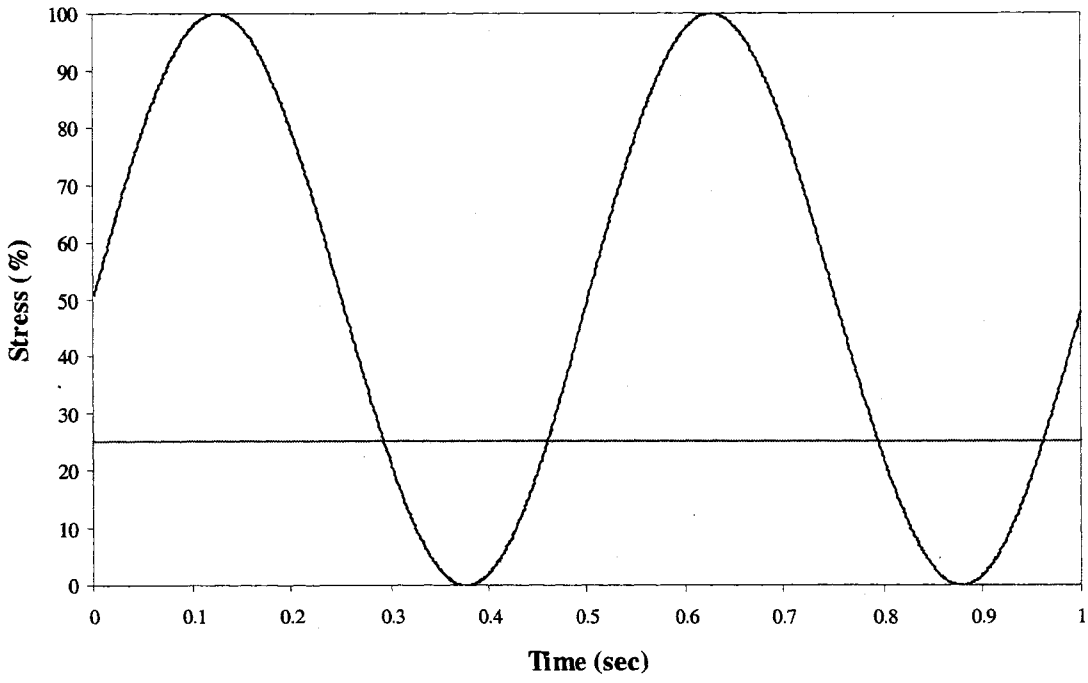

Figure 3.8: Loading Conditions that Create Crack Propagation

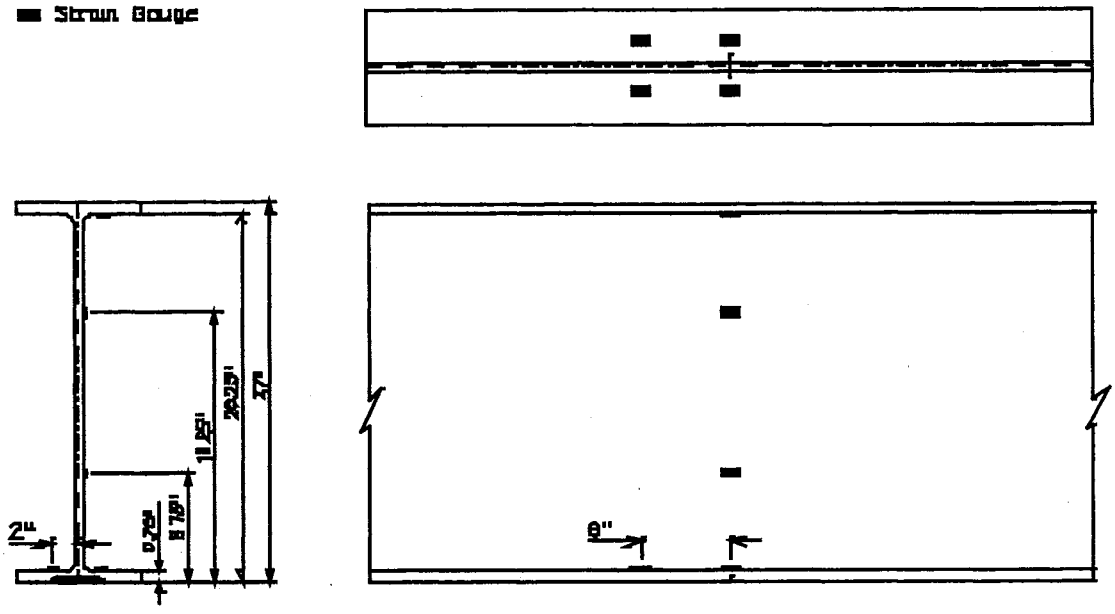

Figure 3.9: Location of Strain Gages Before Retrofit

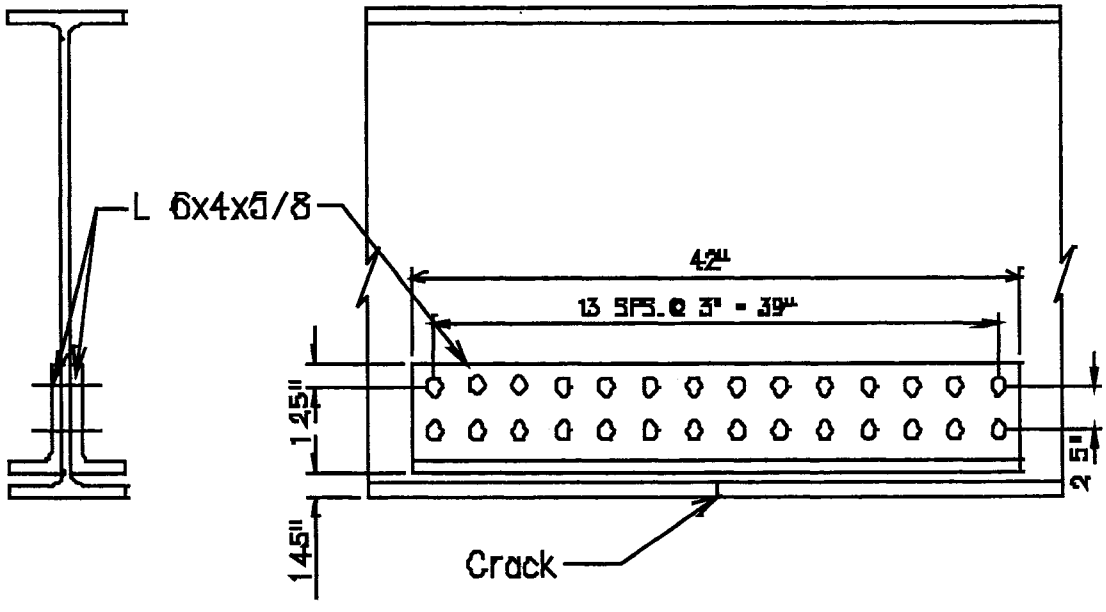

Figure 3.10: Laboratory Double Angle Retrofit Detail

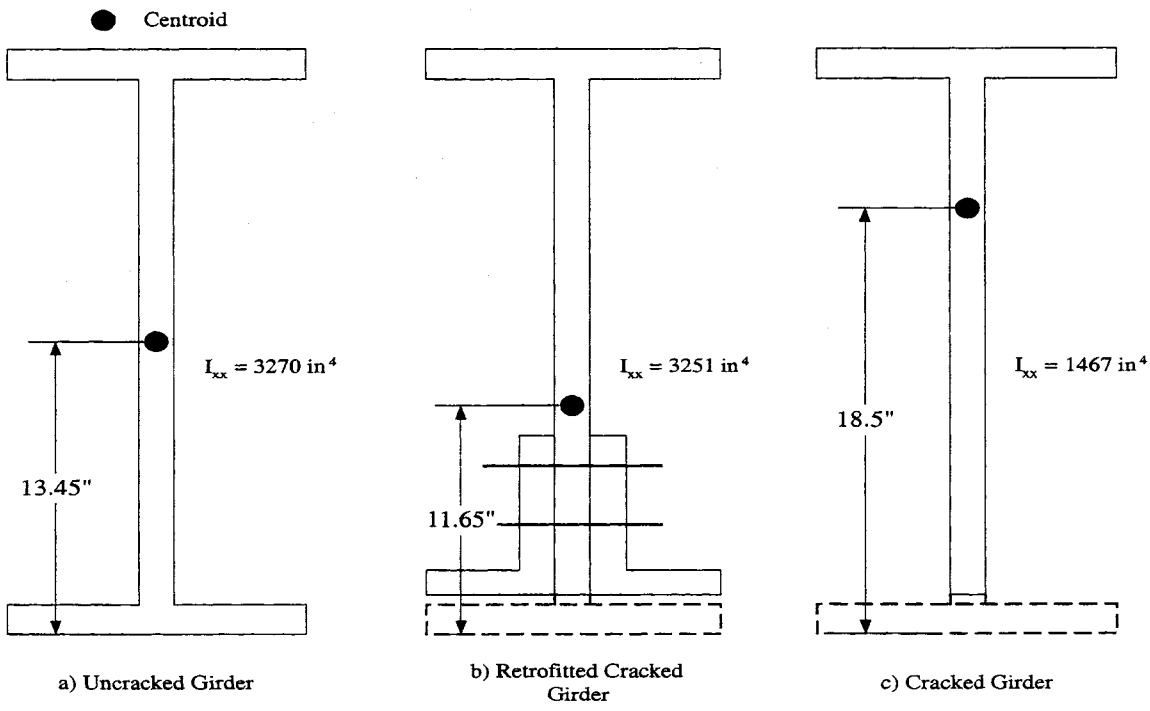

Figure 3.11: Laboratory Beam Moment of Inertia Values
Area Enclosed by Dash Not Included in Moment of Inertia

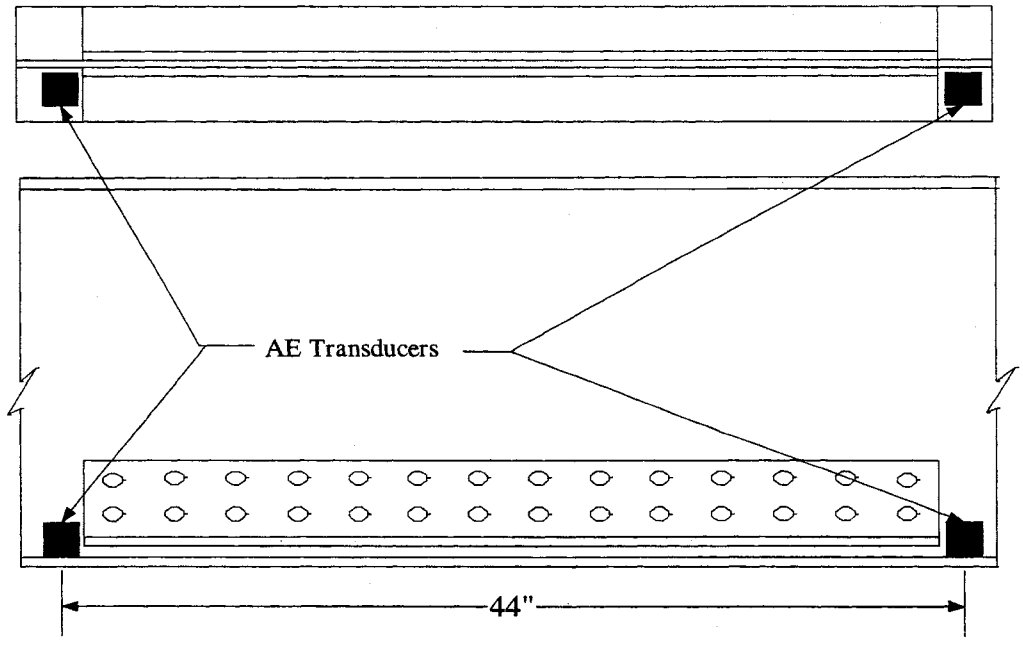

Figure 3.12: AE Transducer Configuration After Retrofit (Single Array)

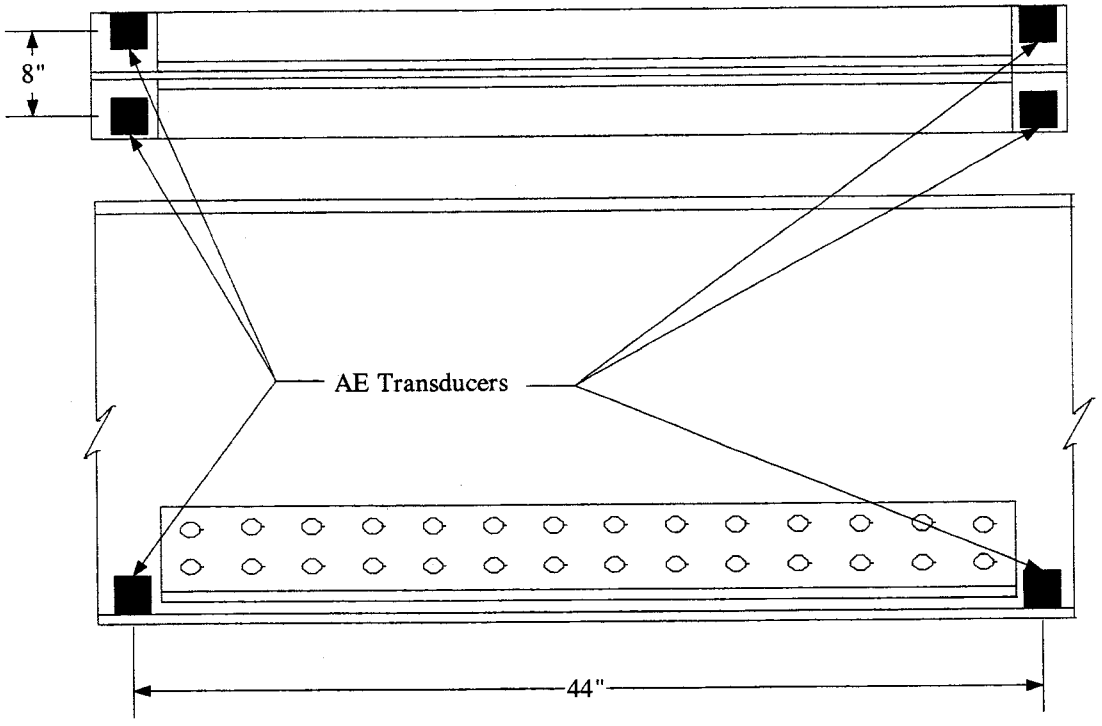

Figure 3.13: AE Transducer Configuration After Retrofit (2-Dimensional Array)

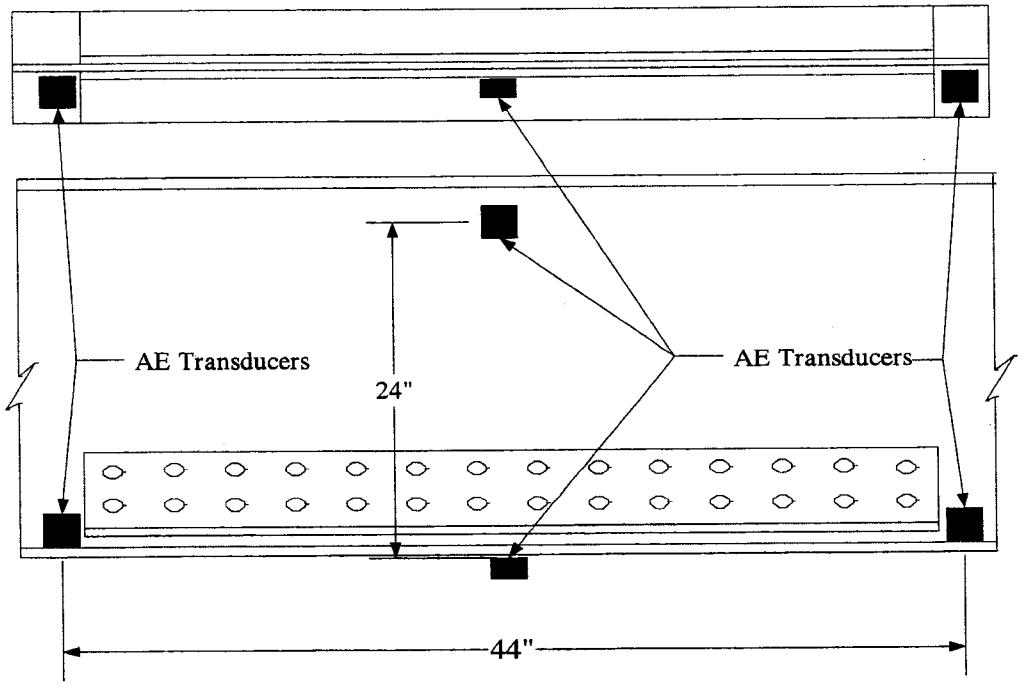

Figure 3.14: AE Transducer Configuration After Retrofit (Double Linear Array)

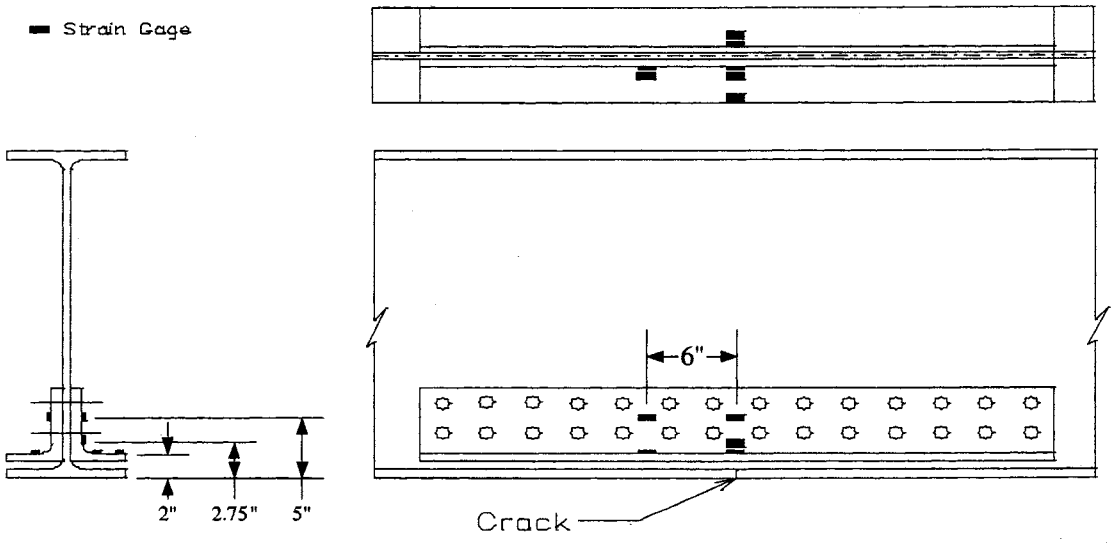

Figure 3.15: Location of Strain Gages on Retrofit

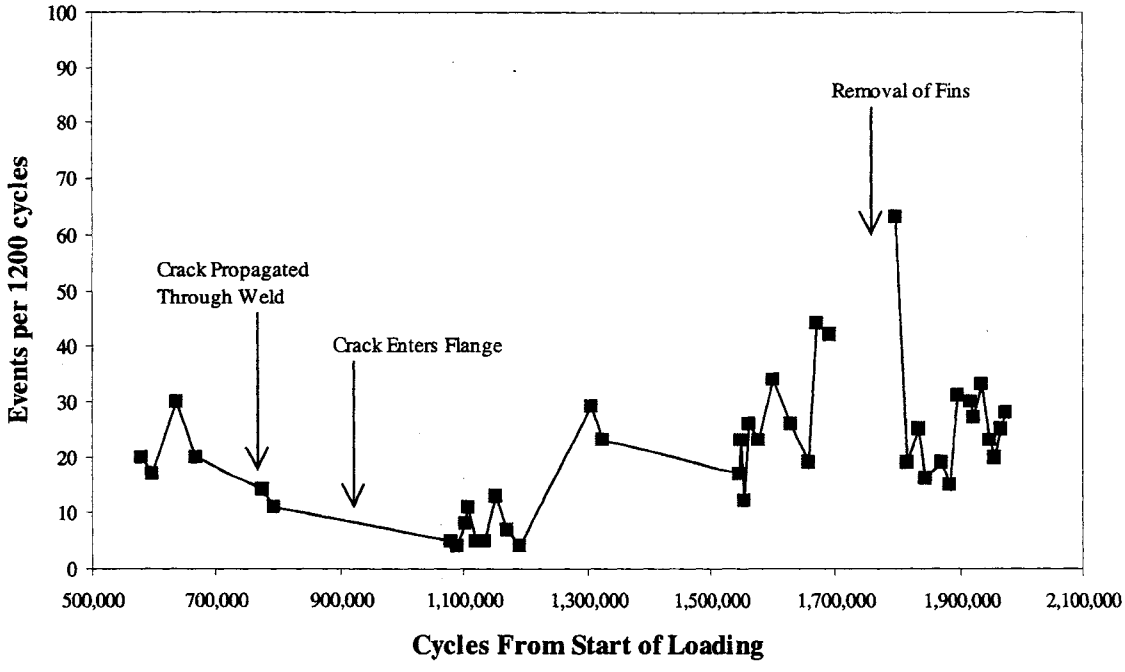

Figure 4.1: AE Crack Events vs. Cycle Before Retrofit

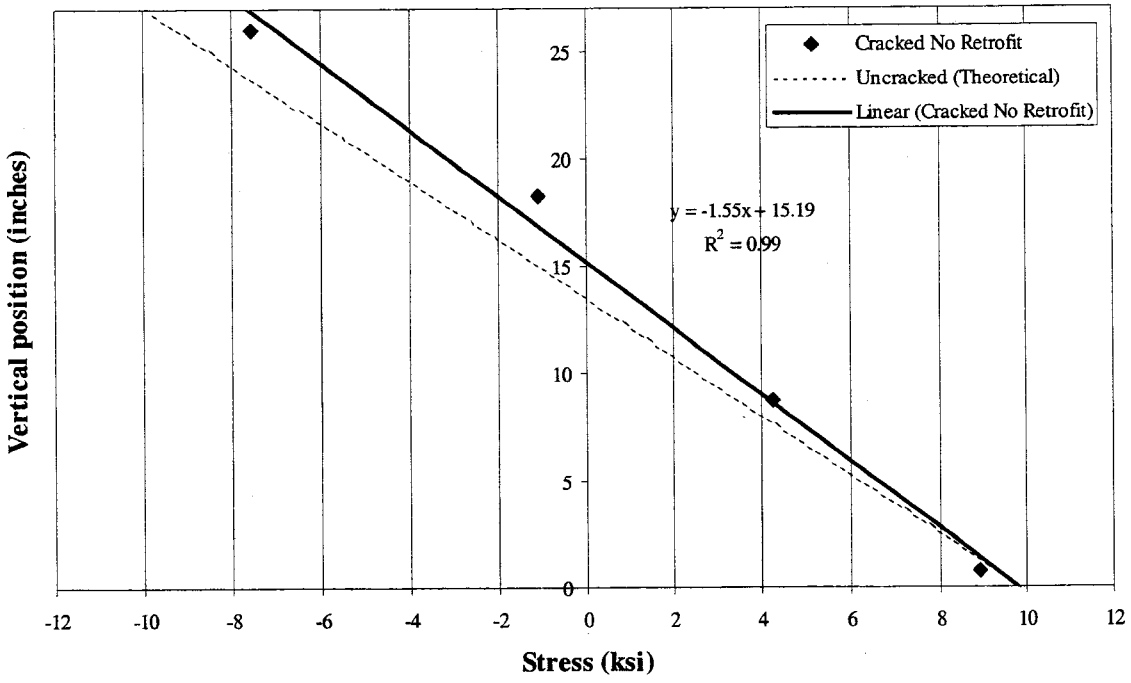

Figure 4.2: Cracked Section Stresses Just Prior to Retrofit

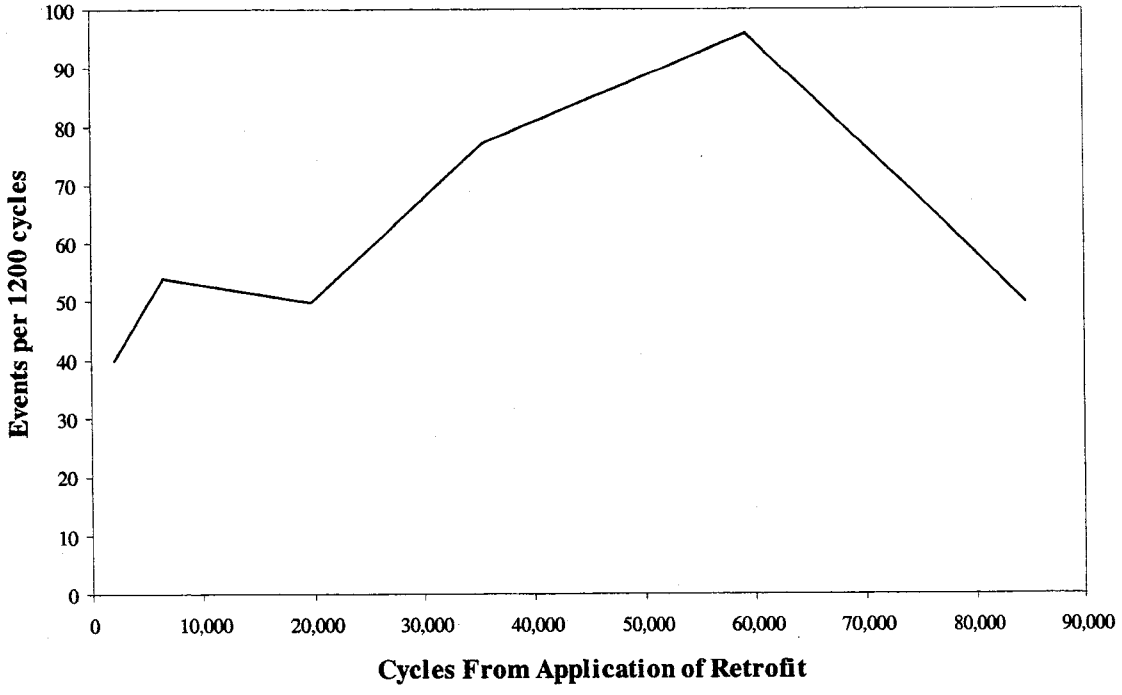

Figure 4.3: AE Crack Events vs. Cycle After Retrofit Application

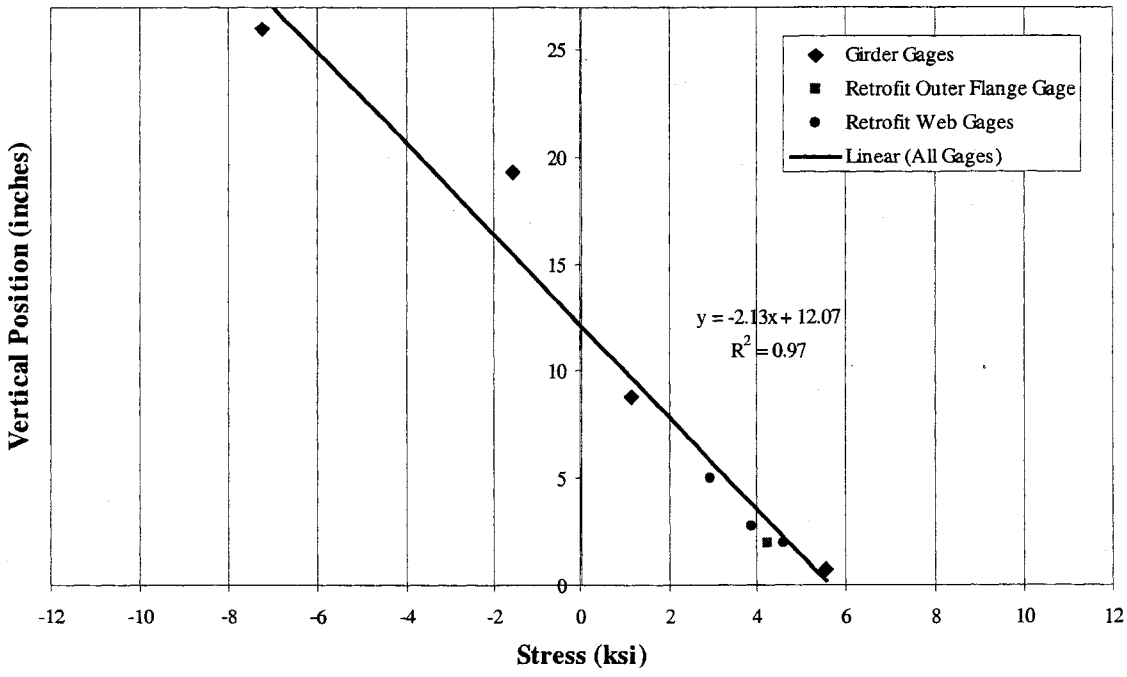

Figure 4.4: Cracked Section Stresses Just After Retrofit Application

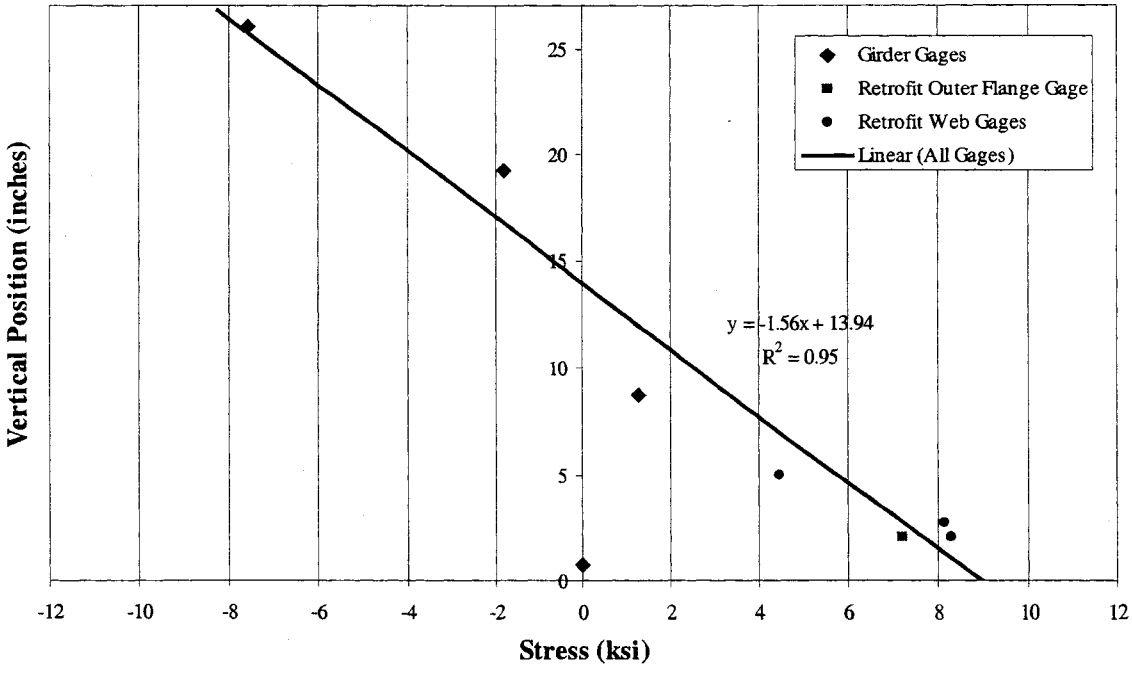

Figure 4.5: Cracked Section Stresses After Full Flange Cracking

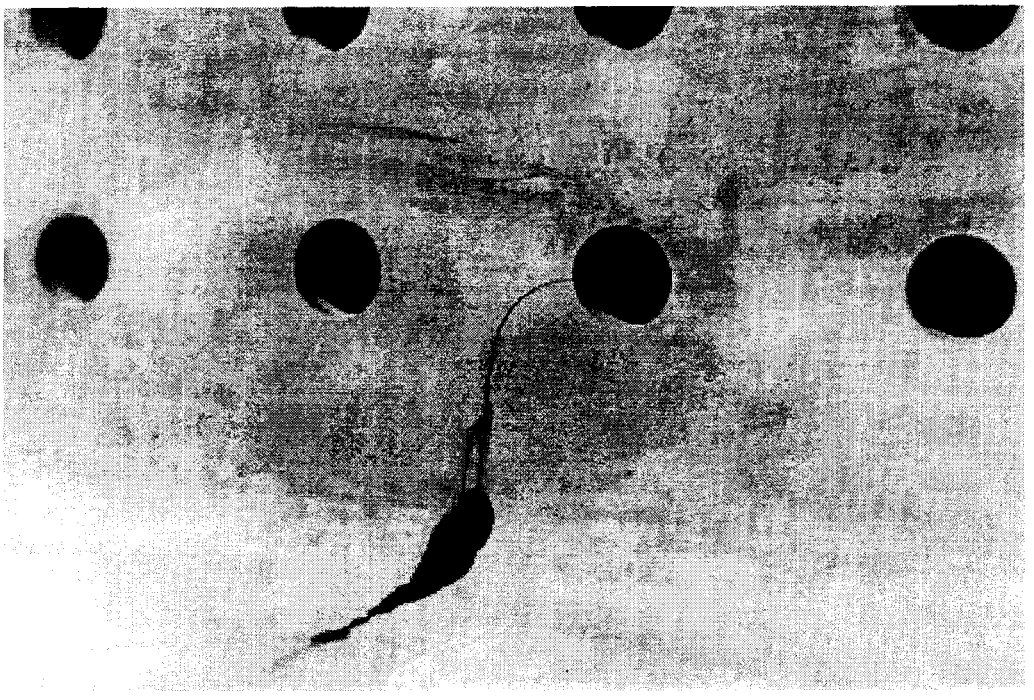

Figure 4.6: Final Web Crack of Laboratory Specimen

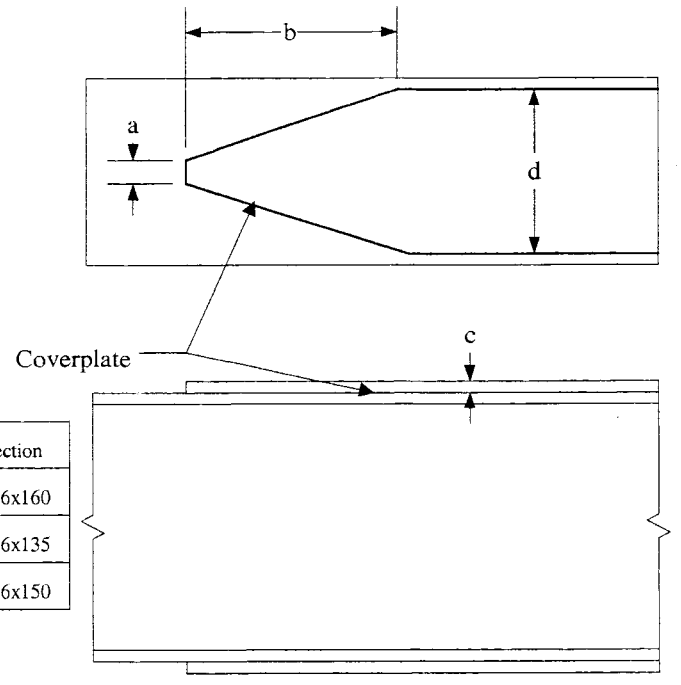

Bridge	a	b	c	d	Section
BR 62066	3 in.	1.5 ft.	1.375 in	10.5 in	W36x160
BR 27855	4 in.	1.5 ft.	0.5 in.	10 in.	W36x135
BR 9276	2 in.	2 ft.	1 in.	10 in.	W36x150

Figure 5.1: Cover Plate Detail

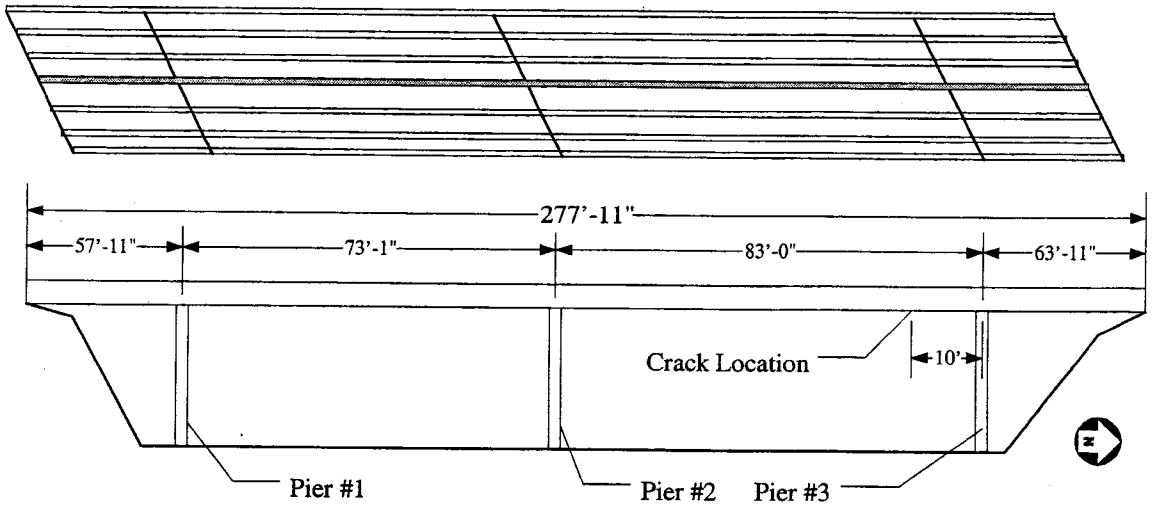

Figure 5.2: Pier Layout West 7th Street Bridge

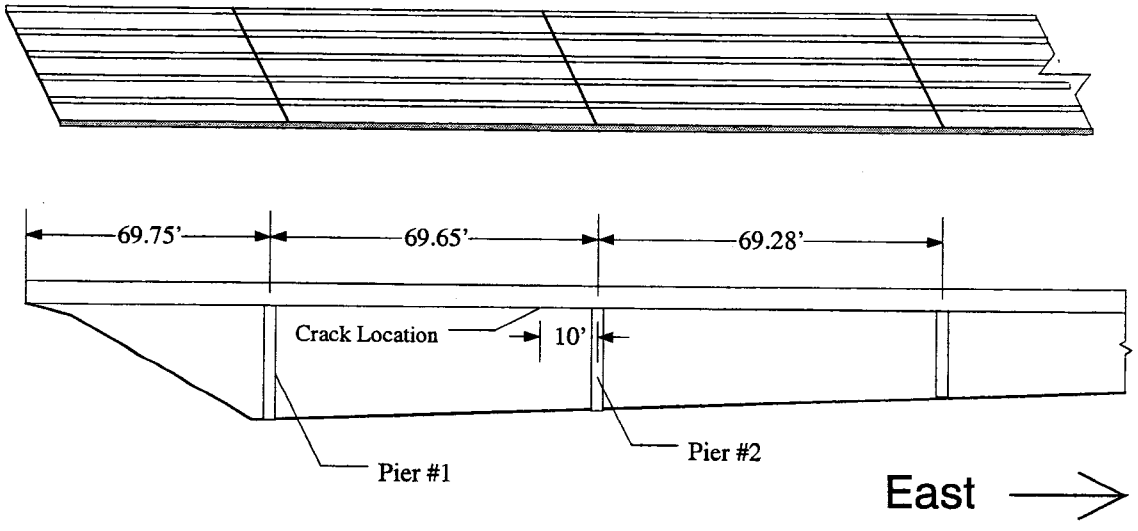

Figure 5.3: Pier Layout I-94

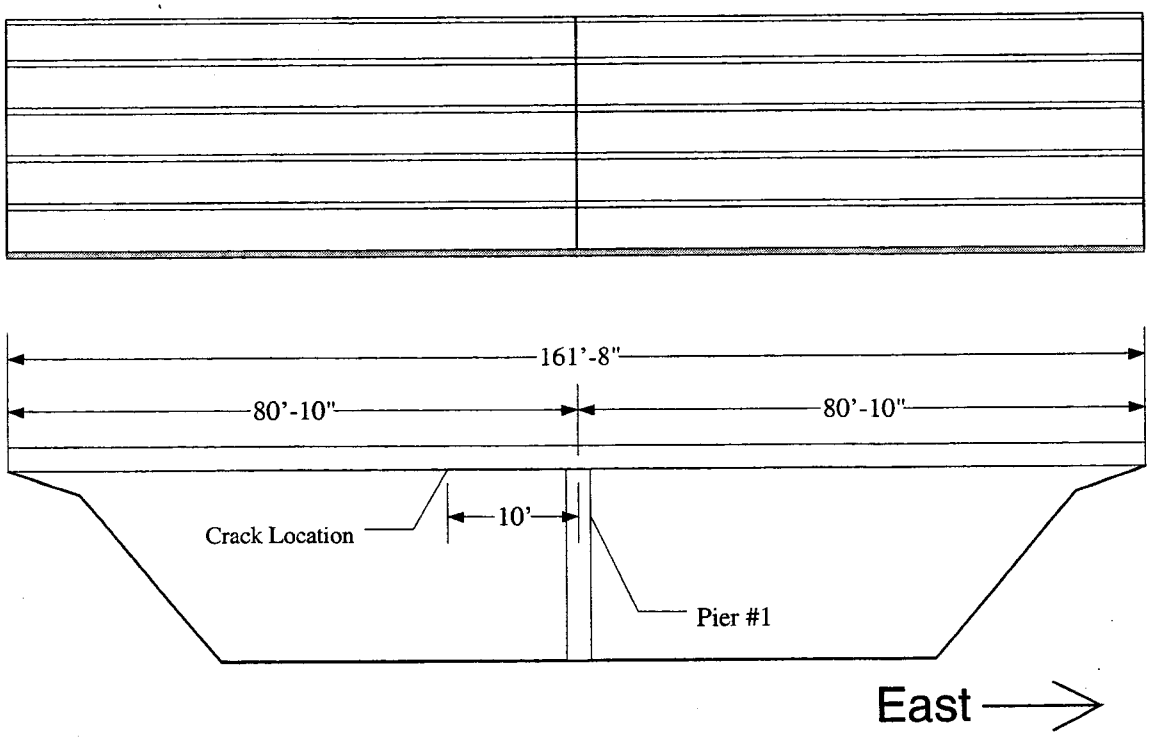

Figure 5.4: Pier Layout TH-36

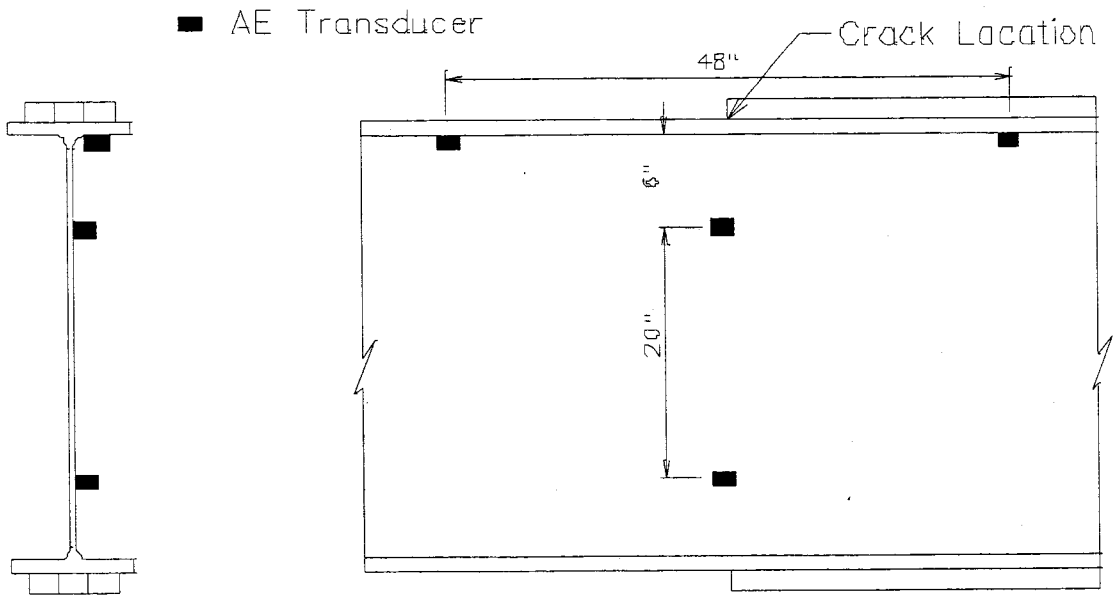

Figure 5.5: Typical AE Transducer Location on Bridges

Bridge	a	b	c	d
BR 62066	1.0"	12"	24"	35"
BR 27855	0.79"	11.79"	24.55"	34.76"
BR 9276	0.94"	11.94"	23.9"	34.9"

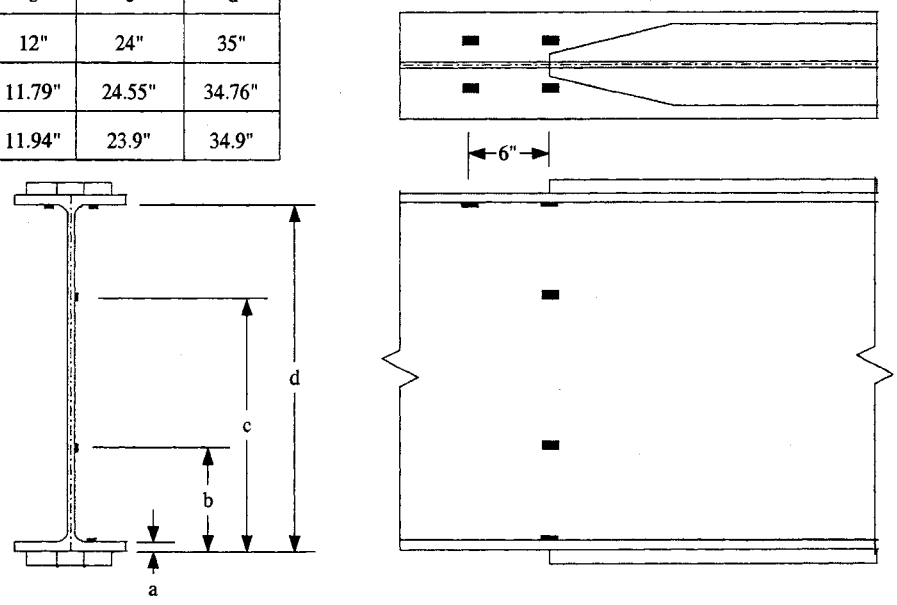

Figure 5.6: Strain Gage Locations on Bridges Before Retrofit

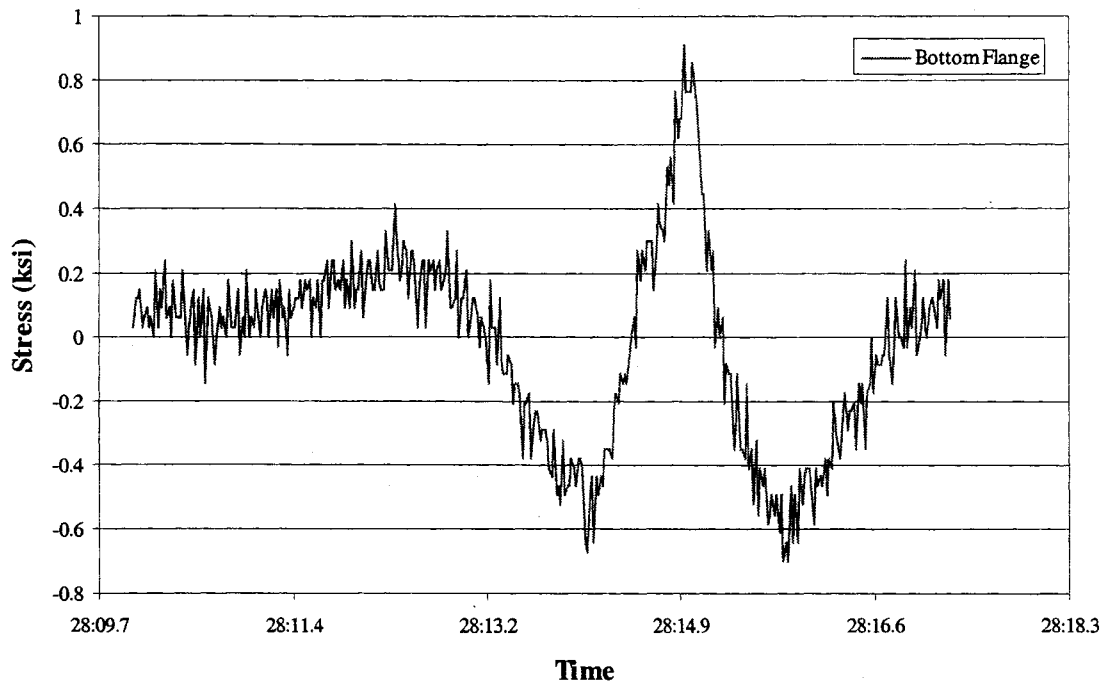

Figure 5.7: Typical Unfiltered Stress Data

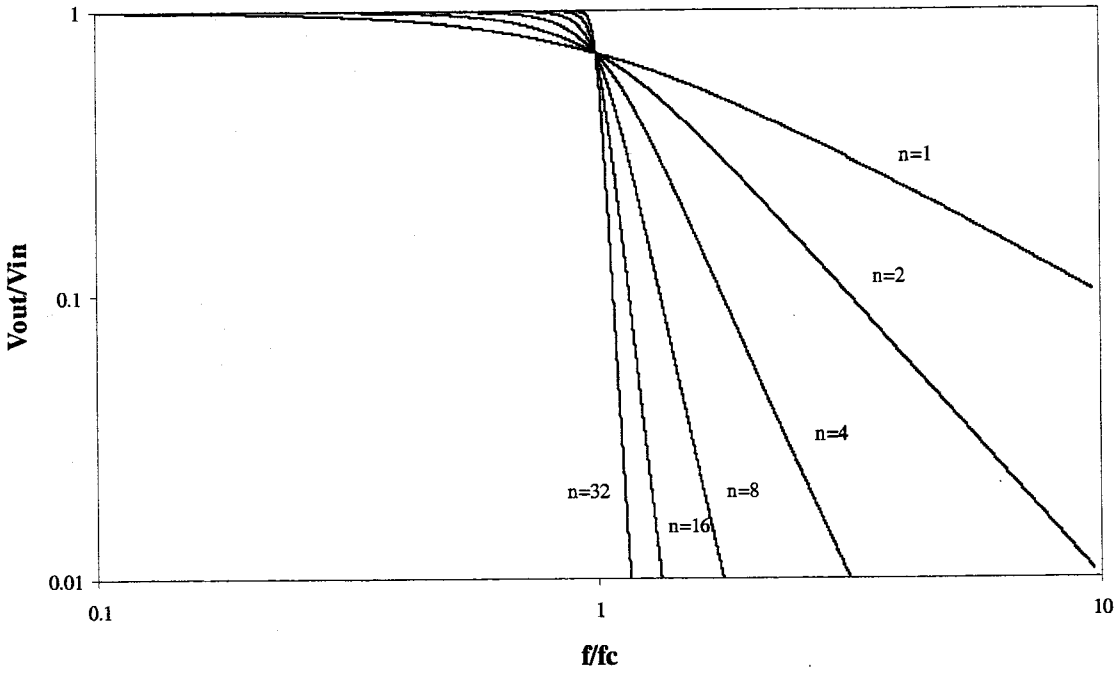

Figure 5.8: Order Effects on Low Pass Butterworth Digital Filter

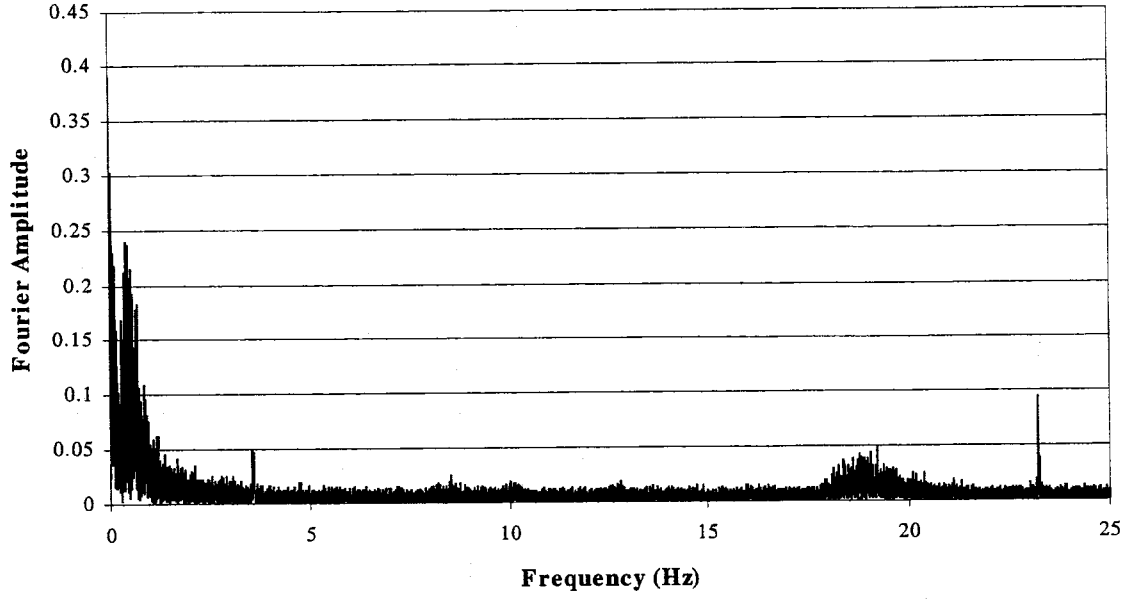

Figure 5.9: Fast Fourier Transform of Unfiltered Data

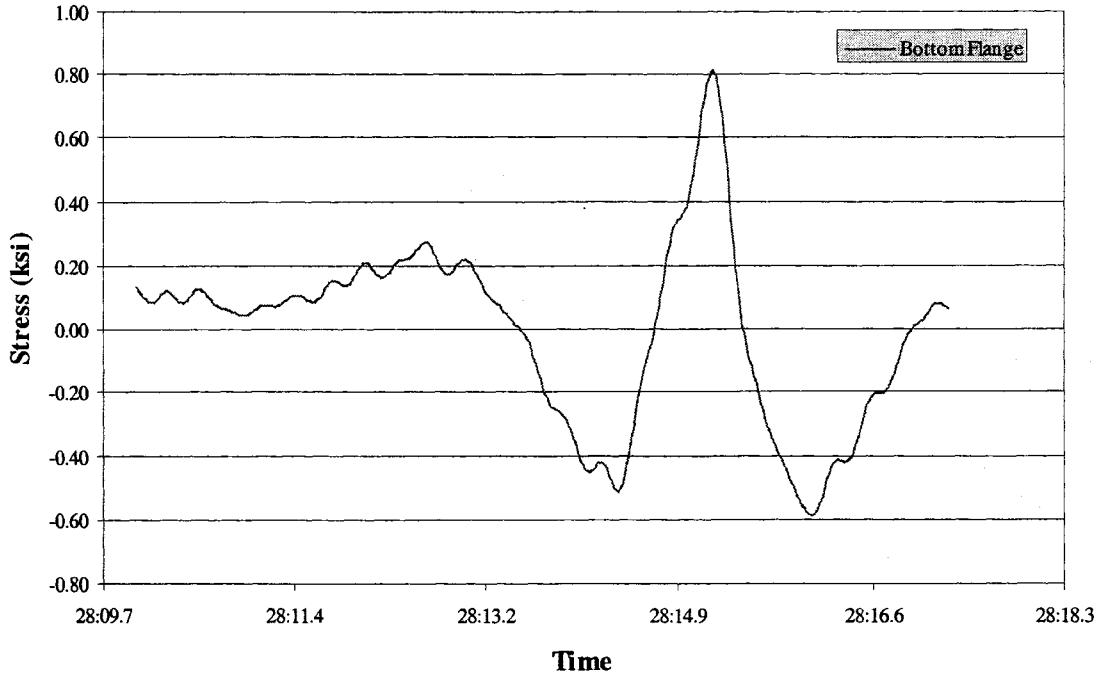

Figure 5.10: Typical Filtered Stress Data

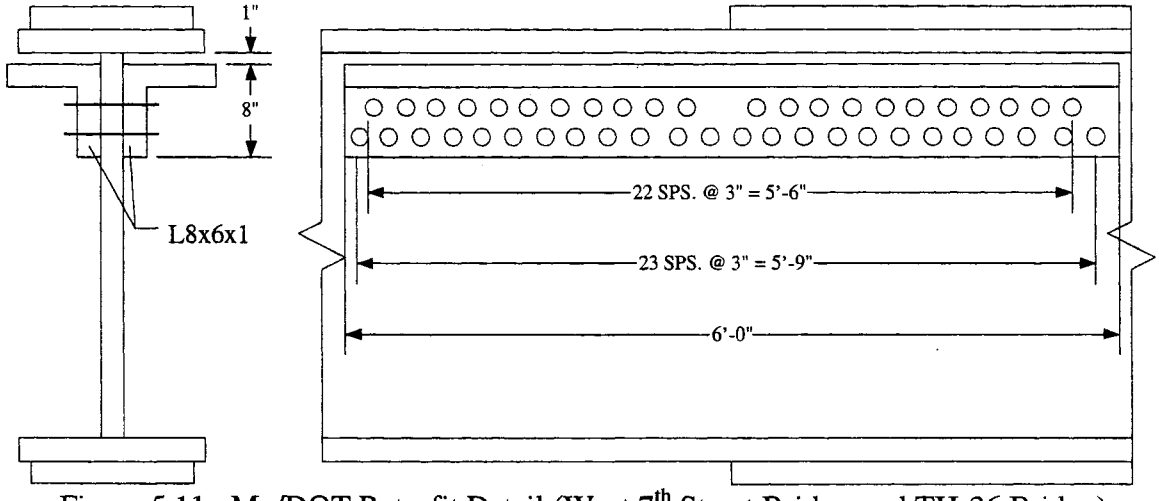

Figure 5.11: Mn/DOT Retrofit Detail (West 7th Street Bridge and TH-36 Bridge)

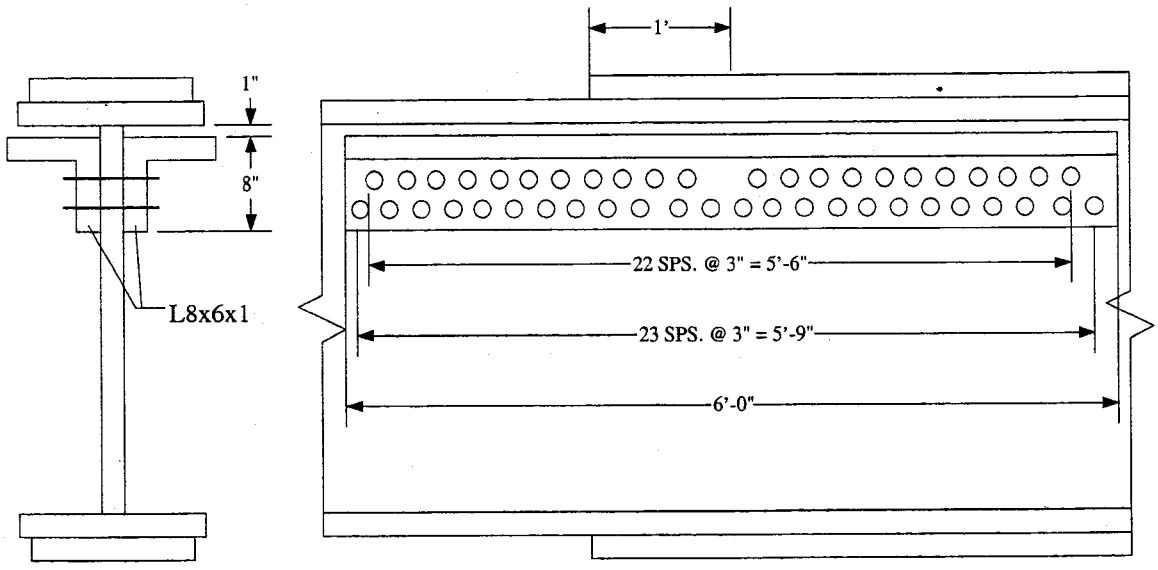

Figure 5.12: Mn/DOT Retrofit Detail (I-94 Bridge)

Bridge	a	b
BR 62066	29.63"	33.13"
BR 27855	29.18"	32.68"
BR 9276	29.48"	32.98"

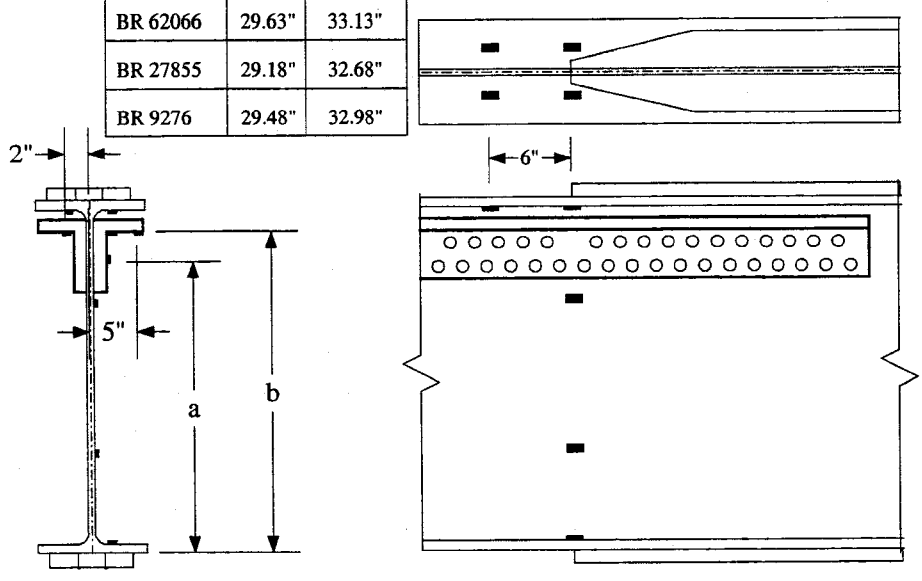

Figure 5.13: Strain Gage Locations for Bridges After Retrofit

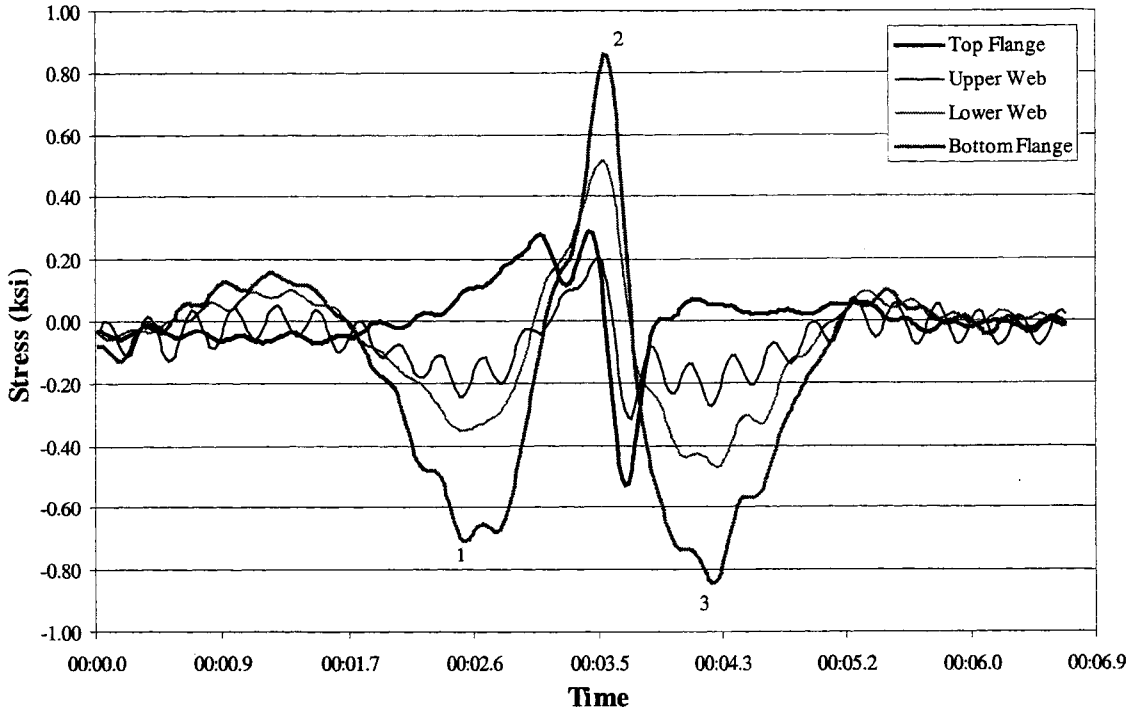

Figure 6.1: West 7th Street Bridge Northbound Stress History

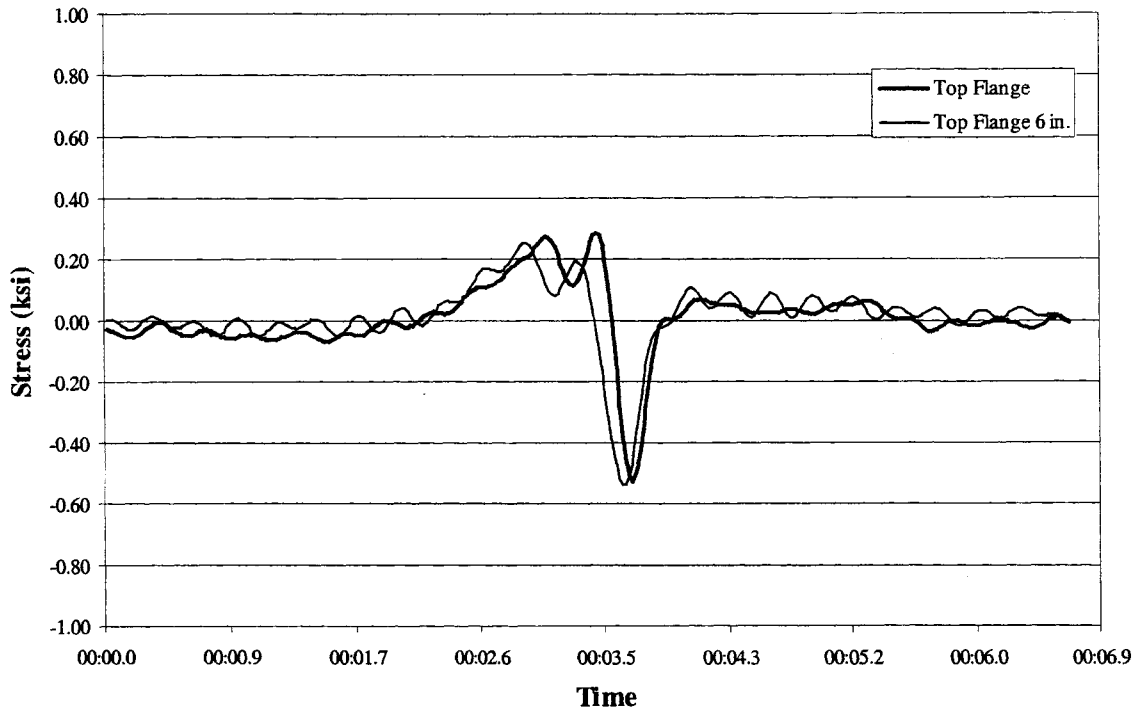

Figure 6.2: West 7th Street Bridge Northbound Stress History Offset Gage

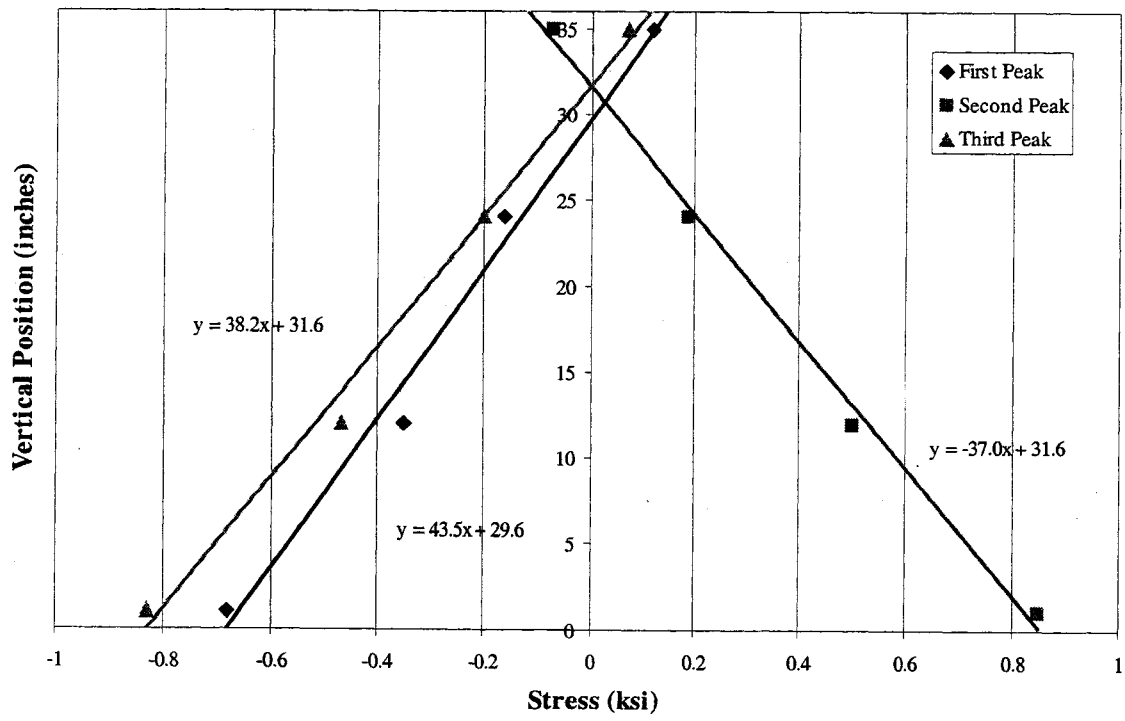

Figure 6.3: West 7th Street Bridge Northbound Stress Distribution

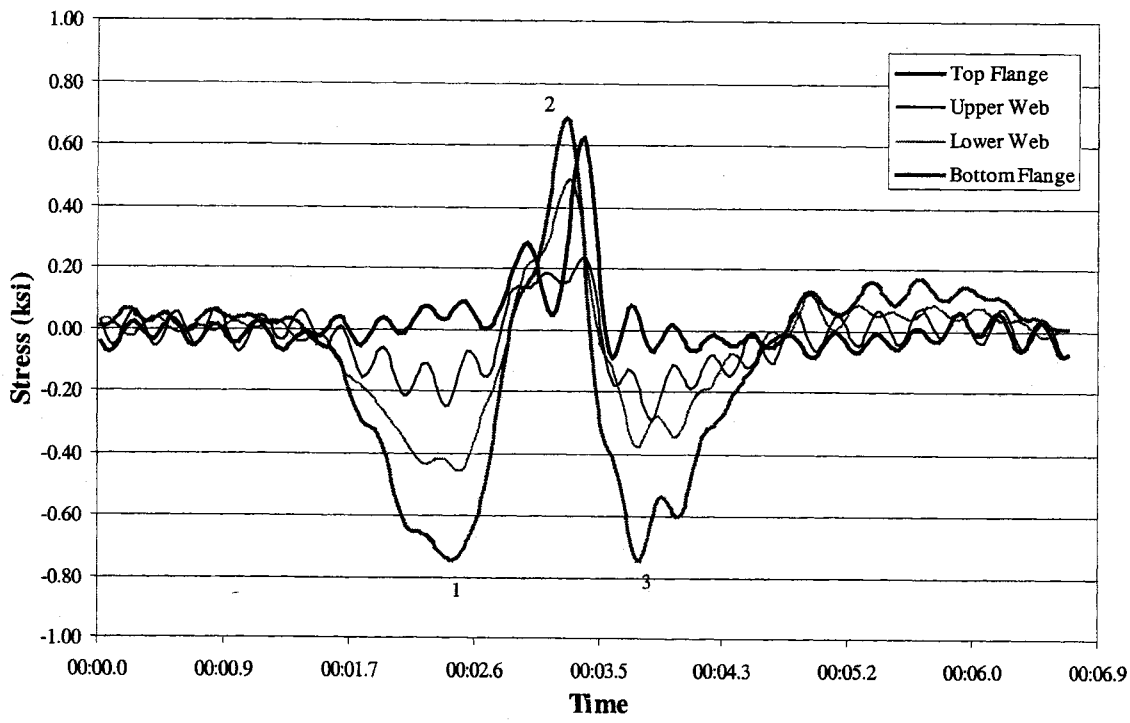

Figure 6.4: West 7th Street Bridge Southbound Stress History

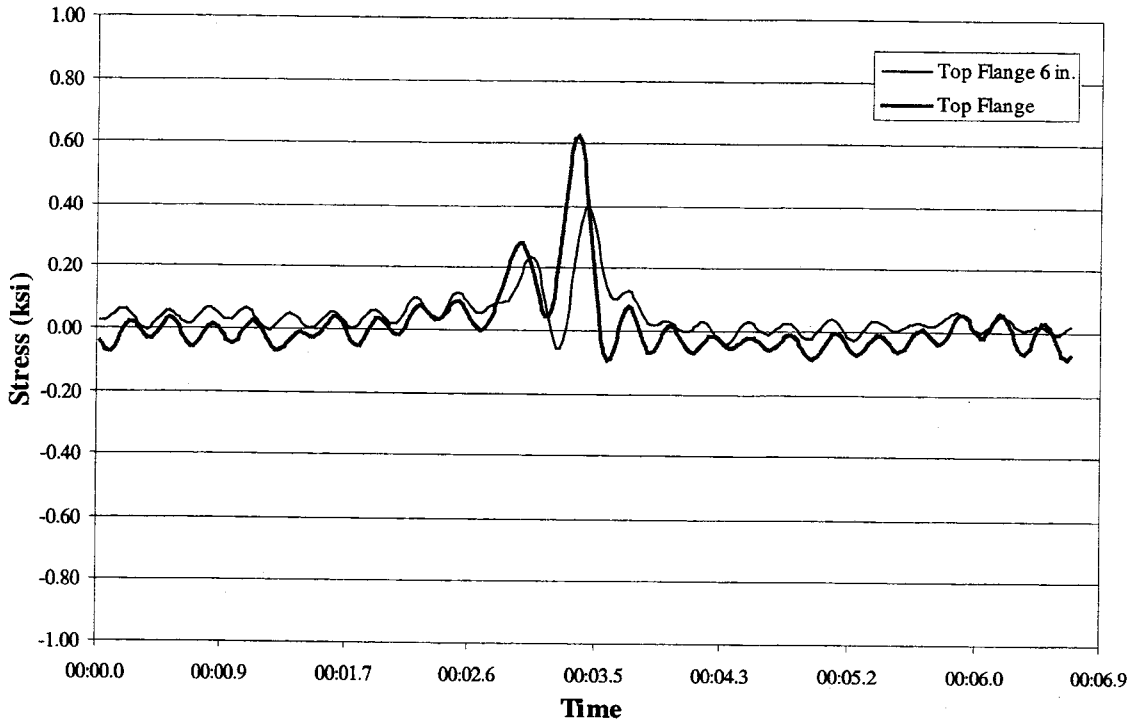

Figure 6.5: West 7th Street Bridge Southbound Stress History Offset Gage

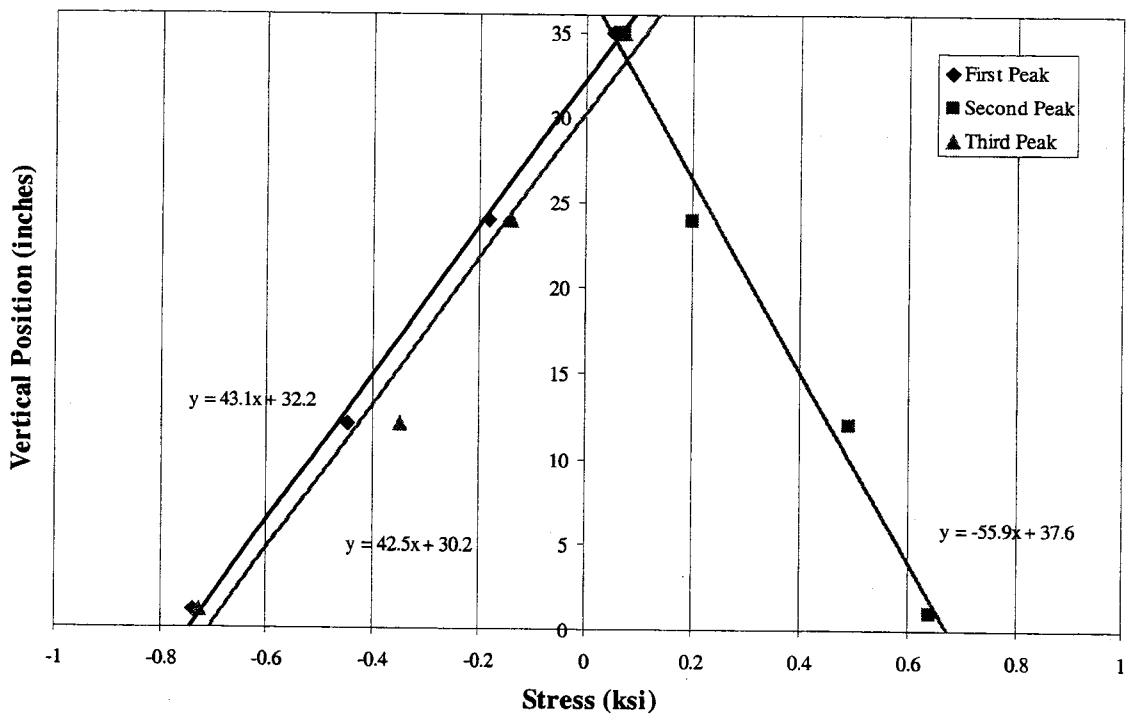

Figure 6.6: West 7th Street Bridge Southbound Stress Distribution

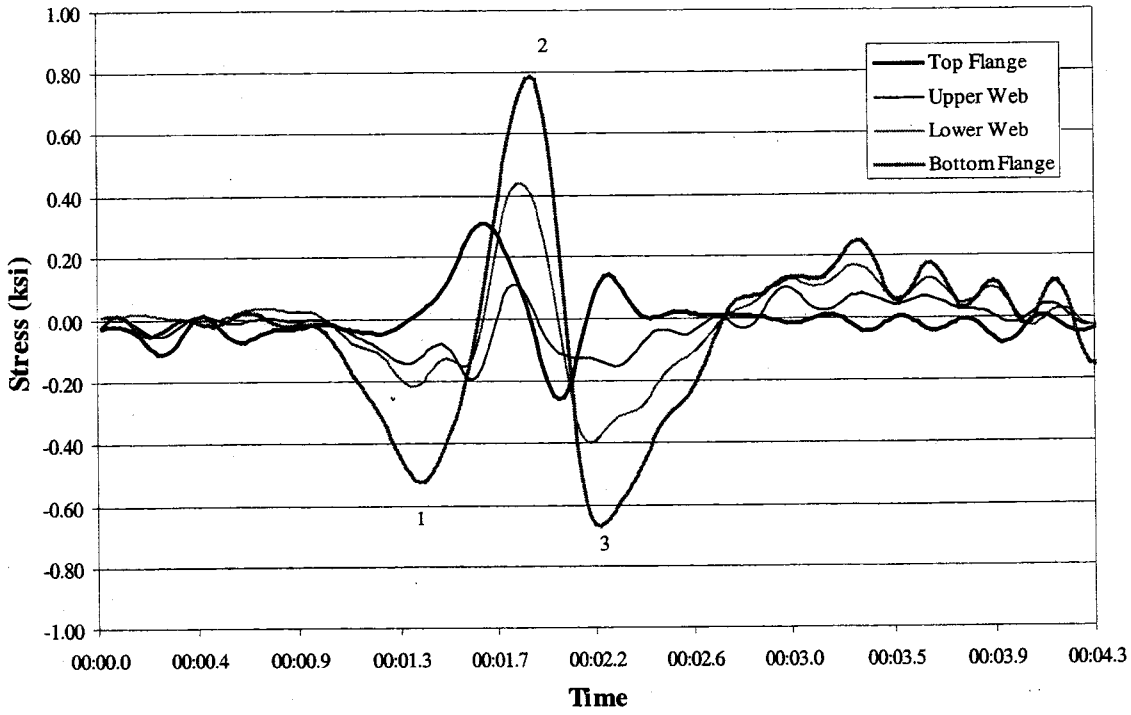

Figure 6.7: I-94 Bridge Stress History Before Retrofit

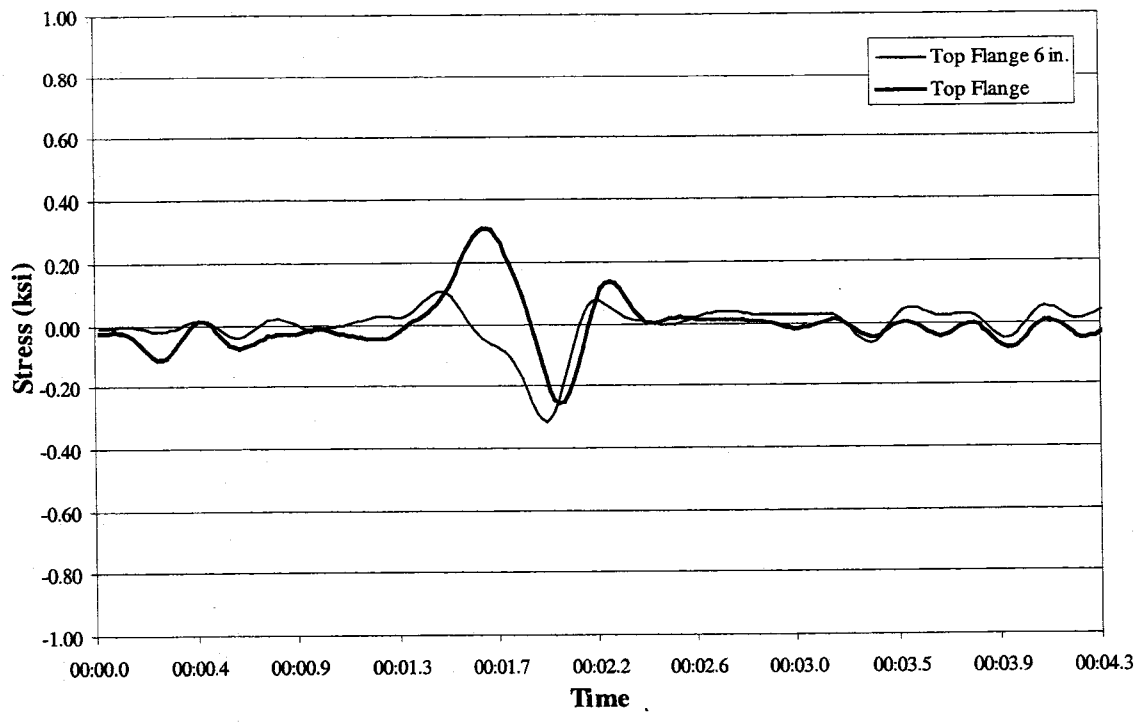

Figure 6.8: I-94 Bridge Stress History Before Retrofit Offset Gage

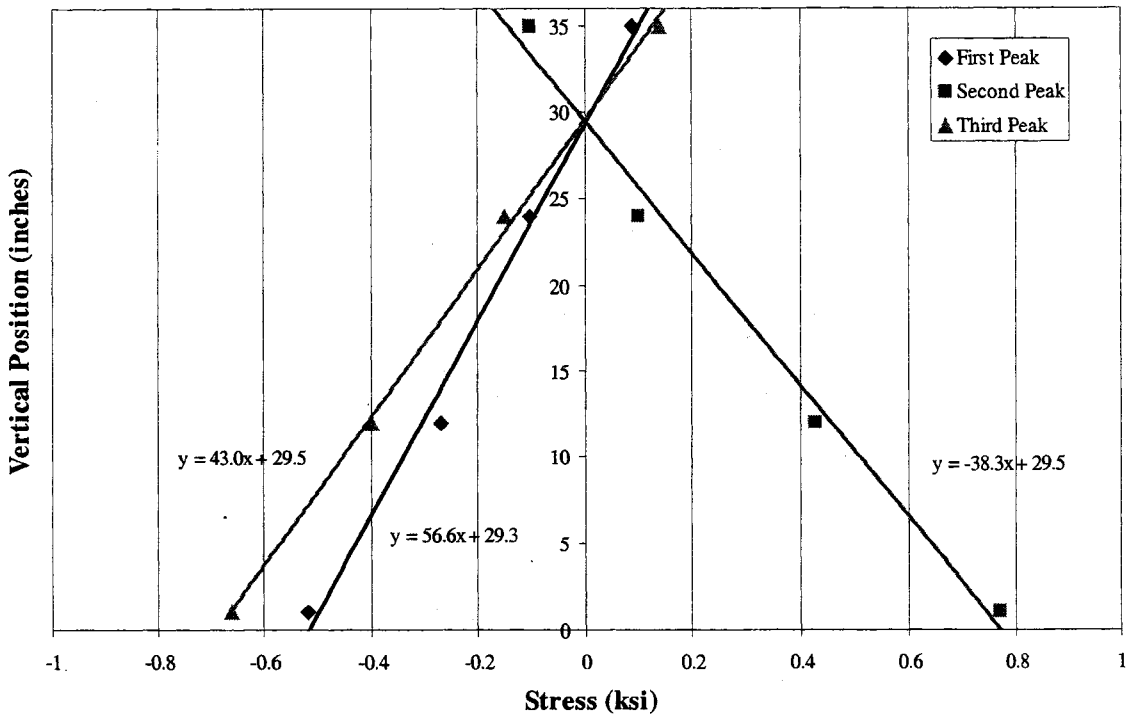

Figure 6.9: I-94 Bridge Stress Distribution Before Retrofit

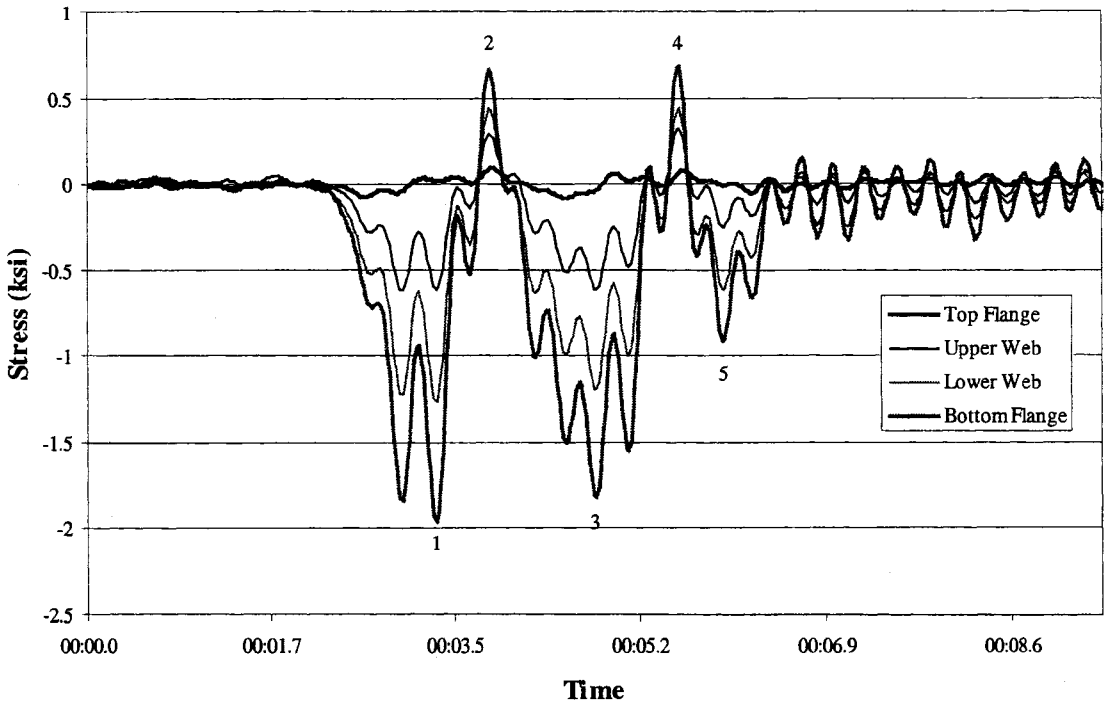

Figure 6.10: TH-36 Bridge Stress History Before Retrofit

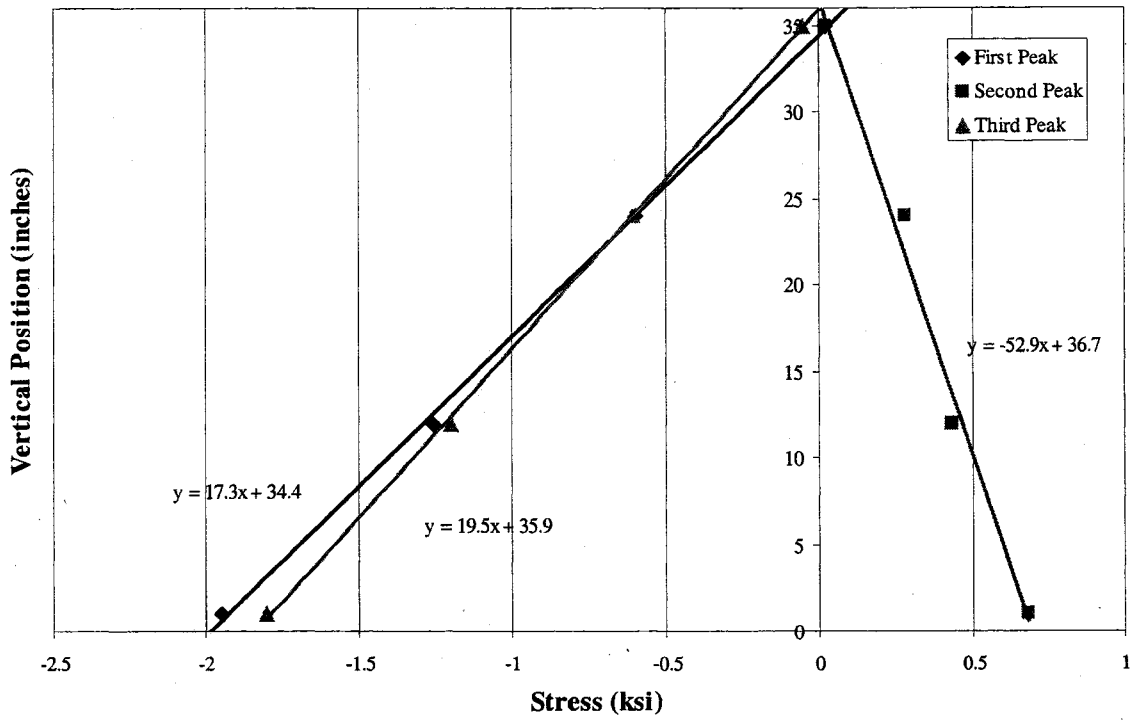

Figure 6.11: TH-36 Bridge Stress Distribution Before Retrofit

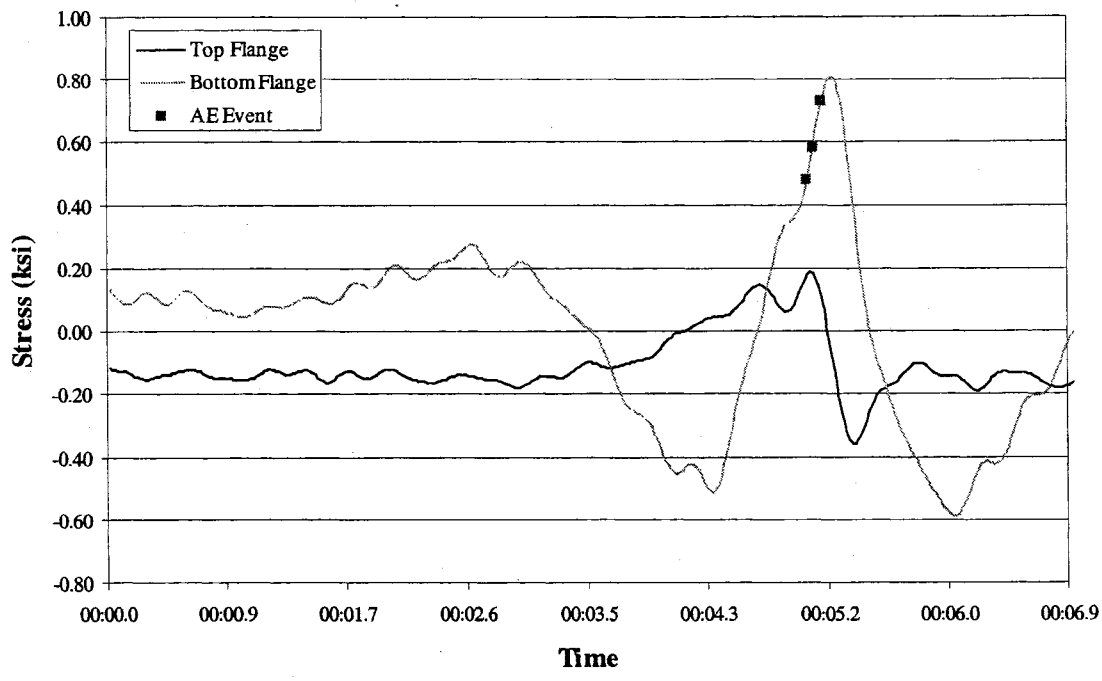

Figure 6.12: Three AE Crack Events for One Truck Pass

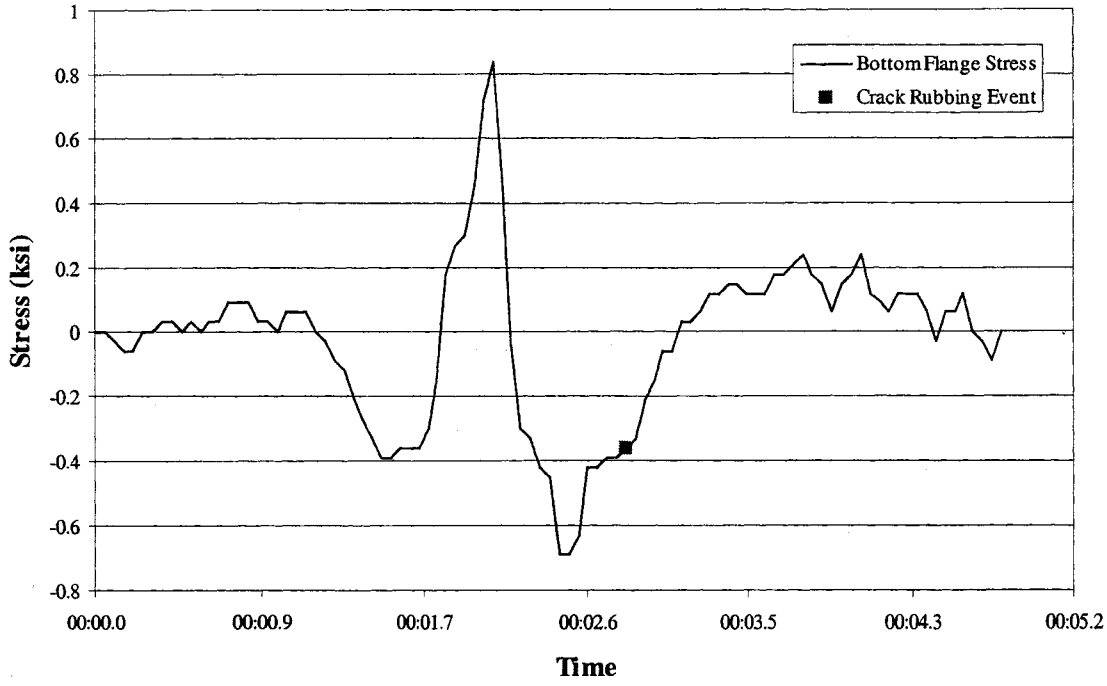

Figure 6.13: Crack Rubbing Event on I-94 Shown Against Bottom Flange Stress

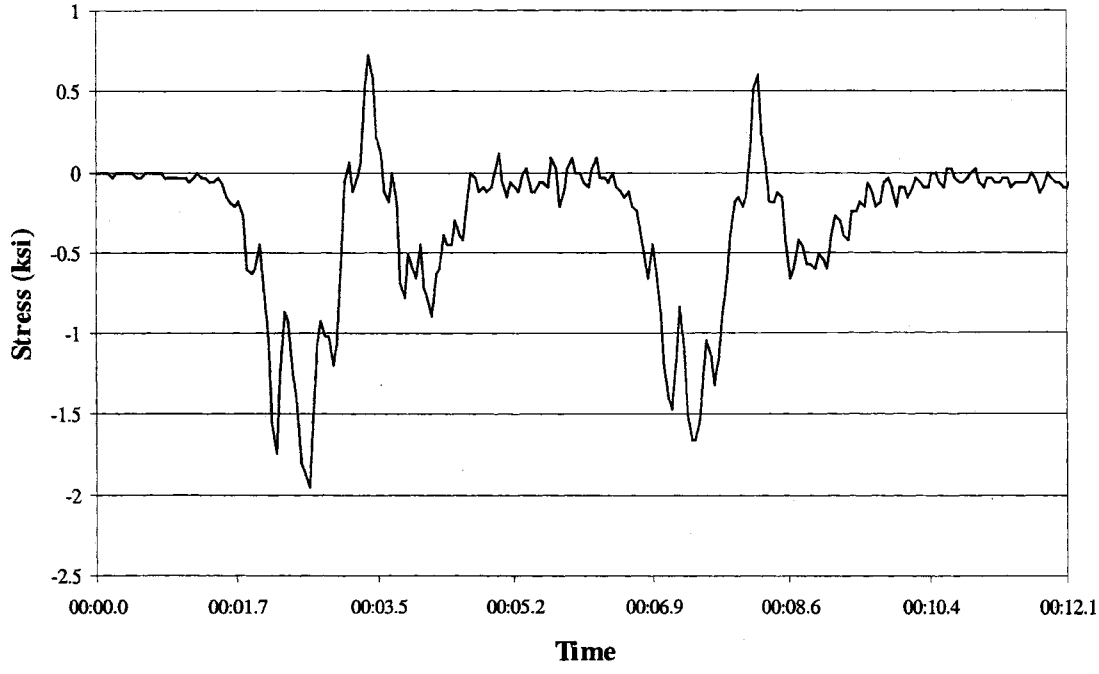

Figure 6.14: Strain in the Bottom Flange of TH-36 with Trucks Adaquately Spaced

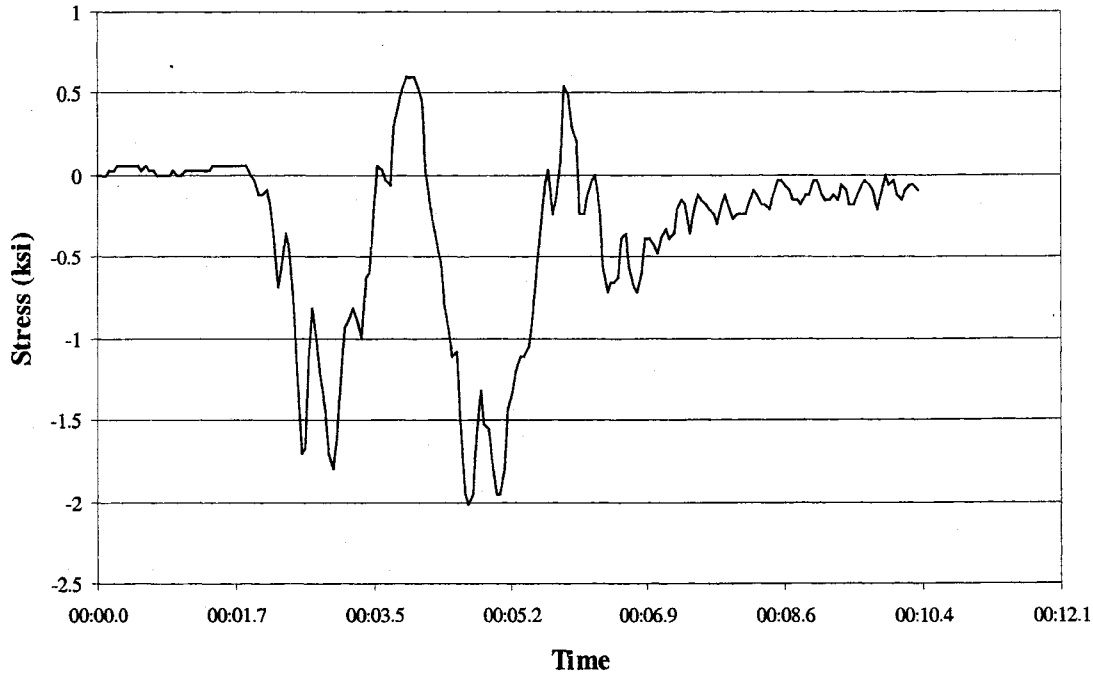

Figure 6.15: Strain in the Bottom Flange on TH-36 with Trucks too Closely Spaced

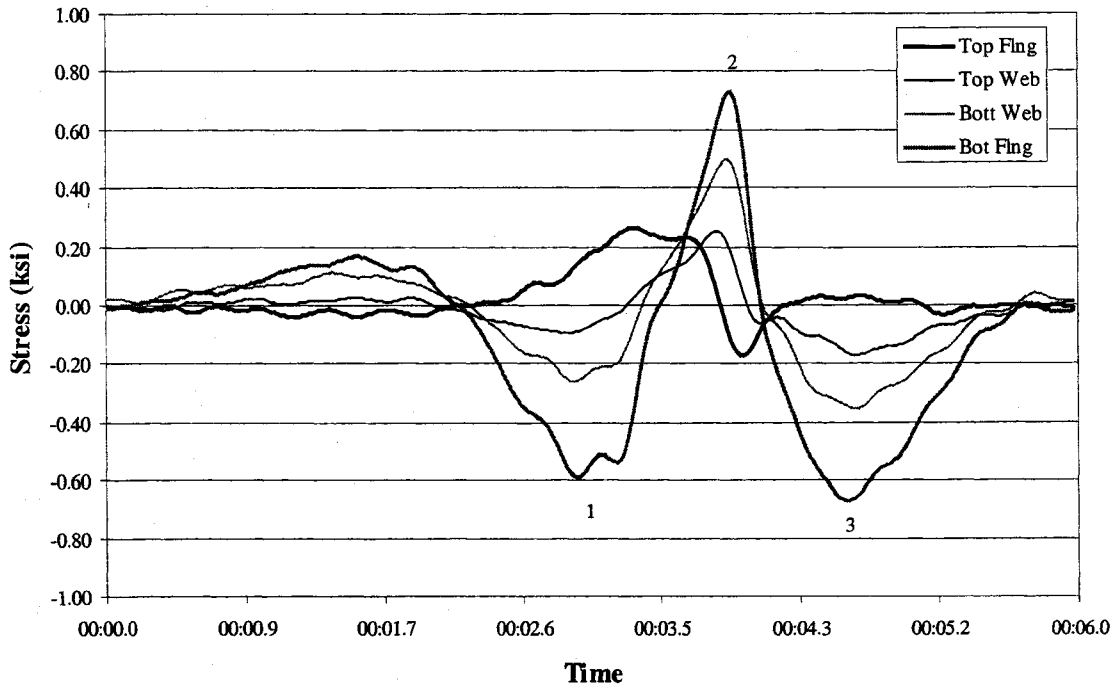

Figure 6.16: West 7th Street Bridge Northbound Stress History After Retrofit

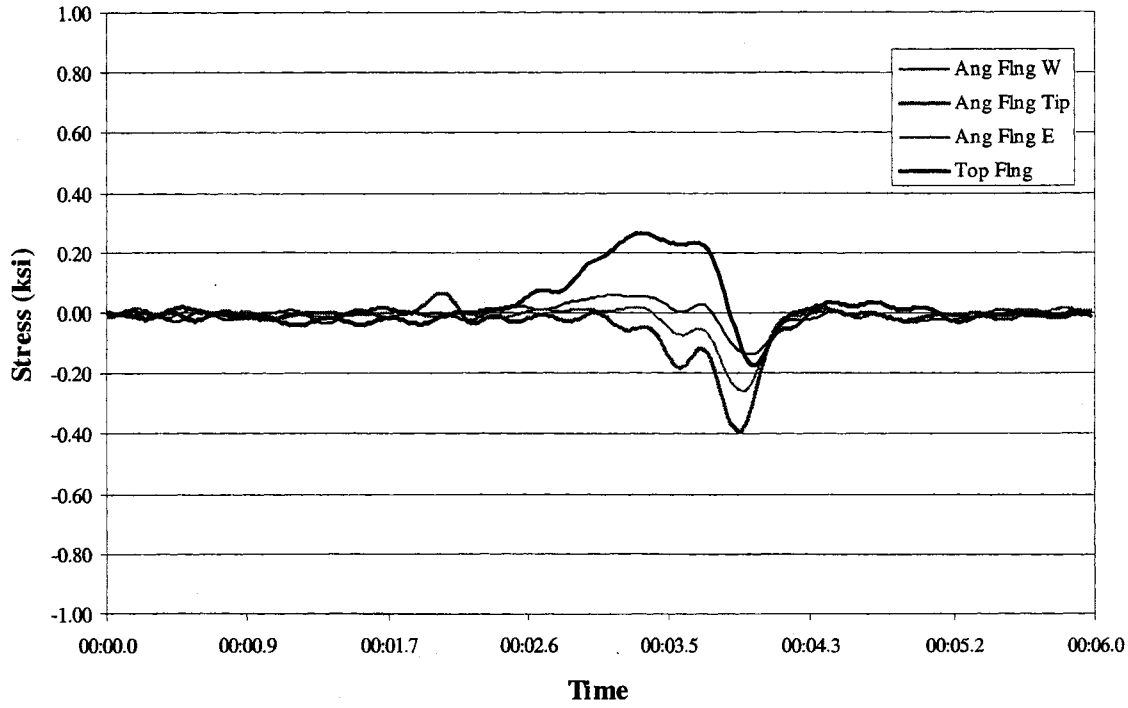

Figure 6.17: West 7th Street Bridge Northbound Stress History Angle Gage After Retrofit

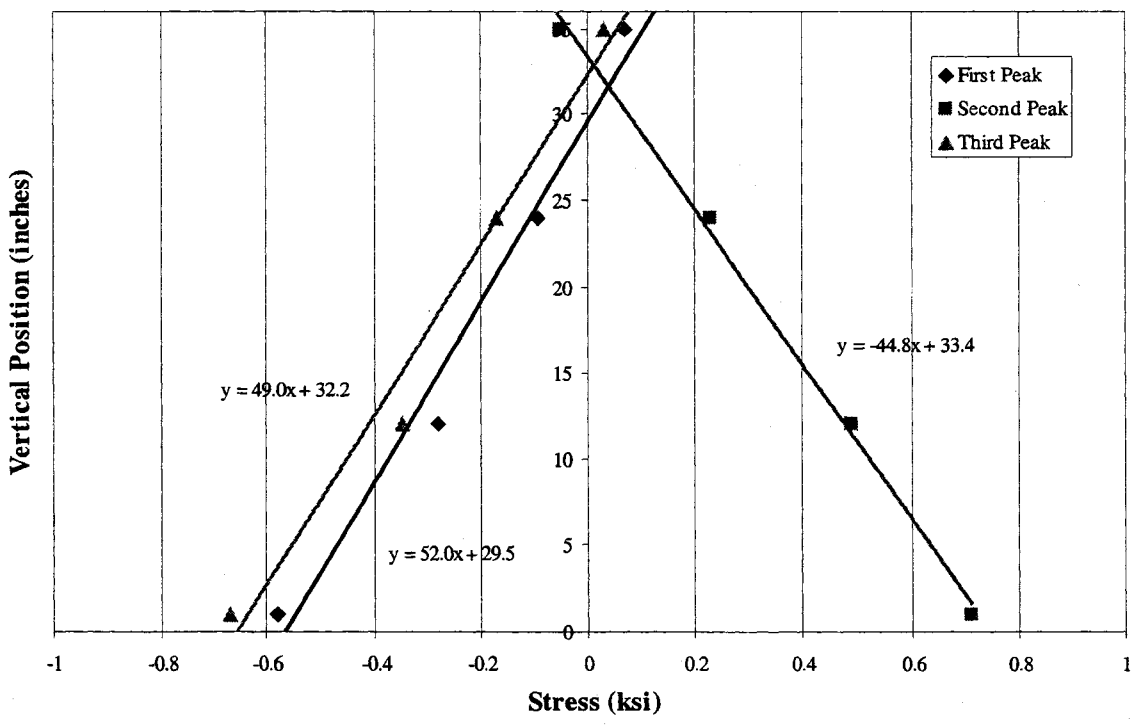

Figure 6.18: West 7th Street Bridge Northbound Stress Distribution After Retrofit

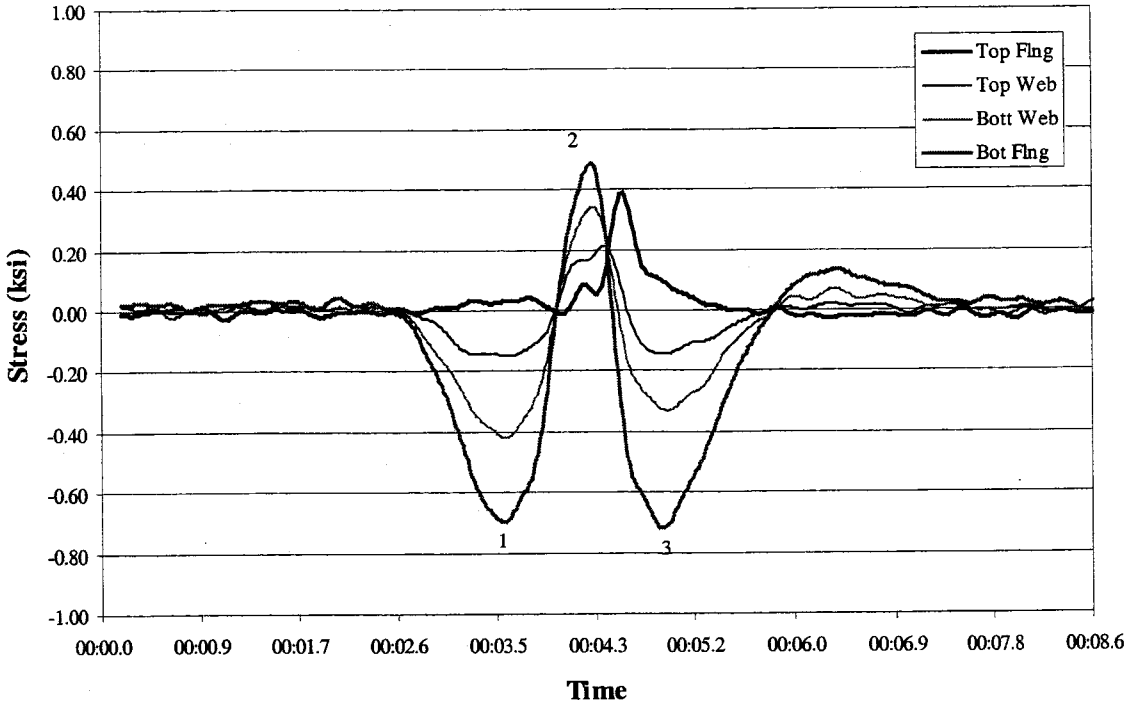

Figure 6.19: West 7th Street Bridge Southbound Stress History After Retrofit

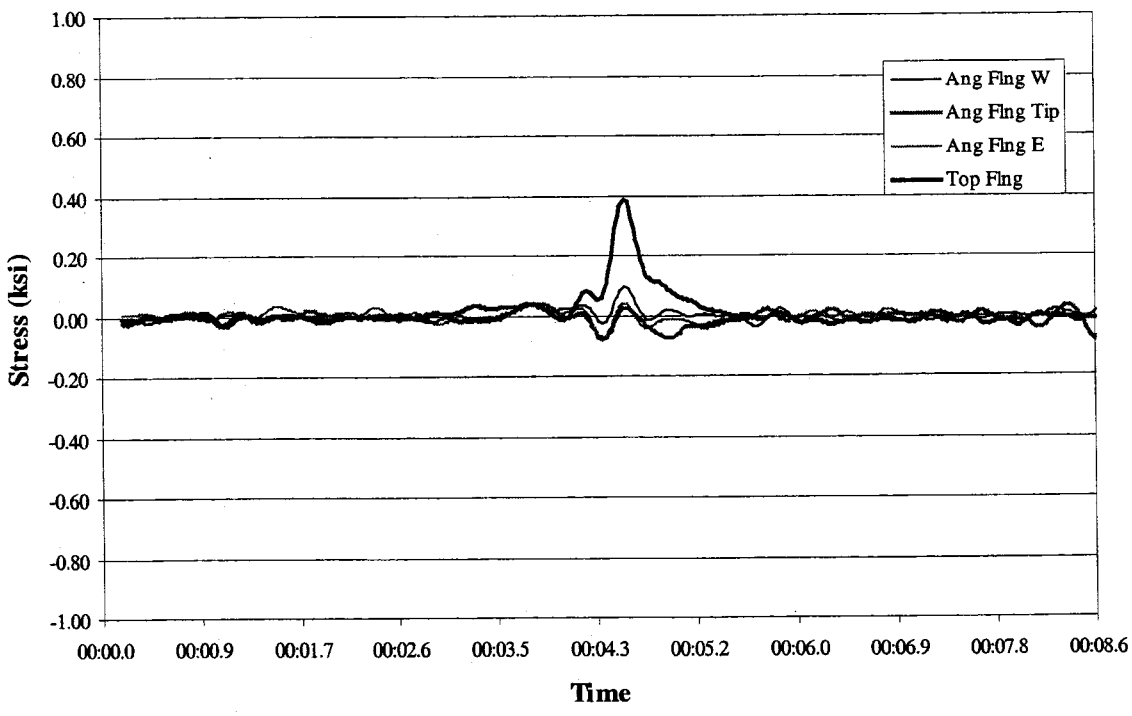

Figure 6.20: West 7th Street Bridge Southbound Stress History Angle Gage After Retrofit

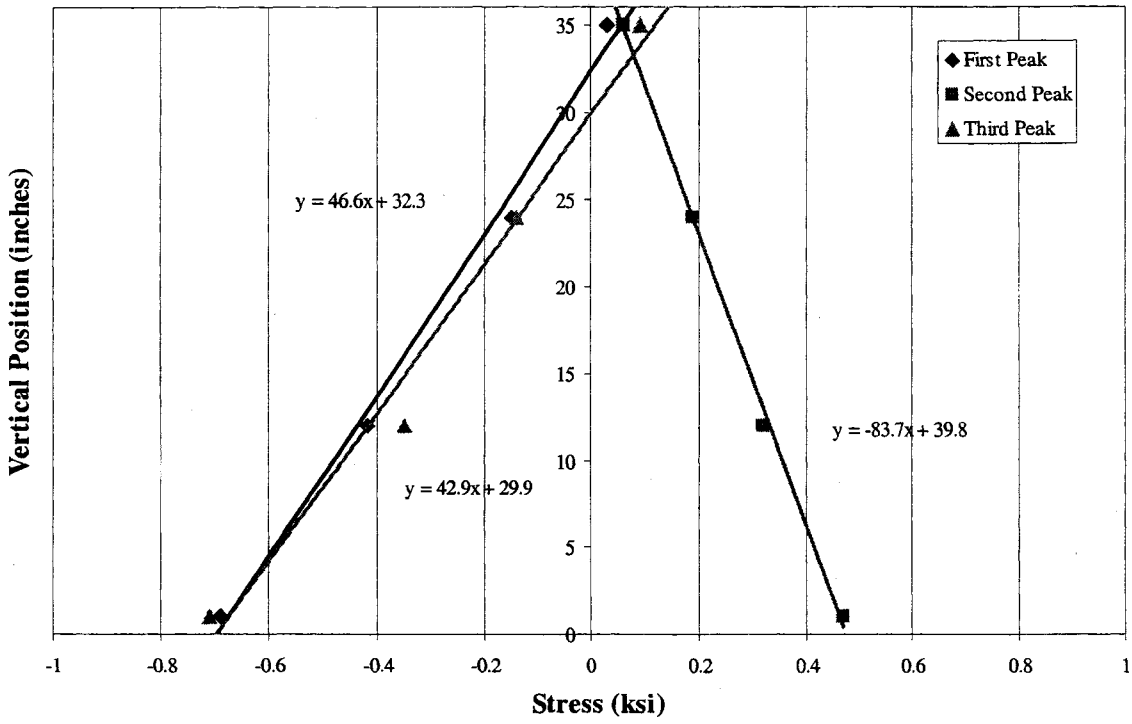

Figure 6.21: West 7th Street Bridge Southbound Stress Distribution After Retrofit

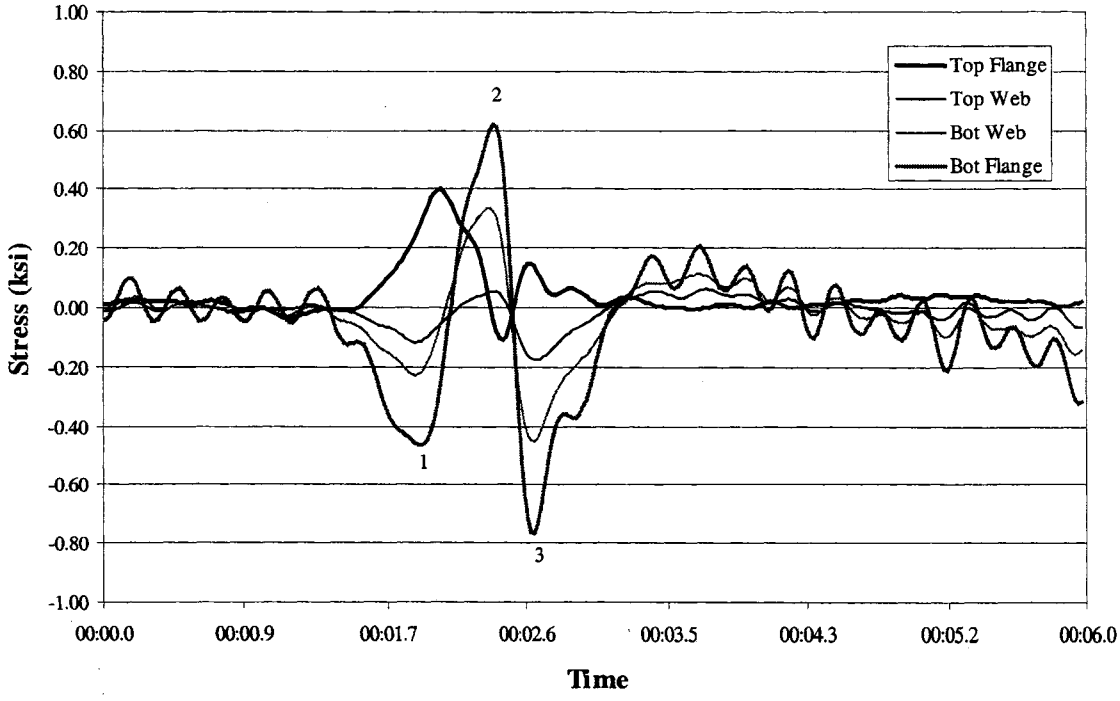

Figure 6.22: I-94 Bridge Stress History After Retrofit

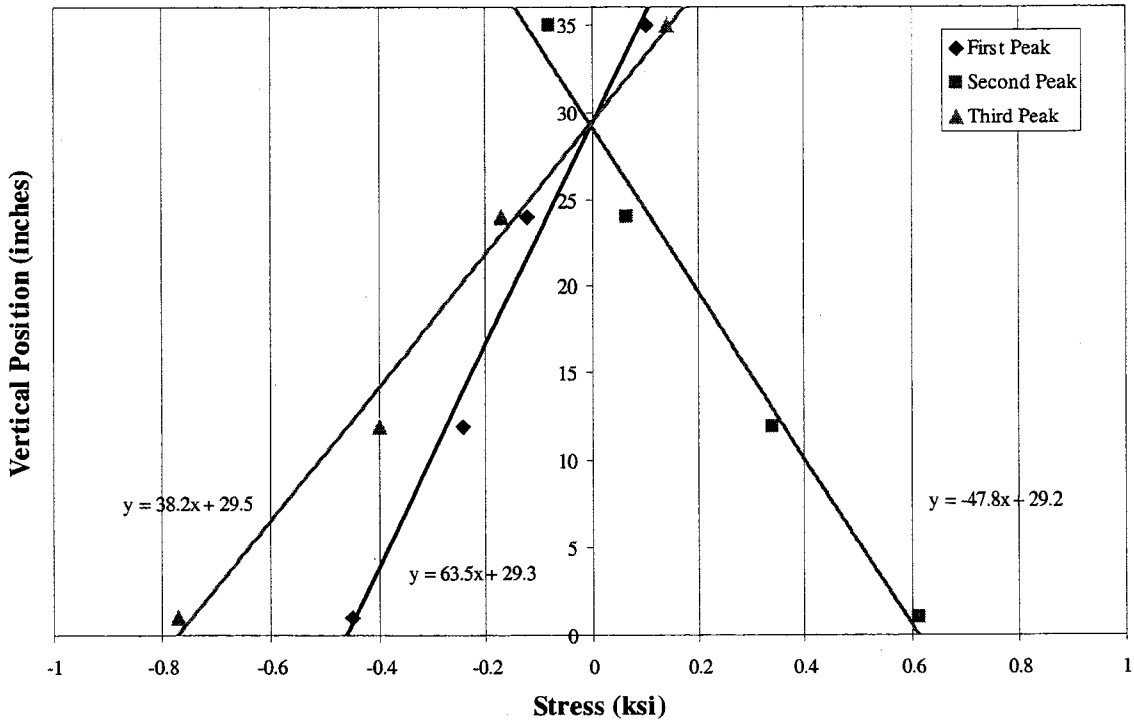

Figure 6.23: I-94 Bridge Stress Distribution After Retrofit

Appendix A

Section Properties

Laboratory Girder Calculation

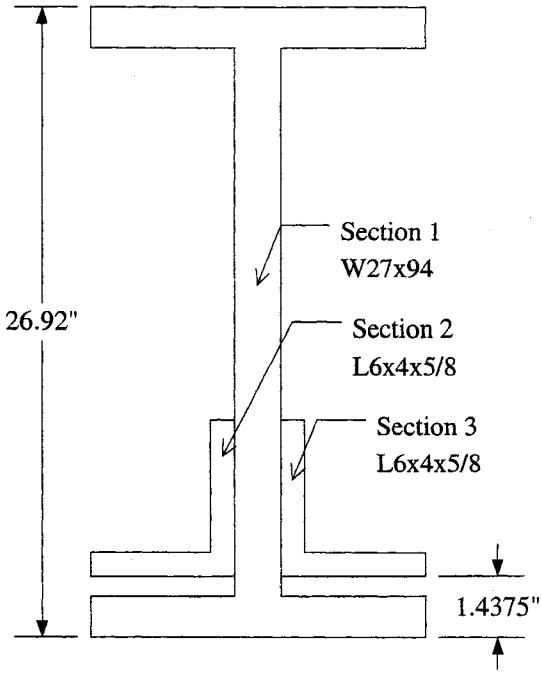

Calculate Moment of Inertia and Centroid from Bottom Fiber

Section	1	2	3
Designation	W27x94	Angle 1	Angle 2
Area (in^2)	27.7	5.86	5.86
I_{xx} (in^4)	3270	21.1	21.1
y (in)	13.46	3.52	3.52

Section	Area (in^2)	y (in)	A * y (in^3)	I_{xx} (in^4)	Y-y (in.)	$A(Y-y)^2$ (in^4)	Total I_{xx} (in^4)
1	27.7	13.46	372.8	3270	-2.96	241.92	3511.92
2	5.86	3.52	20.6	21.1	6.98	285.89	306.99
3	5.86	3.52	20.6	21.1	6.98	285.89	306.99
	39.42		414.1				4125.90

Calculate Centroid

Y = Sum (A*y)/ Sum A = 10.5 in.

New Section Modulus

$S_{bot} := 392.94$

$S_{top} := 251.27$

Old Section Modulus

$S_{bot} := 243$

$S_{top} := 243$

Stress can be calculated using the following:

$$\sigma_{before} := \frac{M_{before}}{S_{before}} \qquad \sigma_{after} := \frac{M_{after}}{S_{after}}$$

Assume the moment imposed before retrofit is equal to that after retrofit attatc

$$M_{before} := M_{after}$$

Then compare stress reduction to section modulus change

$$\frac{\sigma_{before} - \sigma_{after}}{\sigma_{before}} = 1 - \frac{S_{before}}{S_{after}}$$

Bottom Flange Comparison

Reduction in Stress = $\frac{9.8 - 5.7}{9.8} = 0.418$ is 42%

Section Modulus Change = $1 - \frac{243}{392.94} = 0.382$ is 38%

Bridge Girder Calculation

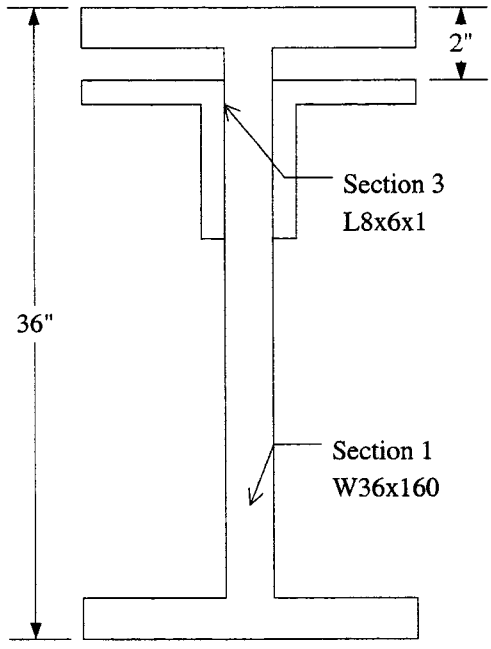

Calculate Moment of Inertia and Centroid from Bottom Fiber

Section	1	2	3
Designatic	W27x94	Angle 1	Angle 2
Area (in^2)	47	13	13
I_{xx} (in^4)	9750	80.8	80.8
y (in)	18	31.35	31.35

Section	Area (in^2)	y (in)	A * y (in^3)	I_{xx} (in^4)	Y-y (in.)	$A(Y-y)^2$ (in^4)	Total I_{xx} (in^4)
1	47	18	846.0	9750	4.75	1062.58	10812.58
2	13	31.35	407.6	80.8	-8.60	960.41	1041.21
3	13	31.35	407.6	80.8	-8.60	960.41	1041.21
	73		1661.1				12895.00

Calculate Centroid

Y = Sum (A*y)/ Sum A = 22.75 in.

$Y := 22.75$

$D := 36$

$I := 12895.0$

New Section Modulus

$$\frac{I}{Y} = 566.813 \qquad \frac{I}{D - Y} = 973.208$$

$$S_{bot} = \frac{I}{Y} \qquad S_{top} = \frac{I}{D - Y}$$

New Section Modulus

$S_{bot} := 566.8$

$S_{top} := 973.2$

Old Section Modulus

$S_{bot} := 542$

$S_{top} := 542$

Stress can be calculated using the following:

$$\sigma_{before} := \frac{M_{before}}{S_{before}} \qquad \sigma_{after} := \frac{M_{after}}{S_{after}}$$

Assume the moment imposed before retrofit is equal to that after retrofit attatcl

$$M_{before} := M_{after}$$

Then compare stress reduction to section modulus change

$$\frac{\sigma_{before} - \sigma_{after}}{\sigma_{before}} = 1 - \frac{S_{before}}{S_{after}}$$

Top Flange Comparison

Reduction in Stress = $\frac{0.76 - 0.43}{0.76} = 0.434$ is 43%

Section Modulus Change = $1 - \frac{542}{973.2} = 0.443$ is 44%

Appendix B

Bridge Details

West 7th Street Beam Detail

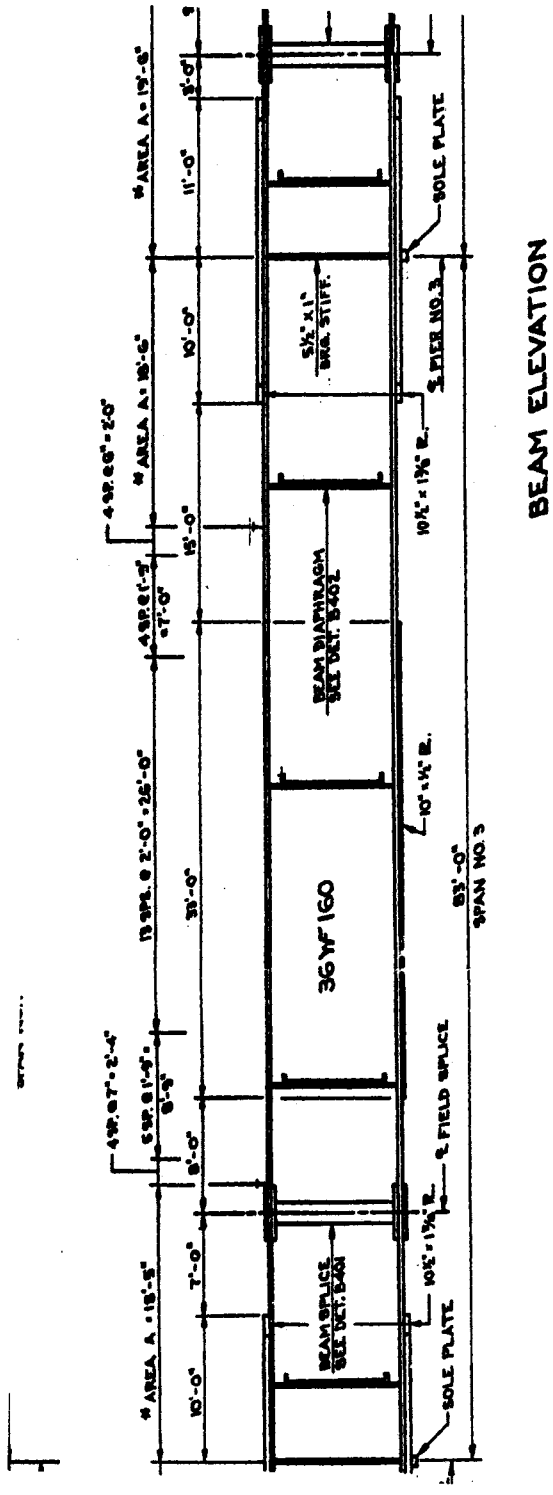

I-94 Beam Detail

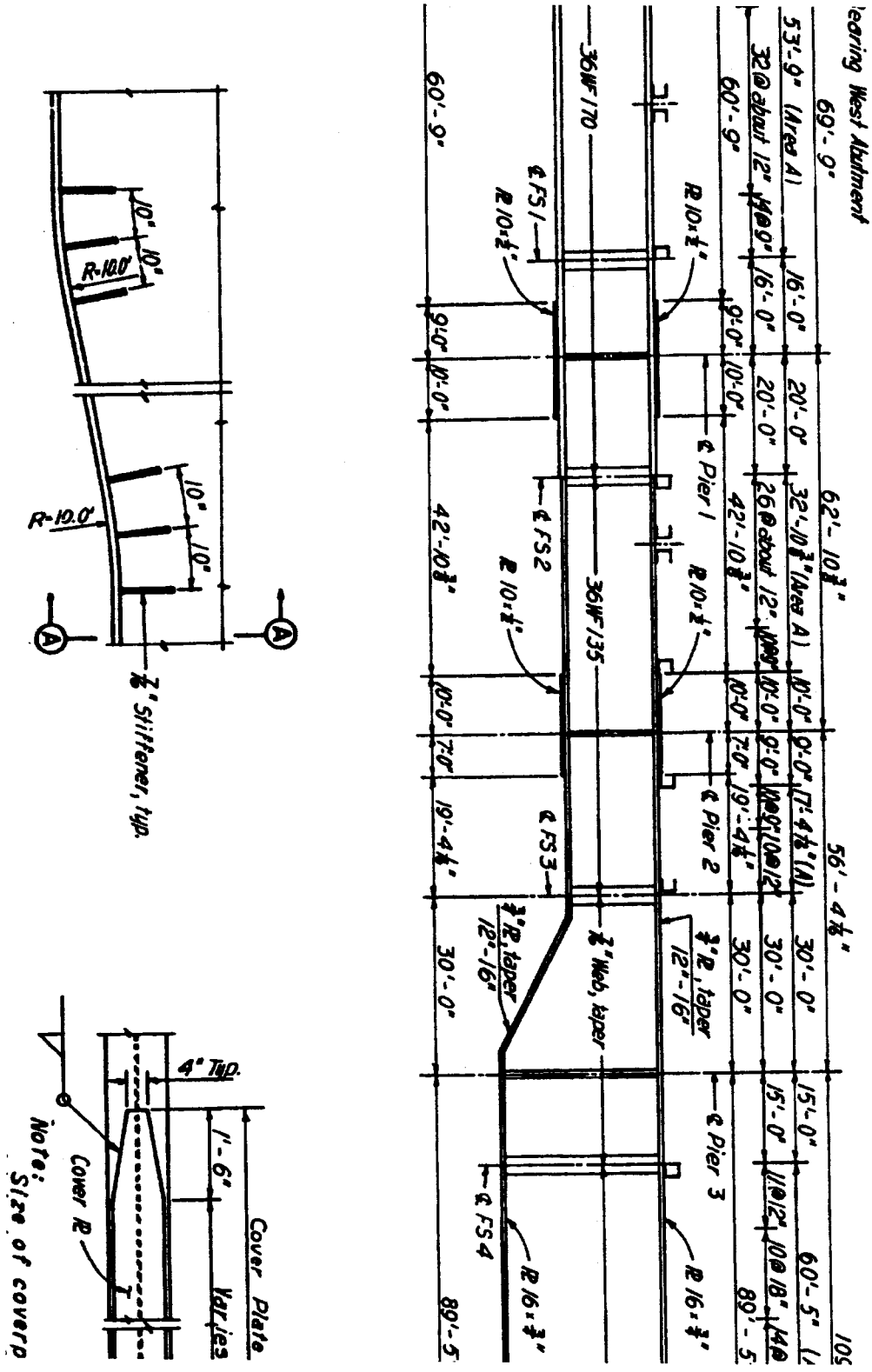

TH-36 Beam Detail

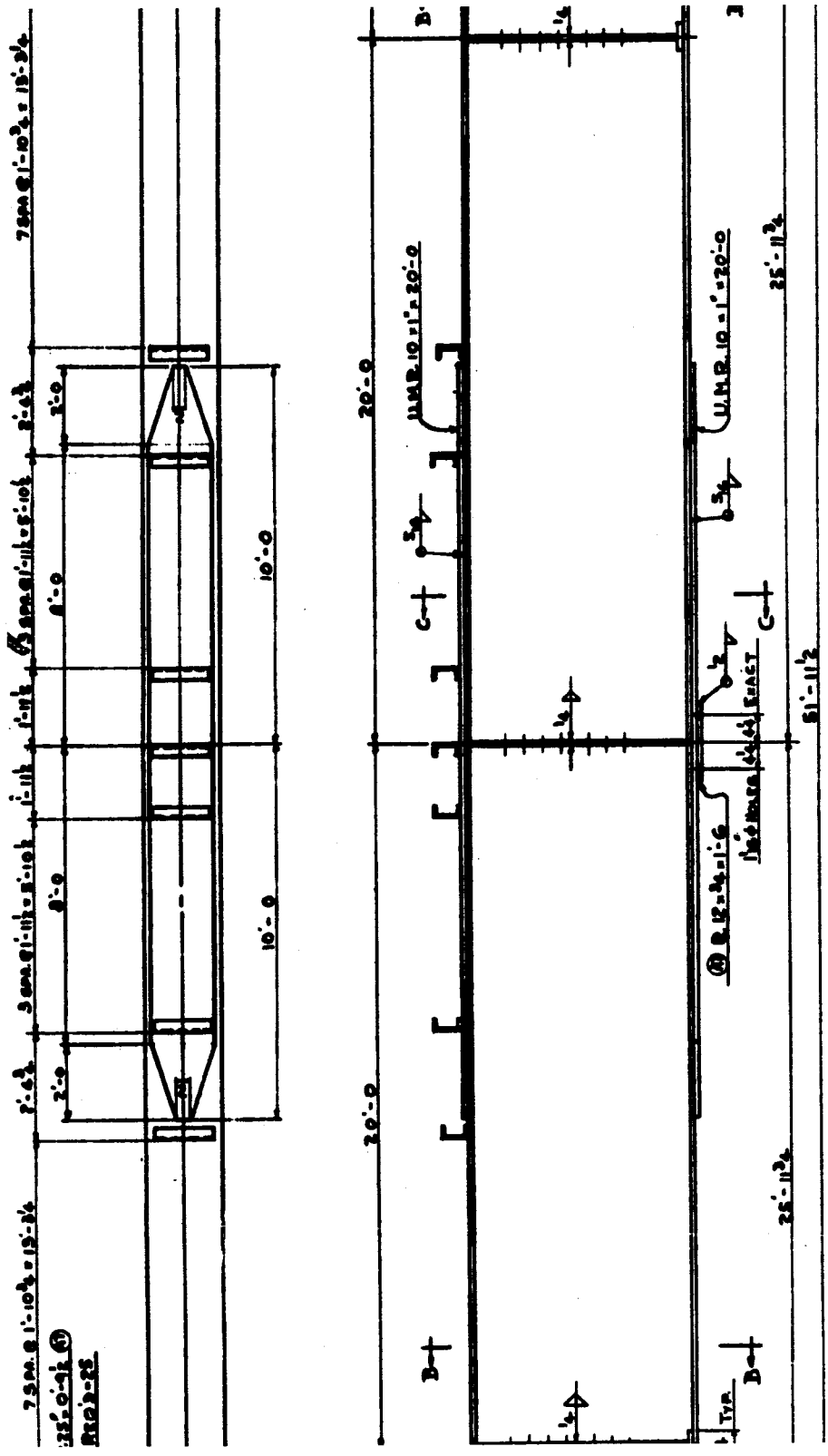

Appendix C

Ultrasonic Inspection Reports

BRIDGES AND STRUCTURES
200 WATERS EDGE BUILDING
1500 W COUNTY ROAD B2
ROSEVILLE, MN 55113
Fax No. 612/582-1161

Monitor - UT remaining cover plates.

REPORT OF ULTRASONIC INSPECTION

Bridge Number: BR62066

Location: West 7th St Over Railroad, St Paul

Date of Inspection: October 7 and 8, 1996

Date of Report: October 8, 1996

Report Prepared By: Eric C. Evens

Introduction:
BR62066 has cover plates welded to the tension flange of the girders. The area of inspection is the top flange where the cover plate terminates. The cover plate terminates with a fillet weld welded transverse to the primary direction of the flange.

Scope of Inspection:
Ultrasonic inspection was performed using an EPOCH III ultrasonic machine with a 60° and 70° transducer. The negative moment flanges were inspected (top flange). Since the top of the flange is not accessible, the inspection was accomplished from the bottom of the flange. The primary area of concern is any indication that is in the flange thickness. Indications that appear beyond the thickness of the flange are of secondary importance. The following girders were inspected (see drawing 1 and 2):

GIRDER	LOCATION	FLANGE THICKNESS
*A	A3 - north and south end of cover plate	1.020"
*B	B3 - north and south end of cover plate	1.020"
*C	C3 - north and south end of cover plate	1.020"
*D	D3 - north and south end of cover plate	1.020"
*E	E3 - north and south end of cover plate	1.020"
F	F3 - north and south end of cover plate	1.020"
G	G3 - north and south end of cover plate	1.020"

* Designates an ultrasonic indication

Results:

Girder A at A3 has a linear indication on the north end cover plate, east and west side of the girder. The indications range in depth from approximately 1/16" (0.0625") on the east side of the girder up to 3/16" (0.1875") on the west side of the girder. All depths are from the top of the flange.

Girder B at B3 has a linear indication on the south end cover plate, east and west side of the girder. The indications range in depth from approximately 1/16" (0.0625") on the west side of the girder up to 1/8" (0.125") deep on the east side of the girder. All depths are from the top of the flange.

Girder C at C3 has a linear indication on the south end cover plate, east and west side of the girder. The indications range in depth from approximately 1/16" (0.0625") on the west side of the girder up to 1/8" (0.125") deep on the east side of the girder. All depths are from the top of the flange.

Girder C at C3 has a linear indication on the north end cover plate, west side of the girder. The indications range in depth from approximately 1/16" (0.0625") deep from the top of the flange.

Girder D at D3 has a linear indication on the south end cover plate, east and west side of the girder. The indication is approximately 3/16" (0.1875") deep from the top of the flange.

Girder E at E3 has a linear indication on the south end cover plate, east side of the girder. The indications range in depth from approximately 1/8" (0.125") deep from the top of the flange.

Girders F and G did not did not have any indications.

Report Prepared By:

Eric C. Evens
Nondestructive Testing Inspector

cc:
Terry Moravec

STATE OF MINNESOTA
BRIDGES AND STRUCTURES
200 WATERS EDGE BUILDING
1500 W COUNTY ROAD B2
ROSEVILLE, MN 55113
Fax No. 612/582-1161

REPORT OF ULTRASONIC INSPECTION

Bridge Number: BR27855

Location: ISTH-94 Over TH-55

Date of Inspection: June 12, 1997

Date of Report: June 18, 1997

Report Prepared By: Eric C. Evens

Introduction:
BR27855 has two girders that have ultrasonic indications that have been previously reported. A follow up inspection was performed to determine the severity of the indications and if the indications had expanded.

Results:
Girder M at M108, west end cover plate, (.8125" flange thickness) refer to the attached drawing for a cross section view of the severity of the indication. The indication does not appear to have propagated beyond the size originally reported.

Girder B at B83, east end cover plate, (1.1875" flange thickness) has a linear indication that is located 0.125" deep from the top of the flange. The indication is approximately 1.5" long. The indication does not appear to have propagated beyond the size originally reported.

Scope of Inspection:
Ultrasonic inspection was performed using an EPOCH III ultrasonic machine with a 30-70-70 transducer. The negative moment flanges were inspected (top flange). Since the top of the flange is not accessible, the inspection was accomplished from the bottom of the flange. The primary area of concern is any indication that is in the flange thickness. Indications that appear beyond the thickness of the flange are of secondary importance.

Report Prepared By:

Eric C. Evens
Nondestructive Testing Inspector

STATE OF MINNESOTA
BRIDGES AND STRUCTURES
200 WATERS EDGE BUILDING
1500 W COUNTY ROAD B2
ROSEVILLE, MN 55113
Fax No. 612/582-1161

REPORT OF ULTRASONIC INSPECTION

Bridge Number: BR9276

Location: TH36 Over Cleveland Ave

Date of Inspection: December 18, 1997

Date of Report: December 22, 1997

Report Prepared By: Eric C. Evens

Introduction:
BR9276 has cover plates welded to the positive and negative moment area of the beams. The primary area of inspection was the end of the cover plates in the negative moment areas. The cover plate terminates with a fillet weld welded transverse to the primary direction of the flange.

Scope of Inspection:
Ultrasonic inspection was performed using an EPOCH III ultrasonic machine with a 30°-70°-70° transducer. Beams that had indications reported on September 16, 1996 were inspected. The inspection was completed to determine if any of the previously reported indications had propagated. The following girders were inspected (see drawing 1):

GIRDER	LOCATION	FLANGE THICKNESS
B	B8 - east & west end of cover plate.	0.9375"
C	B9 - east and west end of cover plate.	0.9375"
F	B12 east & west end of cover plate.	0.9375"

Results:
Girder B at B8 has a linear indication on the east end cover plate, south side of the girder. The indication is approximately 1/16" (0.0625") deep from the top of the flange. The indication is contained to the cover plate weld and has not propagated beyond that originally reported.

Girder C at B9 has a linear indication on the east end cover plate, north side of the girder. The indication is approximately 1/16" (0.0625") deep from the top of the flange. The indication has not propagated beyond that originally reported. The west end cover plate had previously cracked and was repaired.

Girder F at B12 has a linear indication on the west end cover plate, north side of the girder. The indication is approximately 3/16" (0.1875") deep from the top of the flange. The indication extended out towards the end of the flange. See drawing 2 and 3 for a details of the location of the indication.

Report Prepared By:

Eric C. Evens
Nondestructive Testing Inspector

cc:
Terry Moravec
Mark Pribula

Appendix D

Programs

Acquire.c

/* Program for reading voltages and writing data to binary file */

```
#include <formatio.h>
#include <easyio.h>
#include <ansi_c.h>


static long scans; /* number of data points per channel */
static double rate; /* scan rate in hertz */
static double SCANRATE;/* scan rate that is actually achieved */

#define MAXSCANS 5000000
static double SEQ[MAXSCANS];

long nc; /* number of channels being samples */

void die()
{
char temp[100];

        printf("hit <cr> to exit");
        fgets(temp,99,stdin);
        exit(0);
}

void main(void)
{
FILE *fp;
char temp[101],filename[100],f1[100],f2[100];
long fsize,i;
int status;

rate=50.;
nc=7;

printf("Input total time (mins) ");
fgets(temp,100,stdin);
scans = atoi(temp)*60.*rate;
if(nc*scans > MAXSCANS)
{
        printf("maximum scans exceeded (%i)\n",MAXSCANS);
        scans = MAXSCANS/nc;
}
printf("scans = %i \n",scans);
```

```
printf("hit <cr> to start data collection (q=quit) ");
fgets(temp,100,stdin);
if(temp[0] == 'q')
{
        printf("aborted\n");
        exit(0);
}

printf("Working ...\n");


AIAcquireWaveforms (1, "6:0", scans, rate, 5, -5, &SCANRATE,
                                        GROUP_BY_SCAN, SEQ);

printf("Actual scan rate = %f\n",SCANRATE);
fagain:

printf("Input filename to save data in (no ext) = ? ");
fgets(filename,99,stdin);
filename[strlen(filename)-1]='\0';

strcpy(f1,filename);
strcat(f1,".bin");

status=GetFileInfo (f1, &fsize);

if(status == 1)
{
        printf("file exists, try again\n");
        goto fagain;
}
printf("Writing data ...\n");



status = ArrayToFile(f1,SEQ, VAL_DOUBLE, nc*scans,1,VAL_GROUPS_TOGETHER,
        VAL_GROUPS_AS_COLUMNS,VAL_SEP_BY_TAB,1,VAL_BINARY,VAL_OPEN_
AS_IS);

if(status != 0)
{
        printf("write failed (%i), try again\n",status);
        goto fagain;
}
```

```
strcpy(f2,filename);
strcat(f2,".dat");

fp = fopen(f2,"w");
if(fp == NULL)
{
        printf("open on %s failed\n",f2);
        die();
}
else
{
        fprintf(fp,"nc=%i\n",nc);
        fprintf(fp,"scans=%i\n",scans);
        fprintf(fp,"rate=%f\n",SCANRATE);
        fclose(fp);
}


printf("data written to %s and %s \n",f1,f2);



}
```

Read_dat.c

```
/* Program for converting binary data to ASCII */

#include <formatio.h>
#include <easyio.h>
#include <ansi_c.h>


#define MAXSCANS 5000000
static double SEQ[MAXSCANS];

void die()
{
char temp[100];

        printf("hit <cr> to exit");
        fgets(temp,99,stdin);
        exit(0);
}

main()
{
FILE *fp;
char filename[100],f1[100],f2[100],line[100],temp[100],f3[100];
char *pos;
int nc,status;
long scans;
float scanrate;
int i,j;


printf("Input the data file to read (no ext) = ? ");
fgets(filename,99,stdin);
filename[strlen(filename)-1]='\0';

strcpy(f1,filename);
strcat(f1,".bin");
strcpy(f2,filename);
strcat(f2,".dat");

fp = fopen(f2,"r");
if(fp == NULL)
{
        printf("Error on open of %s \n",f2);
```

```
        die();
}

while(!feof(fp))
{
        fgets(line,99,fp);

        if(strncmp(line,"nc=",3) == 0)
        {
                pos = strchr(line,'=')+1;
                nc = atoi(pos);
        }
        if(strncmp(line,"scans=",6) == 0)
        {
                pos = strchr(line,'=')+1;
                scans = atoi(pos);
        }
        if(strncmp(line,"rate=",5) == 0)
        {
                pos = strchr(line,'=')+1;
                scanrate = atof(pos);
        }

}

fclose(fp);

printf("number of channels = %i\n",nc);
printf("number of scans = %i \n",scans);
printf("scan rate = %f \n",scanrate);

if(scans*nc > MAXSCANS)
{
        printf("max array size exceeded\n");
        die();
}

status = FileToArray(f1,&SEQ, VAL_DOUBLE,nc*scans,1,VAL_GROUPS_TOGETHER,
        VAL_GROUPS_AS_COLUMNS,VAL_BINARY);

if(status != 0)
{
        printf("read error occured (%i)\n",status);
        die();
}
```

```
else
{
        printf("Data read ok\n");
}


printf("Convert to ASCII (y/n) <y> =? ");
fgets(temp,99,stdin);

if(temp[0] == 'n')
{
        printf("conversion aborted\n");
        exit(0);
}


printf("saving as text ...\n");

strcpy(f3,filename);
strcat(f3,".txt");

fp=fopen(f3,"w");
if(fp == NULL)
{
        printf("open of %s failed\n",f3);
        die();
}


fprintf(fp,"Scanrate\t%g\n",scanrate);
fprintf(fp,"n chans\t%i\n",nc);
fprintf(fp,"n scans\t%i\n",scans);

for(i=0;i<scans;i++)
{
        for(j=0;j<nc;j++)
        {
    fprintf(fp,"%g",SEQ[nc*i+j]);
    if(j < (nc-1))
    {
        fprintf(fp,"\t");
    }
    else
    {
        fprintf(fp,"\n");
```

```
    }
   }

}
fclose(fp);

printf("done\n");

}
```

Filter.c

```
/* Program for converting from binary to ASCII and filtering data using a Lowpass Butterworth
Digital Filter */

#include <formatio.h>
#include <easyio.h>
#include <ansi_c.h>
#include <analysis.h>

#define MAX 1000000
#define MIN 90003
static double SEQ[MAX], CH7[MIN], CH6[MIN], CH5[MIN], CH4[MIN];
static double CH3[MIN], CH2[MIN], CH1[MIN], CH0[MIN], FIL0[MIN];
static double FIL1[MIN], FIL2[MIN], FIL3[MIN], FIL4[MIN], FIL5[MIN];
static double FIL6[MIN], FIL7[MIN];
void die()
{
char temp[100];

        printf("hit <cr> to exit");
        fgets(temp,99,stdin);
        exit(0);
}

main()
{
FILE *fp;
char filename[100],f1[100],f2[100],line[100],temp[100],f3[100];
char *pos;
double fc;
int nc,status;
int order;
long scans;
float scanrate;
int i,j;


printf("Input the data file to read (no ext) = ? ");
fgets(filename,99,stdin);
filename[strlen(filename)-1]='\0';

strcpy(f1,filename);
strcat(f1,".bin");
```

```
strcpy(f2,filename);
strcat(f2,".dat");

fp = fopen(f2,"r");
if(fp == NULL)
{
        printf("Error on open of %s \n",f2);
        die();
}

while(!feof(fp))
{
        fgets(line,99,fp);

        if(strncmp(line,"nc=",3) == 0)
        {
                pos = strchr(line,'=')+1;
                nc = atoi(pos);
        }
        if(strncmp(line,"scans=",6) == 0)
        {
                pos = strchr(line,'=')+1;
                scans = atoi(pos);
        }
        if(strncmp(line,"rate=",5) == 0)
        {
                pos = strchr(line,'=')+1;
                scanrate = atof(pos);
        }

}

fclose(fp);

printf("number of channels = %i\n",nc);
printf("number of scans = %i \n",scans);
printf("scan rate = %f \n",scanrate);

if(scans*nc > MAX)
{
        printf("max array size exceeded\n");
        die();
}

status = FileToArray(f1,&SEQ, VAL_DOUBLE,nc*scans,1,VAL_GROUPS_TOGETHER,
```

```
        VAL_GROUPS_AS_COLUMNS,VAL_BINARY);

if(status != 0)
{
        printf("read error occured (%i)\n",status);
        die();
}
else
{
        printf("Data read ok\n");
}

printf("Convert to ASCII (y/n) <y> =? ");
fgets(temp,99,stdin);

if(temp[0] == 'n')
{
        printf("conversion aborted\n");
        exit(0);
}


printf("saving as text ...\n");

strcpy(f3,filename);
strcat(f3,".fil");

fp=fopen(f3,"w");
if(fp == NULL)
{
        printf("open of %s failed\n",f3);
        die();
}

fprintf(fp,"Scanrate\t%g\n",scanrate);
fprintf(fp,"n chans\t%i\n",nc);
fprintf(fp,"n scans\t%i\n",scans);
fprintf(fp,"Ch 4\tCh 6\tCh 5\tNo Channel\tCh 3\tCh 2\tCh 1\tCh 0\n");

for(i=0;i<scans;i++)
{
        CH7[i]=SEQ[nc*i];
        CH6[i]=SEQ[nc*i+1];
        CH5[i]=SEQ[nc*i+2];
        CH4[i]=SEQ[nc*i+3];
```

```
        CH3[i]=SEQ[nc*i+4];
        CH2[i]=SEQ[nc*i+5];
        CH1[i]=SEQ[nc*i+6];
        CH0[i]=SEQ[nc*i+7];
}

fc=3.5;  /* Cutoff Frequency of Filter*/
order=8;  /* Filter Order */

        status = Bw_LPF (CH7, scans, scanrate, fc, order, FIL7);
        status = Bw_LPF (CH6, scans, scanrate, fc, order, FIL6);
        status = Bw_LPF (CH5, scans, scanrate, fc, order, FIL5);
        status = Bw_LPF (CH4, scans, scanrate, fc, order, FIL4);
        status = Bw_LPF (CH3, scans, scanrate, fc, order, FIL3);
        status = Bw_LPF (CH2, scans, scanrate, fc, order, FIL2);
        status = Bw_LPF (CH1, scans, scanrate, fc, order, FIL1);
        status = Bw_LPF (CH0, scans, scanrate, fc, order, FIL0);

for (i=0;i<scans;i++)
{
        fprintf(fp,"%g",FIL7[i]);
        fprintf(fp,"\t");
        fprintf(fp,"%g",FIL6[i]);
        fprintf(fp,"\t");
        fprintf(fp,"%g",FIL5[i]);
        fprintf(fp,"\t");
        fprintf(fp,"%g",FIL4[i]);
        fprintf(fp,"\t");
        fprintf(fp,"%g",FIL3[i]);
        fprintf(fp,"\t");
        fprintf(fp,"%g",FIL2[i]);
        fprintf(fp,"\t");
        fprintf(fp,"%g",FIL1[i]);
        fprintf(fp,"\t");
        fprintf(fp,"%g",FIL0[i]);
        fprintf(fp,"\n");
}

fclose(fp);

printf("done\n");

}
```

Stress Counter

```
' Visual Basic Program to count stress ranges

Sub reduction()
Dim i As Long, n As Integer, k As Integer, nscans As Long
Dim nwaste As Integer, Thresh(1 To 1, 1 To 1) As Double
Dim Mean As Double
Dim Stress(1 To 60000, 1 To 2) As Double
Dim Upeak(1 To 10000, 1 To 3) As Double
Dim Fpeak(1 To 10000, 1 To 2) As Double
Dim Sum As Double
Dim Range(1 To 10000, 1 To 2) As Double
Dim Min As Double, imax As Integer
Dim Max As Double, imin As Integer, mi As Long
Dim Dcount As Long, rw As Long, nrange As Long, nfpeaks As Integer
Dim a(1 To 1, 1 To 1) As Integer, b(1 To 1, 1 To 1) As Integer
Dim c(1 To 1, 1 To 1) As Integer, d(1 To 1, 1 To 1) As Integer
Dim e(1 To 1, 1 To 1) As Integer, f(1 To 1, 1 To 1) As Integer
Dim g(1 To 1, 1 To 1) As Integer, h(1 To 1, 1 To 1) As Integer
Dim m(1 To 1, 1 To 1) As Integer, o(1 To 1, 1 To 1) As Integer
Dim p(1 To 1, 1 To 1) As Integer, q(1 To 1, 1 To 1) As Integer
Dim r(1 To 1, 1 To 1) As Integer, s(1 To 1, 1 To 1) As Integer
Dim t(1 To 1, 1 To 1) As Integer, u(1 To 1, 1 To 1) As Integer
Dim v(1 To 1, 1 To 1) As Integer, w(1 To 1, 1 To 1) As Integer
Dim x(1 To 1, 1 To 1) As Integer, y(1 To 1, 1 To 1) As Integer

nscans = Sheets("data").Cells(3, 2).Value
nwaste = 4
n = 0
imax = 0
```

```
imin = 0
npeaks = 0
Mean = 0
Sum = 0

'define thresh and mean
'stress(i,1) is stress value
'stress(i,2) is mean stress value at that location

For n = 1 To 100
    For i = ((n - 1) * nscans / 100) + 1 To (n * nscans / 100)
        Stress(i, 1) = 6# * Sheets("data").Cells(i + nwaste, 1).Value
        Sum = Sum + Stress(i, 1)
        Mean = Sum / (nscans / 100)
    Next i

    For mi = ((n - 1) * nscans / 100) + 1 To (n * nscans / 100)
        Stress(mi, 2) = Mean
    Next mi
    Mean = 0
    Sum = 0
Next n
n = 0
mi = 1

'find the individual peaks
For k = 1 To 1
  For i = 2 To nscans - 1
    inslope = Stress(i, k) - Stress(i - 1, k)
    outslope = Stress(i + 1, k) - Stress(i, k)
```

```
        If inslope >= 0 And outslope <= 0 Then
        n = n + 1
        Upeak(n, 2) = Stress(i, 1)
        Upeak(n, 1) = i
        Upeak(n, 3) = Stress(i, 2)
        End If

        If inslope <= 0 And outslope >= 0 Then
        n = n + 1
        Upeak(n, 2) = Stress(i, 1)
        Upeak(n, 1) = i
        Upeak(n, 3) = Stress(i, 2)
        End If

    Next i
    npeaks = n
    n = 0
Next k

'print the peaks and peak locations on sheet ranges
For rws = 1 To npeaks
    For cols = 1 To 3
        Sheets("ranges").Cells(rws, cols).Value = Upeak(rws, cols)
    Next cols
Next rws

'filter peaks so only big ranges kept
Max = Upeak(1, 2)
Min = Upeak(1, 2)
```

```
For i = 1 To npeaks - 1
   If Upeak(i, 2) >= Max Then
      Max = Upeak(i, 2)
   End If

   If Upeak(i, 2) <= Min Then
      Min = Upeak(i, 2)
   End If

   If Upeak(i, 2) <= Upeak(i, 3) And Upeak(i + 1, 2) >= Upeak(i, 3) And (Upeak(i + 1, 2) -
Upeak(i, 2)) > 0.04 And n = 0 Then
      n = 1
   End If

   If Upeak(i, 2) >= Upeak(i, 3) And Upeak(i + 1, 2) <= Upeak(i, 3) And (Upeak(i, 2) - Upeak(i
+ 1, 2)) > 0.04 And n = 1 Then
      n = 2
   End If

   If Upeak(i, 2) <= Upeak(i, 3) And Upeak(i + 1, 2) >= Upeak(i, 3) And (Upeak(i + 1, 2) -
Upeak(i, 2)) > 0.04 And n = 2 Then
      n = 3
   End If

   If n = 3 Then
      Range(mi, 2) = Max - Min
      Range(mi, 1) = Upeak(i, 1)
      mi = mi + 1
      Max = Upeak(i, 3)
      Min = Upeak(i, 3)
```

```
        n = 0
        i = i - 1
    End If
Next i

nrange = mi - 1

'print the ranges and locations of them
For rws = 1 To nrange
    For cols = 1 To 2
        Sheets("ranges").Cells(rws, cols + 3).Value = Range(rws, cols)
    Next cols
Next rws


'group data to create histogram
For k = 1 To 1
    a(1, k) = 0
    b(1, k) = 0
    c(1, k) = 0
    d(1, k) = 0
    e(1, k) = 0
    f(1, k) = 0
    g(1, k) = 0
    h(1, k) = 0
    m(1, k) = 0
    o(1, k) = 0
    p(1, k) = 0
    q(1, k) = 0
```

```
k = 1
  For i = 1 To 3000
    If Range(i, 2) <= 0.5 And Range(i, 2) > 0.0001 Then
      a(1, k) = a(1, k) + 1
    ElseIf Range(i, 2) <= 1# And Range(i, 2) > 0.0001 Then
      b(1, k) = b(1, k) + 1
    ElseIf Range(i, 2) <= 1.5 And Range(i, 2) > 0.0001 Then
      c(1, k) = c(1, k) + 1
    ElseIf Range(i, 2) <= 2# And Range(i, 2) > 0.0001 Then
      d(1, k) = d(1, k) + 1
    ElseIf Range(i, 2) <= 2.5 And Range(i, 2) > 0.0001 Then
      e(1, k) = e(1, k) + 1
    ElseIf Range(i, k) <= 3# And Range(i, 2) > 0.0001 Then
      f(1, k) = f(1, k) + 1
    ElseIf Range(i, k) < 3.5 And Range(i, 2) > 0.0001 Then
      g(1, k) = g(1, k) + 1
    ElseIf Range(i, 2) < 4# And Range(i, 2) > 0.0001 Then
      h(1, k) = h(1, k) + 1
    ElseIf Range(i, 2) < 4.5 And Range(i, 2) > 0.0001 Then
      m(1, k) = m(1, k) + 1
    ElseIf Range(i, 2) < 5# And Range(i, 2) > 0.0001 Then
      o(1, k) = o(1, k) + 1
    ElseIf Range(i, 2) < 5.5 And Range(i, 2) > 0.0001 Then
      p(1, k) = p(1, k) + 1
    ElseIf Range(i, 2) < 6# And Range(i, 2) > 0.0001 Then
      q(1, k) = q(1, k) + 1

    End If
  Next i
Next k
```

```
'print a chart for number of hits at each level
For k = 1 To 1
   rw = 0
   Sheets("ranges").Cells(rw + 1, 9 + k) = a(1, k)
   Sheets("ranges").Cells(rw + 2, 9 + k) = b(1, k)
   Sheets("ranges").Cells(rw + 3, 9 + k) = c(1, k)
   Sheets("ranges").Cells(rw + 4, 9 + k) = d(1, k)
   Sheets("ranges").Cells(rw + 5, 9 + k) = e(1, k)
   Sheets("ranges").Cells(rw + 6, 9 + k) = f(1, k)
   Sheets("ranges").Cells(rw + 7, 9 + k) = g(1, k)
   Sheets("ranges").Cells(rw + 8, 9 + k) = h(1, k)
   Sheets("ranges").Cells(rw + 9, 9 + k) = m(1, k)
   Sheets("ranges").Cells(rw + 10, 9 + k) = o(1, k)
   Sheets("ranges").Cells(rw + 11, 9 + k) = p(1, k)
   Sheets("ranges").Cells(rw + 12, 9 + k) = q(1, k)
Next k

'Print lables for stress ranges
Sheets("ranges").Cells(rw + 1, 9) = "0 to 0.5"
   Sheets("ranges").Cells(rw + 2, 9) = "0.5 to 1"
   Sheets("ranges").Cells(rw + 3, 9) = "1 to 1.5"
   Sheets("ranges").Cells(rw + 4, 9) = "1.5 to 2"
   Sheets("ranges").Cells(rw + 5, 9) = "2 to 2.5"
   Sheets("ranges").Cells(rw + 6, 9) = "2.5 to 3"
   Sheets("ranges").Cells(rw + 7, 9) = "3 to 3.5"
   Sheets("ranges").Cells(rw + 8, 9) = "3.5 to 4"
   Sheets("ranges").Cells(rw + 9, 9) = "4 to 4.5"
   Sheets("ranges").Cells(rw + 10, 9) = "4.5 to 5"
   Sheets("ranges").Cells(rw + 11, 9) = "5 to 5.5"
```

```
    Sheets("ranges").Cells(rw + 12, 9) = "5.5 to 6"


End Sub
```